

Aircushion Supported
Mega-Floaters

J.L.F. van Kessel

This research was funded by:

The Water Research Centre of Delft University of Technology
&
SBM Gusto

Aircushion Supported Mega-Floaters

PROEFSCHRIFT

ter verkrijging van de graad van doctor
aan de Technische Universiteit Delft,
op gezag van de Rector Magnificus prof. ir. K.C.A.M. Luyben,
voorzitter van het College van Promoties

Op maandag 1 februari 2010 om 12:30 uur
door

Johannes (Jan) Lambertus Franciscus VAN KESSEL

Scheepsbouwkundig ingenieur

Geboren te Bergeijk

Dit proefschrift is goedgekeurd door de promotoren:

Prof. dr. ir. R.H.M. Huijsmans

Prof. ir. C.A. Willemse

Samenstelling promotiecommissie:

Rector Magnificus,	voorzitter
Prof. dr. ir. R.H.M. Huijsmans,	Technische Universiteit Delft, promotor
Prof. ir. C.A. Willemse,	Technische Universiteit Delft, promotor
Prof. dr. ir. J.A. Pinkster,	Technische Universiteit Delft
Prof. dr. A.V. Metrikine,	Technische Universiteit Delft
Prof. ir. J. Meek,	Technische Universiteit Delft, reserve lid
Prof. O.M. Faltinsen,	Norwegian Institute of Technology, Norway
Prof. dr. ir. H.W.M. Hoeijmakers,	Technische Universiteit Twente
Dr. ir. A.P. van 't Veer,	SBM Gusto

ISBN 978-90-8570-496-6

Copyright © 2010 by J.L.F. van Kessel

Keywords: mega-float, very large floating structure (VLFS), aircushion support, compressibility, fluid-structure interaction, hydroelastic analysis, motions, dynamic behavior, wave forces, drift forces, wave field, shear forces, bending moments, stresses, frequency domain, floating runway.

All rights reserved. No part of this publication may be reproduced, stored in a retrieval system or transmitted in any form or by any means, electronic, mechanical, photocopying, recording or otherwise, without prior written permission of the author.

Printed in the Netherlands by: Wöhrmann Print Service, Zutphen.

*To my parents & brother,
my parents Jan & Mariet
my brother Lart*

Contents

Acknowledgement	xi
Summary	xv
List of Symbols	xvii
1 Introduction	1
1.1 History of mega-floaters	1
1.2 Aircushion support in the offshore industry.....	6
1.3 The need for ocean space	8
1.4 Objective of the research.....	9
1.5 Outline of the thesis	9
2 Rigid aircushion supported structures	11
2.1 Introduction.....	11
2.2 Definitions	13
2.3 Aircushion theory.....	13
2.3.1 Theory of air columns	14
2.3.2 Theory of aircushion supported structures	15
2.3.3 Restoring coefficients and stability	16
2.3.4 Resonance frequencies of the aircushion	20
2.4 Fluid dynamics.....	21
2.5 Numerical approach	23
2.6 Validation of the numerical approach	29
2.6.1 Oscillation tests	30
2.6.2 Captive tests	35
2.6.3 Free-floating tests.....	38

2.7	Comparison with a conventional barge.....	42
2.7.1	Tuning the aircushion characteristics.....	42
2.7.2	Drift forces and wave field	46
2.7.3	Wave induced shear forces and bending moments	51
2.8	Conclusions	56
3	Flexible aircushion supported structures	59
3.1	Introduction	59
3.2	Structural model.....	60
3.2.1	Principal coordinates.....	62
3.2.2	Equation of motion	62
3.3	Hydromechanical model	63
3.3.1	Equation of motion	67
3.4	Numerical results and discussion.....	68
3.4.1	Natural frequencies	68
3.4.2	Fluid-structure interaction.....	74
3.4.3	Fluid-gas-structure interaction.....	84
3.4.4	Structural loads	88
3.4.5	Number of principal modes required	96
3.5	Conclusions	98
4	Technical feasibility of an aircushion supported mega-floater	99
4.1	Introduction	99
4.2	Suitable locations for mega-floaters	99
4.2.1	Most probable location	100
4.2.2	Environmental conditions	101
4.3	Main particulars and numerical settings	102
4.4	Wave induced bending moments and stresses	105
4.5	Conclusions	111
5	Conclusions and recommendations	113
5.1	Main conclusions.....	113
5.2	Recommendations.....	114
	Bibliography	117

Appendices	127
A Compressibility of aircushions.....	127
B Behavior of a large rigid aircushion supported structure	131
C Orthogonality condition	133
D Flexible aircushion supported structures.....	135
E Responses in irregular seas	141
 Samenvatting (summary in Dutch)	 143
 Curriculum Vitae	 145

Acknowledgement

When I was still a student at Delft University of Technology I sometimes got carried away by the enthusiasm of Jan Meek and George Lagers when they were talking about their experiences in the offshore industry. Their enthusiasm was contagious, and after a few meetings with them at the university in the spring of 2004, I decided to take the challenge to start a Ph.D. research.

Jo Pinkster, my professor in ship hydromechanics, proposed to investigate the '*behavior of aircushion supported mega-floaters in waves*'. This was a very interesting subject, but unfortunately there was no funding for it. I considered this to be a minor problem and started to write a research proposal.

Marcel Stive, head of the Water Research Centre, was enthusiastic about the subject and decided to fund the first part of the research. The second part of the research was funded by SBM Gusto after some discussions with Wim Janse and Marco Beenen.

Gentlemen, I am very grateful that you gave me the opportunity to carry out the research the way it was. I am very thankful for your enthusiasm, cooperation and funding.

The first part of the research was performed at Delft University of Technology under the supervision of Jo Pinkster and Jan Meek. During regular meetings we discussed the progress of the research and they provided me with new thoughts for future investigations. Jo Pinkster was the person who taught me everything I needed to know about diffraction theory and the basics of aircushion theory. Eventually, this proved to be a fruitful basis for a new numerical method as described in this thesis. Jo, I am very grateful for that!

After retirement of Jo Pinkster the supervision of the research was handed over to René Huijsmans with whom I had the pleasure to work during the last three years. René, I enjoyed working with you, your enthusiasm, your advices, and the way you inspired me to tackle new problems on the way to my Ph.D. The fact that your working day at the university started before 7 AM was a privilege to me, which I frequently used to pose you some questions or to discuss new results. I am also very thankful for the opportunity you gave me to present my research at different conferences at often beautiful (exotic) locations like Wuxi (China), Lisbon (Portugal),

San Diego (USA), Estoril (Portugal), Vancouver (Canada), Southampton (UK) and Hawaii (USA). For sure, these were the greatest scientific moments I experienced during my research!

The second part of the research was carried out at the office of SBM Gusto in Schiedam, the Netherlands. It was great to be back after being away for almost three years. I enjoyed the new cooperation with all my colleagues, especially those in the naval architect department with whom I worked closely together. Two of these people really stand out and I particularly like to thank them for their contributions during my research.

First of all, Riaan van 't Veer, thank you for your critical opinions and the interesting discussions we had about hydrodynamic problems, which I stubbornly called 'issues' or 'challenges'.

Secondly, Timo de Beer, thank you for sharing your structural expertise with me. Sorry for the times I kept you in the office with my never ending questions and new results. I am grateful for our conversations, especially the ones on Friday evenings in a desolated office, which provided me with many new thoughts not to be bored during the weekends.

The second part of this thesis describes the dynamic behavior of flexible floating structures. When I started this part of the research, I had the intention to solve the fully coupled hydro-structural problem without making use of the well-known simplifications. At this stage Martin van Gyzen helped me a lot with 'issues' related to sparse eigenvalue solvers. Unfortunately, but for good reasons, this approach was abandoned. Nevertheless, Martin, I really appreciated your help.

Johan Tuitman, I already know you for many years. We started studying naval architecture at Delft University on the same rainy day in 1999. Then, we graduated in the same week in 2004. Next, we both started a Ph.D. research, and whether it is coincidence or not, we will both defend our own thesis in the same month. I wonder what the next milestone will be that we will share together. Retirement?

Although there were many differences in our researches, we both carried out our research in the field of fluid-structure interaction. This was a good excuse for some interesting discussions during pleasant dinners in the culinary centre of Delft, for which I would like to thank you. Johan, I would also like to thank you for the computations you performed with your hydroelastic code HydElast. These results were used in the verification process of my new hydroelastic code for aircushion supported structures as described in this thesis.

In addition, I am grateful to Fabien Remy for providing measurements of the model tests performed at the BGO-first basin in France in 2006.

I am also very thankful to Henk den Besten, Stefanie Lunshof and Erwin van den Berg for proof-reading the thesis and for providing me with final comments that certainly improved the quality of this thesis.

Most importantly, I wish to thank my parents and brother for their continues encouragement and never ending support. Sorry for all those times that you had to put up with ‘me and my laptop’. This thesis is dedicated to you!

Last, but certainly not least, I wish to thank all my friends and colleagues at the university for their support and the great moments of joy that we shared during the last years. You know who you are!

Jan van Kessel

Delft, December 2009

Summary

Aircushion Supported Mega-Floaters

The increase of the global population and expanding coastal mega-cities will necessitate an innovative pursuit of the utilization of the ocean space in which mega-floaters will play an important role in the future. These types of structures are very large floating artificial islands that can be used for various facilities and purposes similar to those on land. Compared to landfill methods mega-floaters generally have a smaller environmental impact than traditional land reclamation projects. They are indifferent to earthquakes and can be constructed at relatively low cost in a short period of time, independent of ocean depth and seabed conditions. Furthermore, the existing facilities can be easily expanded while they are functional and the space available inside the structure offers prospects for various activities and different use.

This thesis describes a method to predict the dynamic behavior of aircushion supported mega-floaters in waves. These types of structures are supported by a large volume of air which is entrapped underneath the structure by vertical walls that extend sufficiently far underneath the water surface in a way that no air will escape when waves pass by. The method is based on a linear three-dimensional potential theory using modal expansions and a linear adiabatic law to describe the air pressure within the aircushion. It is the first method that is able to accurately predict the three-dimensional dynamic behavior and stresses of flexible aircushion supported structures of arbitrary shape in waves. The structure around the aircushion is modeled in the usual way by means of panels representing pulsating sources which are distributed over the mean wetted surface of the body. The free water surface underneath the structure is modeled by panels laying in the mean free surface of each aircushion. All panels associated with an aircushion represent a body without material mass, but having added mass, damping, hydrostatic restoring and aerostatic restoring characteristics.

The results of this study indicate that the behavior of aircushion supported structures can be well predicted by means of a three-dimensional linear potential method. In case of rigid bodies, the numerical results were validated with model tests. Model tests with a conventional flexible barge served to validate the hydroelastic method. Unfortunately no experimental results are

available for flexible aircushion supported structures. Therefore the numerical results of these structures are verified with analytical and FEM computations.

Both the model tests and computations have shown that the application of aircushions can significantly influence the behavior of floating structures. The effect on the structural loads is significant and is particularly pronounced in the wave induced bending moments which are considerably reduced by the aircushions.

A conventional mega-float structure has to be protected by breakwaters if it is located in open seas. These breakwaters will reduce the wave loads on the structure, but add to the total costs of the mega-float project. Another option is to support the structure by aircushions to reduce the wave induced bending moments and consequently the stresses.

In general, the results of this study have shown that an aircushion supported structure will have significant advantages compared to conventional mega-floaters. In addition, the computational method as developed and proposed proved to be a suitable tool to optimize the cushion configuration for a particular application.

List of Symbols

Hydromechanical

x	surge displacement
y	sway displacement
z	heave displacement
ϕ	roll angle
θ	pitch angle
ψ	yaw angle

ω wave frequency

λ wave length

BB_ϕ shift of the centre of buoyancy due to a roll angle ϕ

$BB_{\phi,s}$ shift of the centre of buoyancy related to the buoyant part of the structure

$BB_{\phi,c}$ shift of the centre of buoyancy related to the aircushions

BM distance from the centre of buoyancy to the metacentric height

GM distance from the centre of gravity to the metacentric height

KB distance from the keel to the centre of buoyancy

KG distance from the keel to the centre of gravity

Structural

u displacement in x-direction

v displacement in y-direction

w displacement in z-direction

θ_x rotation around x-axis

θ_y rotation around y-axis

θ_z rotation around z-axis

Constants

e	2.7182818...
π	3.1415927...

General

\vec{A}	location of a source, (A_1, A_2, A_3)
A_c	area of the aircushion
A_{nj}	added mass coupling coefficients
A_w	the total waterline area of the structure (including the aircushions)
\mathbf{a}	generalized mass matrix
a_{ss}	generalized mass associated with the s^{th} mode
B	centre of buoyancy
B_{nj}	damping coupling coefficients
\mathbf{B}^*	structural damping matrix
C_C	restoring coefficients associated with aircushion contributions
C_D	restoring coefficients associated with distortion modes of the structure
C_{DC}, C_{CD}	restoring coupling coefficients between distortion modes and cushion elements
C_{nj}	restoring coupling coefficient
C_p	specific heat capacity of air at constant pressure
C_{ij}^A	aerostatic restoring coefficients
C_{ij}^H	hydrostatic restoring coefficients
C_R	restoring coefficients associated with rigid-body modes
C_{RC}, C_{CR}	restoring coupling coefficients between the rigid structure and the cushion elements
C_{RD}, C_{DR}	restoring coupling coefficients between the rigid structure and the distortion modes
C_v	specific heat capacity of air at constant volume
$C_{33,c}$	heave restoring coefficient of the aircushions
\mathbf{c}	generalized stiffness matrix
c	speed of sound, 343 m/s in dry air of 20 °C
c_{ss}	generalized stiffness coefficient associated with the s^{th} mode
\mathbf{D}	matrix of principal modes, $(\mathbf{D}_1, \mathbf{D}_2, \dots, \mathbf{D}_m)$
\mathbf{D}_r	r^{th} eigenvector, $(D_{r1}, D_{r2}, \dots, D_{rN})$
\mathbf{D}_{rj}	generalized displacement vector at node j due to the r^{th} principal mode, $(u_r, v_r, w_r, \theta_{x_r}, \theta_{y_r}, \theta_{z_r})$
E	modulus of elasticity
\mathbf{F}	vector of external forces
G	shear modulus of elasticity, centre of gravity

$G(\bar{X}, \bar{A})$	Green's function of a source in \bar{A} relative to a field point \bar{X}
g	gravity acceleration, $g = 9.80663 \text{ m/s}^2$ (average)
H_s	significant wave height
h	water depth
h_c	height of the aircushion
I	area moment of inertia
I_T	transverse area moment of inertia of the waterline
I_{nj}	mass moment of inertia
I_L	longitudinal area moment of inertia of the waterline
i	imaginary number, $i = \sqrt{-1}$
\mathbf{K}	structural stiffness matrix
K_{xx}	roll radius of gyration
k	wave number
L	length of the structure
L_c	length of the cushion
\mathbf{M}	mass matrix, wave induced bending moments
M_{nj}	mass coupling coefficient
m	mass
N_{AC}	number of aircushions
N_c	number of panels in cushion c
N_D	number of distortion modes
N_m	number of mode shapes, $m \geq 6$
N_t	total number of panels used to describe the structure and free surfaces of all cushions
n	normal vector
P	pressure of the aircushion
P_a	atmospheric pressure
P_c	pressure resulting from draft of the aircushion, $P_c = \rho g T_c$
P_0	initial pressure inside the aircushion, $P_0 = P_a + P_c$
$P(t)$	pressure inside the aircushion at time instant t
$p(X)$	pressure in the fluid
$p_r(t)$	set of principal coordinates
\mathbf{Q}	vector of concentrated nodal loads
S	wetted surface of the structure
S_C	free surface area of cushion c
S_c	area of dry elements of the structure laying at the boundary of the aircushion
ΔS_s	surface element of the body or the mean free surfaces of the aircushions

t	time
T	draft, period of regular wave
T_c	vertical distance between mean sea level and the free surface within the aircushion, i.e. the draft of the aircushion
T_z	mean zero-crossing period
T_p	peak period
ΔT	draft variation
\mathbf{U}	vector of nodal displacements
\mathbf{u}_j	vector containing displacements due to j^{th} modal shape
\mathbf{V}	wave induced shear forces
V	volume of the aircushion
V_0	initial volume of the aircushion
$V(t)$	volume of the aircushion at time instant t , $V(t) = V_0 + \Delta V$
ΔV	volume variation of the aircushion
w_j	vertical displacement of element j
\mathbf{X}	vector (X_1, X_2, X_3)
\bar{X}	field point (X_1, X_2, X_3)
X_n	wave force in direction n
$X_{n,p}$	force on cushion element n due to the p - mode of motion
$\overline{X_r}$	generalized fluid force
x_c	distance in x-direction from COG to centre of the aircushion
x_{cf}	coordinate of the centre of the water plane relative to the origin of the axis system
$\overline{x_j}$	rigid body motion in the j -mode
y_c	distance in y-direction from COG to centre of the aircushion
$\overline{y_{cf}}$	coordinate of the centre of the water plane relative to the origin of the axis system
z_c	mean change of the cushion height

Greek symbols

δ_{rs}	Kronecker delta function
ε	compressibility factor of air
$\Phi(\mathbf{X}, t)$	total velocity potential
$\phi(\mathbf{X})$	velocity potential of harmonic waves
ϕ_0	undisturbed wave potential
ϕ_c	wave radiation potential of the aircushions, i.e. potentials associated with vertical motions in cushion c
ϕ_d	wave diffraction potential
$\phi_{d,k}$	diffraction potential at panel k

$\phi_{j,k}$	motion potential value at panel k
ϕ_j	wave radiation potential
$\phi_j(\bar{X})$	potential in point \bar{X} due to the j -mode of motion
κ	gas law index, 1.4 for air
ρ	density of the fluid
σ	stress
σ_{sj}	strength of a source on surface element s due to motion mode j
ζ_0	amplitude of the undisturbed incoming wave
ζ_c	vertical motion of free surface in cushion c
ω_r	r^{th} eigenvalue
ω_{di}	i^{th} distortion mode of the dry structure in vacuum

Special symbols

∇	displaced volume of the structure
∇^2	Laplacian

Chapter 1

Introduction

1.1 History of mega-floaters

Jules Verne, the 19th century novelist and one of the fathers of science fiction, was probably the first to write about large floating islands in his book *L'île à hélice* in 1895 [60]. Nevertheless it was not before the beginning of the 20th century that the first detailed plans for building a *Mega-Floater* were made. These plans were driven by the need for fast transport of passengers and cargo between Europe and the US. At that time, non-stop air transportation of cargo and passengers across the Atlantic Ocean was considered to be unsafe, unreliable and inefficient. Besides, it was not expected that airplanes could economically fly more than 500 miles in the near future. This conclusion was strengthened by the first non-stop flight of Charles Lindberg across the Atlantic Ocean for which he used a specially designed airplane which was basically a flying fuel tank.

Driven by great commercial interest, Edward Armstrong came up with a solution and proposed to build strings of floating airports across the Atlantic. These floating structures were called Seadromes and would serve as refueling stations for transatlantic flights. Each Seadrome would have a length of approximately 335 m, a width of 100 m and a displacement of 50,000 tons [48]. Figure 1.1 shows the design of a Seadrome and a 1/32 scale model which was tested in Chesapeake Bay.

On October 22nd of 1929, the New York Times announced that construction of the first Seadrome would begin within sixty days. Seven days later, on what we now call Black Tuesday, the stock markets crashed and the Great Depression began. When the global economy recovered, the feasibility of transatlantic flights increased and the Seadrome became superfluous.

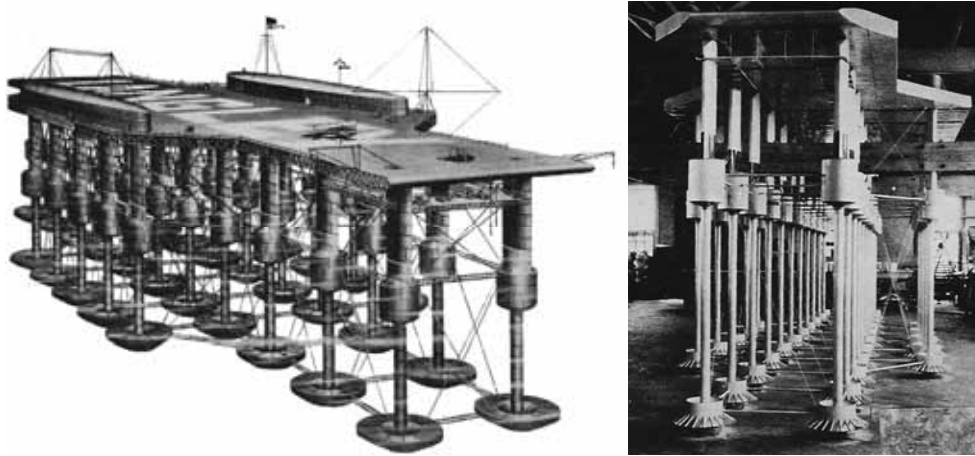


Figure 1.1: Seadrome designed by Edward R. Armstrong in 1929. The right figure shows the 1/32 scale model which was tested in Chesapeake Bay.

The first large floating runway was actually constructed by the US Navy Civil Engineering Corps in 1943. The structure measured 552 m x 83 m x 1.5 m and consisted of 10,920 pontoons as shown in figure 1.2 [63, 65, 77, 78].

During the same period a top-secret military project was executed with code name Habbakuk. The Allies suffered heavy merchant shipping losses from German U-boats during the war, particularly due to the limiting range of patrolling aircrafts in the mid-Atlantic. Geoffrey Pyke came up with a solution and submitted a memorandum to the Chief of Combined Operations in which he proposed that a natural or artificial iceberg should be hollowed out to shelter aircrafts. The structure would have a length of 600 m, a width of 90 m, a depth of 60 m, consisted of 280,000 blocks of ice and would be leveled to provide an adequate runway. The displacement amounted to 2 million tons and the walls would have a thickness of 12 m.

In December 1942, the project got the highest priority by Winston Churchill. Nevertheless the concept did not look very hopeful in February 1943 as mechanical strength tests pointed out that natural ice was unreliable and the resistance against explosives was unpredictable. The outlook suddenly transformed when Mark and Hohenstein discovered that the inclusion of a small percentage of wood pulp improves the mechanical properties of ice in a spectacular manner, see table 1.1 [52]. In view of the similarity to concrete and in honor of Geoffrey Pyke, the frozen wood pulp was given the name pykrete (Pyke's concrete).

Construction of a 1/50 scale model of the Habbakuk started in Patricia Lake in the Canadian Rocky Mountains in March 1943, see figure 1.3. By the fall, the Canadian National Research Council had shown that it was technically possible to build a ship of ice. However the costs of material and labor of the full-scale structure were excessive and the project was cancelled in January 1944.



Table 1.1: Mechanical properties of pykrete and ice (at -15 °C)

		Pykrete	Ice
Ultimate strength in compression	MPa	7.60	4.27
Ultimate strength in tension	MPa	4.80	1.14
Density	kg/m ³	980	910

Figure 1.2: SOCK flight deck and parking area (1943)

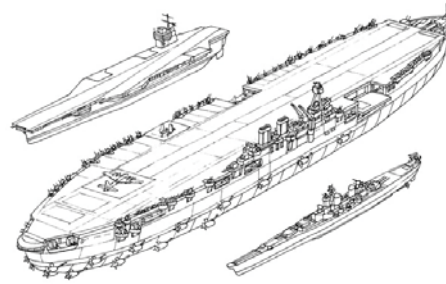


Figure 1.3: Construction of the scale model of the Habbakuk in ice (left) and the final full-scale design compared to an aircraft carrier and battle ship (right)

The Japanese picked up the idea of a floating airport as a national project in 1995 and called it Mega-Float. This project was driven by new needs and the fact that Japan has a shortage of land as less than 13% of the country is arable while its ocean space amounts to 4.5 million sq. km. [2, 76]. From these figures it becomes clear that the limited land resources, large population and extensive marine exclusive zone (EEZ) necessitated an aggressive and innovative pursuit of the utilization of the ocean space.

Basically, the Japanese Mega-Float project consisted of two phases. The first phase was a three year program to identify the wide range of associated problems. Seventeen leading Japanese shipbuilding companies established the Technological Research Association of Mega-Float (TRAM) to investigate the feasibility of a floating airport. Nine equally sized modules were

connected afloat and they together formed a model with a length of 300 m. The total budget of the first phase of the project amounted to \$ 86.2 million [62].

The first phase was continued with a second phase for which a budget of \$ 103.6 million was available. Five modules were built in different shipyards that, together with the modified model of the first phase, formed the final structure of the Mega-Float project. The structure had a length of 1 kilometer and was located behind an existing breakwater in Tokyo Bay near Yokosuka City. Figure 1.4 shows the assembly of the modules as well as the final structure. Real landing and take-off experiments were carried out with small airplanes during the second phase of the project, see figure 1.5. Finally, it was concluded that no significant differences between a land-based runway and the Mega-Float structure existed.

After completion of the project the Mega-Float structure was broken up in parts which were used for a wide range of different applications like car and fishing parks, floating piers and an information centre.

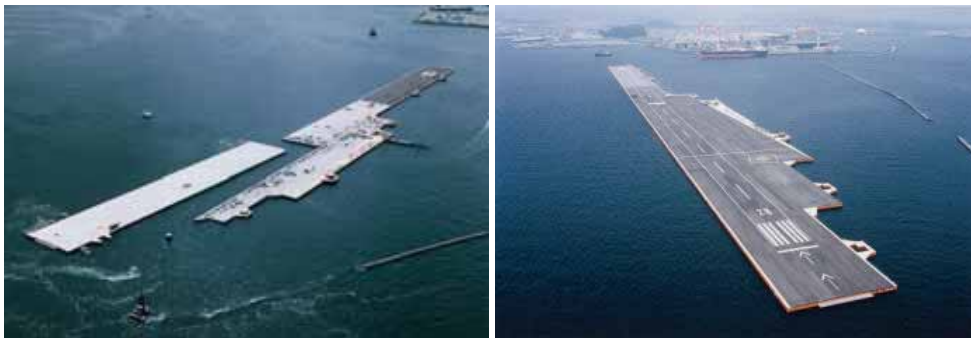


Figure 1.4: Phase 2 of the Mega-Float structure in Japan, assembly (left) and final model (right)



Figure 1.5: Take-off and landing of an airplane on the Mega-Float structure

Simultaneously with the Mega-Float project, the U.S. Office of Naval Research (ONR) started to investigate the feasibility of a Mobile Offshore Base (MOB). Such a base was intended for logistical support of U.S. military operations in areas where fixed bases were expected not to be available or to be inadequate.

The MOB is a self-propelled floating platform consisting of one or more serially connected modules which together form a runway of 1500 m. Several conceptual designs were made by different contractors and extensive studies were carried out to investigate the connections between the individual floating modules. Figure 1.6 shows four conceptual designs.

The ONR research program was finished in 2000 with the conclusion that it is possible to build a Very Large Floating Structure (VLFS) like the MOB with present knowledge and technology [40, 41]. One of the main deliverables of the project was the MOB Classification Guide published by ABS [1]. This document provides guidelines for the design of an MOB, but may also be valuable for other Mega-Float structures in the future.



Figure 1.6: Conceptual designs of the Mobile Offshore Base

With the exception of one monohull concept, both the Japanese and U.S. studies resulted in rather conventional solutions. A completely different approach is a structure that is supported by a large aircushion. The air underneath the structure distributes the wave loads equally over the bottom of the body. The main advantage of an aircushion supported structure is the reduction of the wave induced bending moments [57, 74]. Additionally, the wave induced motions, second order drift forces, and resistance of an aircushion supported structure may be reduced as well [26, 56]. For these reasons an aircushion supported structure can be a good alternative for a conventional Mega-Float structure.

For many years, much attention has been paid to the development of relatively small and fast waterborne sea transport based on aircushion technology, see for example [16, 17, 34, 47, 81]. A large number of these vessels are in service world-wide and much experience in aircushion technology has been gained as a result.

1.2 Aircushion support in the offshore industry

In addition, the use of aircushions to support large floating structures has been known for a long time in the offshore industry. In most of these cases the draft of bottom-founded structures was temporarily decreased by pumping compressed air underneath the structure to allow transportation from a shallow building dock to deeper water.

The Khazzan Dubai oil storage tanks installed in the Arabian Gulf in 1969 are probably the first offshore structures which were passively supported by air. Three subsea storage tanks with a storage capacity of 500,000 barrels were installed on the seabed with use of aircushion technology.

Figure 1.7 shows the construction of two storage tanks and the towing to the final location. In order to float the open bottom structures and to tow them from the construction yard to the final location 60 miles offshore, air was pumped underneath the structure and pressurized until it supported the weight of the tank. Once on location, the structure was submerged by venting the air under the structure. The sudden release of air reduced the pressure and caused a dynamic descent. Submergence continued by pumping water into the internal bottle [10, 12, 8]. The installation process is shown in figures 1.8 and 1.9.



Figure 1.7: Construction and towing of the Khazzan Dubai storage tanks

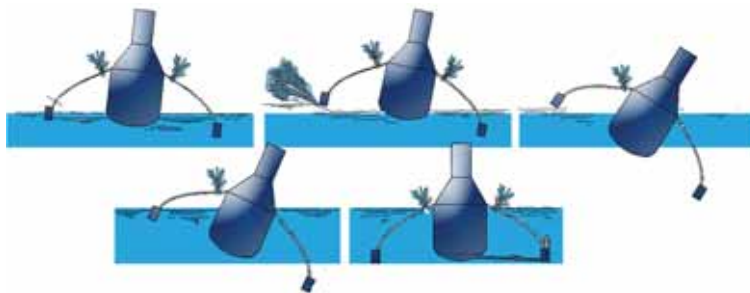


Figure 1.8: Installation process of the Khazzan Dubai storage tank



Figure 1.9: Installation of Khazzan Dubai storage tank No. 1

Another example of aircushion technology is the installation of the Maureen Gravity platform in 1983 [4]. In this case, compressed air was pumped underneath the construction to float the 42,600 t structure before it was towed from the dry dock to the final location in the North Sea.

Aircushions were also used to lift the 218,000 t bottom section of the Gullfaks C Condeep structure to a buoyant condition from the construction dock in 1987. During this operation, about 96% of the buoyancy was provided by aircushions. The use of air to improve the floatability of a structure was not new since it was already used on the first Condeep's in 1974. To some extent aircushions were used in all subsequent Condeep projects as described by Kure and Lindaas [37].

Chakrabarti [9] described how aircushions were used in launching a semi-submersible from the construction yard of Chicago Bridge & Iron in Pascagoula (USA) on the Gulf of Mexico. A unique launching procedure was developed as the launching dock had a much greater elevation than the existing water level adjacent to the dock. Open-bottom buoyancy cans (up to 10.7 m in diameter) were designed to support the structure on a cushion of compressed air during the launch operation and load out in the sheltered bay off the Gulf of Mexico. Before final towing started, the buoyancy cans were ballasted and submerged underneath the structure in deeper water in the bay.

In the 1970s the Seatek Slo-Rol system was introduced to reduce the wave-induced motions of jack-up platforms while floating. As a result of the application of this system, the transverse and longitudinal stability of the platform were reduced by bringing the natural roll and pitch frequencies outside the range of the wave frequencies. In addition, the angular motions in waves were reduced as well as the dynamic loads in the jack-up legs in the wet-tow mode.

Blood [7] presented a pneumatically stabilized platform (PSP) as a floating concept for a Mobile Offshore Base (MOB) in 1996. The final MOB report [41] of the science and technology program showed that the response of a PSP did not only depend on wave excitation but also on the mass of the water column, air pocket stiffness and air pressure distribution. In case of a PSP these characteristics can be tuned resulting in small dynamic responses in a particular sea state. In addition to the MOB program, Pinkster [57] described the dynamic behavior of a large Mobile Offshore Base supported by one aircushion and carried out model experiments at the Ship Hydromechanics Laboratory of Delft University of Technology [56, 57].

The behavior of an open-bottom semi-submersible supported by air was investigated by Xin-Yuan [79]. Model tests indicated that the structure was more stable and mooring forces were lower compared to a conventional semi-submersible.

1.3 The need for ocean space

While the 20th century may have been the century of land, the 21st century is expected to become the century of the ocean. According to UN forecasts [15], the global population is expected to grow from 6.8 billion today to 8.9 billion in 2050. This will have a large effect on metropolitan cities which are often located in the coastal zone. At the moment 60% of the global population lives in the coastal zone, i.e. 150 km from the sea or ocean [18]. Figure 1.10 shows the UN forecast of the global population density [85]. Especially the population density of India and the city-state Singapore show a sharp increase. In

case of Singapore this is due to a limited amount of arable land. Besides, the lack of land and sand make traditional landfill methods difficult, this problem and a possible future solution will be described in more detail in chapter 4.

A large floating structure may be an ideal solution for coastal mega-cities like Singapore. Such a structure can be used for any facilities and purposes similar to those on land. In addition, mega-floaters are often less environmentally destructive than traditional land reclamation projects. They are indifferent to earthquakes and can be constructed at relatively low cost in a short period of time independent of ocean depth and ground conditions. Furthermore, the existing facilities can be easily expanded while they are functional and the space inside the structure offers prospects for various activities and different use.

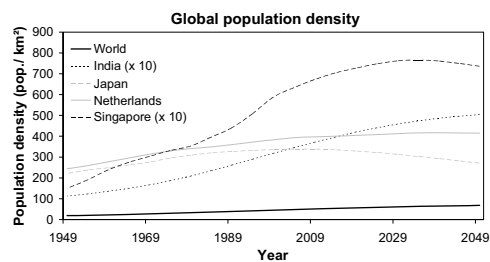


Figure 1.10: United Nations estimation and prediction of the global population density

1.4 Objective of the research

Examples from the past have indicated that aircushions can modify the behavior of structures in waves considerably and justify a more detailed investigation into aircushion technology applied to mega-floaters. The objective of the research is to *predict the behavior of very large floating aircushion supported structures in waves*. This includes an assessment of the technical feasibility of aircushion supported structures and a comparison with a conventional box-shaped structure. The hydroelastic behavior has to be investigated as well since mega-floaters may not show the same behavior as rigid bodies.

Much of the effort will be put into development of numerical methods in order to evaluate design concepts by means of simulations. The results from model tests performed by Tabeta [64], Pinkster et. al. [54, 55, 57] and Remy et. al. [58] will serve to validate the numerical method. As such, the new numerical method may be used in future designs of large aircushion supported structures.

1.5 Outline of the thesis

This thesis is subdivided into three main chapters. Chapter 2 describes a method to compute the behavior of rigid aircushion supported structures. Model experiments are described which served to validate the results of an oscillating structure in still water, a captive structure in waves and a free-floating structure without forward speed in waves. In addition a comparison will be made between an aircushion supported structure and a conventional barge with respect to dynamic behavior, drift forces, wave field and structural loads.

Chapter 3 describes a method to compute the hydro-elastic behavior of flexible aircushion supported structures. First the results of a conventional flexible barge will be discussed which are validated by model experiments. Next, the hydro-elastic behavior and structural loads of flexible aircushion supported structures will be discussed.

Chapter 4 describes the step from the academic world to a practical application and discusses the technical feasibility of an aircushion supported mega-floater. For this purpose an assessment will be made of different locations in order to find the most likely location where the first mega-floater will be operated. Next, the environmental conditions of this location are used to assess the feasibility of different types of mega-float structures.

The main conclusions and thoughts for future research are summarized in chapter 5.

Chapter 2

Rigid aircushion supported structures

2.1 Introduction

For many years much attention has been paid to the development of fast waterborne sea transport based on aircushion technology as applied to Surface Effect Ships (SES) and hovercrafts. Figure 2.2 shows an example of a hovercraft at high speed. Different numerical methods to compute the behavior of high-speed aircushion crafts are described by Kaplan et. al. [34], Nakos et. al. [47] and Moulijn [46].

On the other hand, little research has been performed on free-floating aircushion supported structures without forward speed in waves as shown in figure 2.1. There are some distinct differences between fast aircushion crafts and the free-floating structures which will be discussed in this thesis.

The most obvious difference is the difference in forward speed. Furthermore, the vertical walls underneath the free-floating structures extend sufficiently far below the mean water line to prevent air from escaping underneath the structure. The structures considered in this thesis are passively supported by aircushions.

Contrary to these structures, hovercrafts and Surface Effect Ships are actively supported by air, i.e. a continuous flow of air is required to maintain the aircushion pressure underneath the structure. For this reason large fans have to be installed on the deck of such structures.

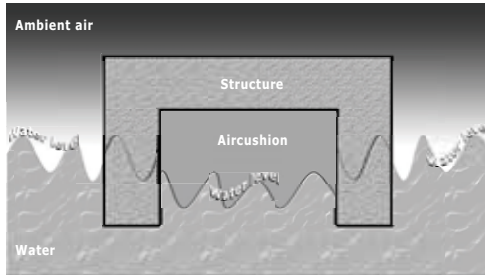


Figure 2.1: Cross-section of an aircushion supported structure



Figure 2.2: Hovercraft at high speed

In recent years, Pinkster et. al. [54, 55, 57] studied the behavior of large free-floating aircushion supported structures in waves at Delft University of Technology. Their results were validated by means of model tests which were performed by Tabeta [64].

Malenica and Zalar [42] solved the linear hydrodynamic problem of aircushion supported vessels. However, their approach corresponds to a great extent to the one presented by Pinkster [53]. In addition, Gueret and Hermans [20, 21] extended the analytical work of Malenica and Zalar for aircushion supported structures in regular waves at zero speed.

On the other hand, Lee and Newman [39, 50] performed computations which provided a good description of acoustic disturbances in the aircushion. Particular attention was paid to the resonant frequencies of the air inside the cushion. These resonances are analogous to the cobblestone effect suffered by high-speed aircushion vessels as demonstrated by Steen [61] and Ulstein et. al. [71].

The wave induced motions of aircushion supported offshore structures in shallow water were investigated by means of an analytical approach and model tests performed by Thiagarajan et. al. [66, 67, 68]. In addition it was shown by Chenu [11] that aircushions reduce the stability of the structure and changes the natural frequency and added mass.

Ikoma et. al. [29, 30] investigated the dynamic behavior of rigid aircushion supported structures at the College of Science and Technology at Nihon University. In recent years they extended their research to the field of hydroelasticity [24, 25, 27, 28]. This subject will be discussed in chapter 3.

The present chapter describes a linear potential method to compute the dynamic behavior of large aircushion supported structures. The method is based on Pinkster's approach [53] with small changes in the numerical model of the cushion and the coupling with the rigid body. The results of the numerical method will be compared with model tests and the results presented by Pinkster [55].

Paragraph 2.7.1 will show the effect of a pressure change within the aircushion on the dynamic behavior of the structure. Next paragraphs 2.7.2 and 2.7.3 describe the behavior of large

aircushion supported structures subjected to waves from different headings. The motions will be discussed as well as the drift forces and structural loads. In order to show the effect of the aircushions on the behavior of the full-scale structure, the results will be compared with those of a conventional floating barge.

2.2 Definitions

A right handed axis system (x, y, z) will be used in the analysis of the dynamic behavior of the floating structure. The displacements at the centre of gravity (COG) of the floating body are defined in the six degrees of freedom surge (x), sway (y), heave (z), roll (ϕ), pitch (θ) and yaw (ψ). The first three degrees are translations in the x -, y - and z -direction respectively. Roll, pitch and yaw are the rotations around these axes as illustrated in figure 2.3.

A floating body may be subjected to waves from different headings. In this case head waves are associated with a wave heading of 180° and stern waves correspond to a wave heading of 0° . All other wave directions and their headings are shown in figure 2.4.

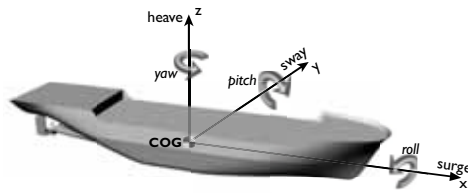


Figure 2.3: six degrees of motion

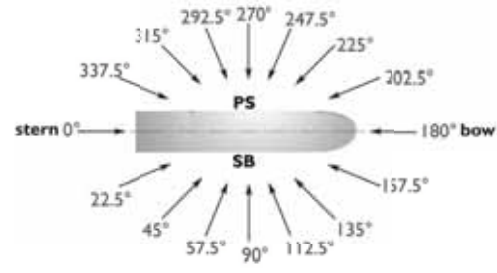


Figure 2.4: Wave directions

2.3 Aircushion theory

This section describes the theory of aircushion supported structures at zero speed in waves. The structure is assumed to be rigid and supported by one or more aircushions that may or may not be interconnected. The floater is passively supported by the cushions, which implies that no fans are needed to maintain the air pressure within the cushion. The aircushions are bounded by the rigid part of the structure which extends sufficiently far below the mean water level in order to ensure that no air leakage will occur from the cushion. Furthermore, it is assumed that air from the cushion does not dissolve in the water underneath.

2.3.1 Theory of air columns

The volume change in the aircushion underneath the structure is reversible and describes an adiabatic process of the form:

$$P V^{\kappa} = \text{constant} \quad (2.1)$$

The pressure within the aircushion changes due to wave motions and oscillations of the structure. With use of the previous equation, the resulting pressure inside the aircushion may be expressed as:

$$P(t) = P_0 \left(\frac{V_0}{V(t)} \right)^{\kappa} \quad (2.2)$$

in which:

- V_0 = initial volume of the aircushion
- $V(t)$ = volume of the aircushion ($V_0 + \Delta V(t)$) at time instant t
- P_0 = initial pressure inside the aircushion ($P_a + P_c$)
- $P(t)$ = pressure inside the aircushion at time instant t

P_a is the atmospheric pressure and P_c is the pressure required to support the structure. In addition, ΔV is the volume variation of the aircushion and κ is the gas law index, which is the ratio between the specific heat capacity at constant pressure (C_p) and constant volume (C_v):

$$\kappa = \frac{C_p}{C_v} \quad (2.3)$$

A gas law index of 1.4 is generally used for air. The non-linear expression of the pressure in equation (2.2) may be simplified to a linear form by making use of a Taylor expansion of $(V_0 + \Delta V)^{-\kappa}$ around $\Delta V = 0$. In this case it is assumed that the volume variations are small compared to the total volume of the aircushion. This simplification results in the following linear expression:

$$P(t) = P_0 - \kappa P_0 \frac{\Delta V(t)}{V_0} \quad (2.4)$$

The pressure variations within the aircushion result in pressure changes on the structure. These pressure changes may be rewritten as restoring coefficients which can be used in a general equation of motion.

If the structure is supported by N_{AC} aircushions, then the total restoring coefficient can be derived from the previous equation by making use of $V_0 = h_c A_c$, in which h_c is the initial cushion height and A_c the cushion area:

$$C_{33,c} = \sum_{i=1}^{N_{AC}} \kappa P_0 \frac{A_{c,i}}{h_{c,i}} \quad (2.5)$$

The spring coefficient $C_{33,c}$ in this equation is related to the aircushions only, i.e. the restoring term of the buoyant part of the structure is not taken into account.

2.3.2 Theory of aircushion supported structures

Henceforward the buoyant part of the floating body will be taken into account. When the structure moves slowly in vertical direction, the free water surface inside the aircushions will move in the same direction. However, due to the compressibility of air, the displacement of the free water surface within the cushions will be smaller than the vertical motion of the structure. For this reason the compressibility of air should be added to equation (2.5) in order to obtain the restoring coefficient of the total structure including the aircushions.

The compressibility of the aircushion mainly depends on the height of the air chamber underneath the structure. If this parameter is taken into account, the polytropic process as described in equation (2.1) may be written as:

$$\left(\frac{P(t)}{P_0} \right)^{1/\kappa} \cdot h_c(t) = \text{constant} \quad (2.6)$$

On the other hand the air pressure within the cushion may also be expressed as:

$$P(t) = P_a + \rho g T_c(t) \quad (2.7)$$

with $T_c(t)$ being the vertical distance between mean sea level and the free surface within the aircushion. Initially, when the structure is fully supported by the rigid skirts, the air pressure P_0 within the cushion is equal to the atmospheric pressure P_a .

If the structure moves ΔT downward and the compressibility of air is written as a small non-dimensional parameter ε , then the aircushion will be compressed by $\varepsilon \Delta T$. This is graphically shown in figure 2.5.

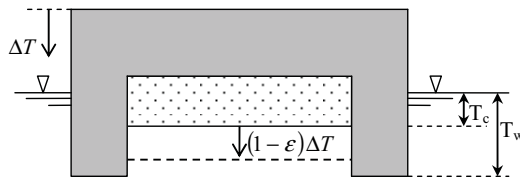


Figure 2.5: Vertical motion of an aircushion supported structure and compression of the cushion

Substitution of equation (2.7) in (2.6) and making use of the compressibility of air provides:

$$\left(1 + \frac{\rho g}{P_a} T_c(t)\right)^{1/\kappa} \cdot h_c(t) = \left(1 + \frac{\rho g}{P_a} \{T_c(t) + (1 - \varepsilon) \Delta T\}\right)^{1/\kappa} \cdot (h_c(t) - \varepsilon \Delta T) \quad (2.8)$$

If the right hand side of this equation is rewritten by a Taylor expansion around $\Delta T = 0$, the following compressibility factor of the aircushion will be obtained:

$$\varepsilon = \frac{\rho g h_c}{\kappa P(t) + \rho g h_c} \quad (2.9)$$

This procedure is described in appendix A.

2.3.3 Restoring coefficients and stability

Displacing the structure in the heave mode will change the volume of the aircushion. Consequently the volume variation results in a pressure change on the structure. The pressure change may be rewritten as a restoring coefficient of the aircushion supported structure and the heave restoring coefficient may be expressed as:

$$C_{33} = (A_w - \varepsilon A_c) \rho g \quad (2.10)$$

where A_w is the total waterline area of the structure (including the aircushions). Substitution of equation (2.9) results in:

$$C_{33} = \rho g (A_w - A_c) + C_{33,c} - \frac{C_{33,c}^2}{C_{33,c} + \rho g A_c} \quad (2.11)$$

The first term represents the hydrostatic restoring force of the buoyant part of the structure, the second and third terms are contributions of the aircushions as described in appendix A.

The centre of buoyancy (B) of a conventional floating body will shift when the structure is subjected to a small roll angle ϕ as shown in figure 2.6. A shift of the centre of buoyancy results in an increase of the restoring moment. It is common practice in ship building applications to define the stability of a floating body by the following expression:

$$GM = KB + BM - KG \quad (2.12)$$

$$B M = \frac{B B_{\varphi}}{\tan \varphi} \quad (2.13)$$
[illegible]
$$BB_{\phi,s} = 2 \frac{\int_0^L \int_{y_{c,max}}^{b/2} y_s^2 \tan \phi dy_s dx_s}{\nabla} \quad (2.14)$$
$$BB_{\phi,c} = \frac{\sum_{N_{AC}} \left\{ \int_0^L \int_{y_c, \min}^{y_c, \max} z_c y_c (1 - \varepsilon) dy_c dx_c \right\}}{\nabla} \quad (2.15)$$

in which:

$$\begin{aligned} \overline{z_c} &= \text{mean change of the cushion height, for rectangular shaped structures:} \\ \overline{z_c} &= (y_{c,max} + y_{c,min}) / 2 \tan \phi \\ \overline{y_c} &= \text{centre of the cushion in y-direction} \end{aligned}$$

Substitution of equations (2.14) and (2.15) into (2.13) provides the following expression for rectangular shaped aircushions and small roll angles:

$$BM_T = \frac{\int \int_{A_s} y_s^2 dy_s dx_s + \sum_{N_{AC}} \left\{ (1 - \varepsilon) \overline{y_c}^2 \int \int_{A_c} dy_c dx_c \right\}}{\nabla} \quad (2.16)$$

In order to compute the transverse stability (GM_T), the horizontal components of the air pressure on the skirts of the structure should be taken into account as well. Figure 2.8 shows the air pressure on the vertical walls of a structure supported by two aircushions which is subjected to a heeling angle ϕ . The pressure within each aircushion is constant such that $P_1 = P_{1,H1} = P_{1,H2} = P_{1,H3}$ and $P_2 = P_{2,H1} = P_{2,H2} = P_{2,H3}$.

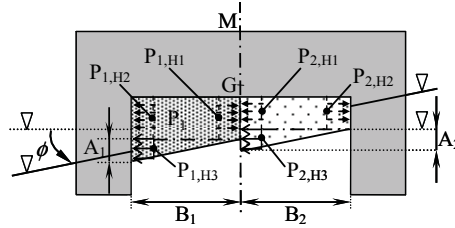


Figure 2.8: Air pressure on the vertical walls of a structure supported by two aircushions.

The horizontal components of the aircushion pressure on the vertical skirts result in an additional heeling moment which may be expressed as:

$$X_{4c} = \sum_{i=1}^{N_{AC}} B_i \tan \phi \cdot L_i \cdot P_{i,H3} (\overline{OG} + T_{c,i} - \varepsilon \overline{z_{c,i}}) \quad (2.17)$$

in which:

$$\begin{aligned} B_i &= \text{width of cushion } i \\ L_i &= \text{length of cushion } i \\ P_{i,H3} &= \text{excess air pressure within cushion } i \quad (P(t) - P_a) \\ T_{c,i} &= \text{initial draft of cushion } i \\ \varepsilon \overline{z_{c,i}} &= \text{additional mean draft of cushion } i \text{ due to heeling angle } \phi \end{aligned}$$

For small heeling angles the previous expression may be simplified to:

$$X_{4c} = \rho g \sum_{i=1}^{N_c} A_i T_{c,i} (\overline{OG} + T_{c,i}) \phi \quad (2.18)$$

with $A_i = L_i B_i$ being the area of cushion i . Combining equations (2.16) and (2.18) and substitution in (2.12) results in a general expression of the GM-value for structures with rectangular aircushions:

$$\overline{GM}_T = \frac{\int \int y^2 dy_s dx_s + \sum_{N_{AC}} \left\{ (1 - \varepsilon) \overline{y_c}^2 A_c - A_c T_c (\overline{OG} + T_c) \right\}}{\nabla} - \overline{BG} \quad (2.19)$$

in which A_c is the area of the aircushion. Accordingly the rotational restoring coefficients may be expressed as:

$$C_{44} = \rho g \left(\iint_{A_s} y^2 ds_s + \sum_{N_{AC}} \left\{ (1 - \varepsilon) \overline{y_c}^2 A_c - A_c T_c (\overline{OG} + T_c) \right\} - \overline{BG} \nabla \right) \quad (2.20)$$

$$C_{55} = \rho g \left(\iint_{A_s} x^2 ds_s + \sum_{N_{AC}} \left\{ (1 - \varepsilon) \overline{x_c}^2 A_c - A_c T_c (\overline{OG} + T_c) \right\} - \overline{BG} \nabla \right) \quad (2.21)$$

and the non-zero coupled restoring coefficients are:

$$C_{34} = C_{43} = C_{33} y_{c,ef} \quad (2.22)$$

$$C_{35} = C_{53} = C_{33} x_{c,ef} \quad (2.23)$$

$$C_{45} = C_{54} = C_{33} x_{c,ef} y_{c,ef} \quad (2.24)$$

in which x_{cf} and y_{cf} are coordinates of the centre of the water plane relative to the origin of the axis system. If the structure and aircushions are rectangular shaped x_{cf} and y_{cf} may be written as:

$$x_{cf} = \left(\frac{x_{max} + x_{min}}{2} \right), \quad y_{cf} = \left(\frac{y_{max} + y_{min}}{2} \right) \quad (2.25)$$

Based on the described restoring coefficients, the restoring matrix of the rigid-body may be expressed in the following general form:

$$C_R = \begin{bmatrix} 0 & 0 & 0 & 0 & 0 & 0 \\ 0 & 0 & 0 & 0 & 0 & 0 \\ 0 & 0 & C_{33} & C_{34} & C_{35} & 0 \\ 0 & 0 & C_{43} & C_{44} & C_{45} & 0 \\ 0 & 0 & C_{53} & C_{54} & C_{55} & 0 \\ 0 & 0 & 0 & 0 & 0 & 0 \end{bmatrix} \quad (2.26)$$

2.3.4 Resonance frequencies of the aircushion

The vertical resonance frequency of the aircushion can be computed by making use of equation (2.5). If the mass of the structure is equal to m , the undamped natural frequency is:

$$\omega = \sqrt{\frac{C_{33,c}}{m}} \quad (2.27)$$

In addition, the waves may cause a resonance effect in the aircushion which is known as the cobblestone effect. S. Steen [61] and O.M. Faltinsen [17] described this effect in detail and showed that the spatially varying air pressures within the cushion have their extreme values at the end of the cushion. These extremes at both ends of the cushion are out of phase and create a pitch moment resulting in a pitch acceleration. As a consequence additional vertical accelerations are present which are well known problems for fast aircushion supported structures like surface effect ships. These vertical accelerations are largest at the far ends of the structure, i.e. at the bow and stern.

Although the structures discussed in this thesis have no forward speed, the cobblestone effect may become dominant if the structure is supported by a large aircushion. In this case the first cobblestone frequency occurs if the length of the acoustic wave in the aircushion is twice the length of the cushion:

$$\omega = \frac{\pi c}{L} \quad (2.28)$$

where c is the speed of sound, i.e. 343 m/s in dry air of 20 °C. For periods of 6 – 9 seconds the acoustic wavelength is 2000 – 3000 m, and the first half-wave resonance will occur in an aircushion of length 1000 – 1500 m.

2.4 Fluid dynamics

The aircushions and the rigid part of the structure are partly bounded by water. The interactions between the aircushions, the structure and the surrounding water may be described by a linear three-dimensional potential theory. In this case the fluid motions in regular waves are described by a potential Φ in point X with earth-bound coordinates X_1, X_2, X_3 :

$$\Phi(X_1, X_2, X_3, t) = \phi(X_1, X_2, X_3) e^{-i\omega t} \quad (2.29)$$

in which ϕ is the spatial part of the total velocity potential, t is the time and ω the circular wave frequency. The velocity potential Φ satisfies the Laplace equation:

$$\nabla^2 \Phi = \frac{\partial^2 \Phi}{\partial x^2} + \frac{\partial^2 \Phi}{\partial y^2} + \frac{\partial^2 \Phi}{\partial z^2} = 0 \quad (2.30)$$

Physically this means that the flow is incompressible and irrotational. Besides, the potential ϕ satisfies the linearized boundary conditions on the free surface outside the body, the boundary condition at the sea-floor and the radiation condition. The boundary condition at the sea-floor, which is assumed to be flat, states that the vertical component of the water particle velocity is zero at the sea bottom:

$$\frac{\partial \Phi}{\partial z} = 0 \quad \text{for: } z = -h \quad (2.31)$$

The free surface boundary condition outside the body equates the vertical component of the water particle velocity to the rate of change of the free surface profile with time. In linear theory, the following condition is satisfied at the still water level:

$$\frac{\partial^2 \Phi}{\partial t^2} + g \frac{\partial \Phi}{\partial z} = 0 \quad \text{for: } z = 0 \quad (2.32)$$

The radiation condition ensures that the sources radiate waves instead of absorbing them and the potentials, due to the body motions ($j = 1, 2, \dots, 6$) and diffraction ($j = 7$), are outgoing at an infinitely large distance r from the oscillating body:

$$\lim_{r \rightarrow \infty} \sqrt{r} \left(\frac{\partial \Phi_j}{\partial r} - i\nu \Phi_j \right) = 0 \quad (2.33)$$

where ν is the dispersion relation which describes the relation between the wave length λ and the wave frequency:

$$\nu = \kappa \tanh \kappa h \quad (2.34)$$

in which $\nu = \omega^2 / g$, h is the water depth and κ is the wave number being equal to $\kappa = 2\pi / \lambda$.

In addition, a no-leak condition has to be satisfied on the rigid part of the body surface while the potential at the free surfaces of the aircushions must satisfy the no-leak condition at the unknown moving free surface. These requirements are not automatically satisfied by the incoming wave potential, so additional potentials are introduced which represent pulsating source distributions over the mean wetted surface of the rigid part of the structure and the mean free surface of the cushions.

The complex potential ϕ follows from the superposition of the undisturbed wave potential ϕ_0 , the wave diffraction potential ϕ_d , the radiation potentials associated with the 6 degrees of freedom of the rigid structure ϕ_j , and the potentials associated with the vertical motions of the free surface within each cushion, ϕ_c . The total potential may be written as:

$$\phi = -i\omega \left\{ (\phi_0 + \phi_d) \zeta_0 + \sum_{j=1}^6 \phi_j x_j + \sum_{c=1}^{N_{AC}} \frac{1}{S_C} \iint_{S_C} \phi_c \zeta_c dS_C \right\} \quad (2.35)$$

in which:

- ζ_0 = amplitude of the undisturbed incoming wave
- x_j = rigid body motion in the j -mode
- ζ_c = vertical motion of the free surface in cushion c
- N_{AC} = total number of independent, non-connected cushions
- S_C = free surface area of cushion c
- ϕ_c = potentials associated with the vertical motions of cushion c

The undisturbed wave potential ϕ_0 and the diffraction potential ϕ_d together describe the flow around the captive structure under the assumption that the free surface within each air cushion is rigid and non-moving. The potentials ϕ_j are associated with the flow around the structure oscillating in still water under the assumption that the free surface within each air cushion is rigid and fixed. The potentials $\phi_{c,i}$ are associated with the flow around the captive structure as induced by the vertical motions ζ_c of the free surface within each cushion.

The velocity potential associated with the undisturbed long-crested regular wave in water of constant depth h is given by:

$$\phi_0 = \frac{g}{\omega^2} \frac{\cosh k(X_3 + h)}{\cosh kh} e^{ik(X_1 \cos \alpha + X_2 \sin \alpha)} \quad (2.36)$$

The fluid pressure follows from Bernoulli's law:

$$p(X_1, X_2, X_3, t) = -\rho \frac{\partial \Phi}{\partial t} = p(X_1, X_2, X_3) e^{-i\omega t} \quad (2.37)$$

With use of equations (2.29) and (2.35), the previous expression of the fluid pressure may be written as:

$$p(X_1, X_2, X_3, t) = p = \rho \omega^2 \left\{ (\phi_0 + \phi_d) \zeta_0 + \sum_{j=1}^6 \phi_j x_j + \sum_{c=1}^{N_{AC}} \frac{1}{S_C} \iint_{S_C} \phi_c \zeta_c dS_C \right\} \quad (2.38)$$

2.5 Numerical approach

When considering a conventional rigid body, the motions of the structure are determined by solving the equation of motion for six degrees of freedom and taking into account wave forces, added mass, damping and restoring terms. It is customary to determine the wave forces on the captive structure based on the undisturbed wave potential ϕ_0 and the solution of the diffraction potential ϕ_d . Added mass and damping coefficients are based on the motion potentials ϕ_j obtained by oscillating the structure in the six modes of motion in still water.

If a floating body is partially supported by one or more aircushions, a different approach should be followed in order to determine the motions of the structure, pressure within the cushions, added mass and damping coefficients and other quantities such as structural loads and drift forces.

In the present approach the rigid body of the aircushion supported structures is modeled in the usual way by means of panels representing pulsating sources distributed over the mean wetted surface of the floater. The free water surface underneath the structure is modeled by panels representing oscillating source distributions laying in the mean free surface of each cushion. The mean surface level of individual cushions may be substantially different from other cushions and the mean water level outside the structure as shown in figure 2.9.

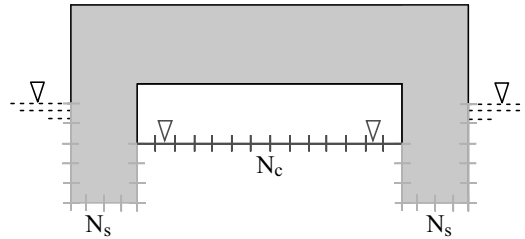


Figure 2.9: Cushion elements (N_c) and structural elements (N_s) of the body.

All panels of the free surface within an aircushion are assumed to represent a body without material mass, but having added mass, damping, hydrostatic restoring and aerostatic restoring characteristics. Cushion c contains N_c free surface panels. Each panel has one degree of freedom being the vertical motion of panel n within cushion c . The total number of degrees of freedom amounts to:

$$D.O.F. = 6 + \sum_{c=1}^{N_{AC}} N_c \quad (2.39)$$

The number 6 in this expression represents the six degrees of freedom of the rigid part of the structure.

In the first step of the numerical approach, the restoring coefficients of the rigid body include the hydrostatic restoring coefficients as well as the aerostatic restoring coefficients. However, in this case the free surface of the aircushion is fixed:

$$C_{33} = \rho g A_w + \sum_{i=1}^{N_c} C_{33,c} \quad (2.40)$$

$$C_{34} = \rho g A_w y_{cf} + \sum_{i=1}^{N_c} C_{33,c} \overline{y_c} \quad (2.41)$$

$$C_{35} = -\rho g A_w x_{cf} - \sum_{i=1}^{N_c} C_{33,c} \overline{x_c} \quad (2.42)$$

$$C_{44} = \rho g (I_t + A_w y_{cf}^2 - BG \nabla) + \sum_{i=1}^{N_c} C_{33,c} \overline{y_c}^2 \quad (2.43)$$

$$C_{45} = -\rho g A_w x_{cf} y_{cf} - \sum_{i=1}^{N_c} C_{33,c} \overline{x_c} \overline{y_c} \quad (2.44)$$

$$C_{55} = \rho g (I_t + A_w x_{cf}^2 - BG \nabla) + \sum_{i=1}^{N_c} C_{33,c} \overline{x_c}^2 \quad (2.45)$$

$$C_{rj} = C_{jr}, \quad j = 3, 4, 5; r = 3, 4, 5 \quad (2.46)$$

The restoring coefficients of the cushion elements are considered if $r = 7, 8, \dots, 6 + N_c$ and $j = 7, 8, \dots, 6 + N_c$. In this case the structure remains fixed and the restoring terms associated with the cushion elements are:

$$C_C = \begin{cases} C_{rj} = \delta_{rj} \kappa P_0 \frac{A_r A_j}{V_c} + \delta_{rj} \rho g A_r & \text{for: } r = j \\ C_{rj} = \delta_{rj} \kappa P_0 \frac{A_r A_j}{V_c} & \text{for: } r \neq j \end{cases} \quad (2.47)$$

in which P_0 is the initial air pressure, V_c is the aircushion volume and A_r is the area of cushion element r . δ_{rj} is the Kronecker delta function, defined by:

$$\delta_{rj} = \begin{cases} 1 & \text{if } r \text{ and } j \text{ are part of the same cushion} \\ 0 & \text{if } r \text{ and } j \text{ are not part of the same cushion} \end{cases}$$

The coupling coefficients between the rigid structure and the cushion elements (C_{RC}, C_{CR}) may be expressed as:

$$C_{rj} = 0, \quad r = 1, 2, 6; j = m + 1, m + 2, \dots, m + N_c \quad (2.48)$$

$$C_{3j} = -\kappa P_0 \frac{A_c A_j}{V_c}, \quad j = m + 1, m + 2, \dots, m + N_c \quad (2.49)$$

$$C_{4j} = -\kappa P_0 \frac{A_c A_j}{V_c} (y - y_G), \quad j = m + 1, m + 2, \dots, m + N_c \quad (2.50)$$

$$C_{5j} = \kappa P_0 \frac{A_c A_j}{V_c} (x - x_G), \quad j = m + 1, m + 2, \dots, m + N_c \quad (2.51)$$

$$C_{rj} = C_{jr}, \quad j = 1, 2, \dots, 6; r = m + 1, m + 2, \dots, m + N_c \quad (2.52)$$

in which A_c is the total area of all cushion elements in cushion c .

It should be noted that the air pressure on the skirts, as described by equation (2.18), is not taken into account in the numerical approach. The contribution of the horizontal forces on the restoring moment is relatively small compared to the contribution of the air pressure on the bottom of the structure.

The wave force X_n , added mass a_{nj} and damping coupling coefficients b_{nj} are determined in the same way as is customary for a multi-body system. The mean underwater part of the structure is discretized into a number of panels representing pulsating sources, this is also the case with each free surface panel within an aircushion.

The contribution of the total potential due to the discrete pulsating source distributions over the structure and the free surface of the aircushions may be expressed as:

$$\phi_j(\bar{X}) = \frac{1}{4\pi} \sum_{s=1}^{N_t} \sigma_{sj}(\bar{A}) G(\bar{X}, \bar{A}) \Delta S_s \quad (2.53)$$

in which:

$$\begin{aligned} N_t &= \text{total number of panels used to describe the wet structure and free surfaces} \\ &\quad \text{of all cushions} \\ \bar{X} &= X_1, X_2, X_3 = \text{a field point} \\ \bar{A} &= A_1, A_2, A_3 = \text{location of a source} \end{aligned}$$

$G(\bar{X}, \bar{A})$	=	Green's function of a source in \bar{A} relative to a field point \bar{X}
ΔS_s	=	surface element of the body or the mean free surfaces in the aircushions
σ_{sj}	=	strength of a source on surface element s due to motion mode j
$\phi_j(\bar{X})$	=	potential in point \bar{X} due to the j -mode of motion

The unknown source strengths σ_{sj} are determined based on boundary conditions placed on the normal velocity of the fluid at the centers of the panels:

$$-\frac{1}{2}\sigma_{mj}(\bar{X}) + \frac{1}{4\pi} \sum_{s=1}^{N_c} \sigma_{sj}(\bar{A}) \frac{\partial}{\partial n} G(\bar{X}, \bar{A}) \Delta S_s = \frac{\partial \phi_j}{\partial n_m}, \quad m=1, 2, \dots, N_t \quad (2.54)$$

The right hand side of the above equation depends on the case to be solved. If the source strengths for determination of the diffraction potential are required, the normal velocity vector becomes:

$$n_{m(D.O.F., +1)} = \frac{\partial \phi_d}{\partial n_m} = -\frac{\partial \phi_0}{\partial n_m} \quad (2.55)$$

In this case the wave loads due to the incoming waves and diffraction effects are defined as being the loads on the structure and the individual free surface panels in the cushions, all being fixed. The initial added mass and damping coupling coefficients are found by applying normal velocity requirements for the six rigid body motions ($j=1,6$) of the structure:

$$\frac{\partial \phi_j}{\partial n_m} = n_{mj} \quad j=1, 2, \dots, 6 \quad (2.56)$$

in which the panel index m covers only the panels on the structure. Furthermore, n_{mj} are the general directional cosines for the panels on the structure given by:

$$\begin{aligned} n_{m1} &= \cos(n_m, x_1) \\ n_{m2} &= \cos(n_m, x_2) \\ n_{m3} &= \cos(n_m, x_3) \\ n_{m4} &= x_{m2} n_{m3} - x_{m3} n_{m2} \\ n_{m5} &= x_{m3} n_{m1} - x_{m1} n_{m3} \\ n_{m6} &= x_{m1} n_{m2} - x_{m2} n_{m1} \end{aligned} \quad (2.57)$$

in which x_{mi} are the coordinates of the centre of a panel relative to the body axes.

If the wave forces on the rigid structure are considered, the normal velocity components on all cushion panels are equal to zero. For the determination of the added mass and damping coupling

arising from the normal motions of individual cushion panels, the normal velocity boundary condition is zero except for one cushion panel at a time for which the following value holds:

$$\frac{\partial \phi_m}{\partial n_m} = -1 \quad (2.58)$$

where the value -1 follows from the fact that the free surface normal is pointing in the negative X_3 -direction. From the solutions of the source strengths for all these cases the wave force vector X_n and the added mass a_{nj} and damping coupling coefficients b_{nj} may be obtained. The wave force follows from:

$$X_n = -\rho \omega^2 \sum_{k=1}^{N_n} (\phi_{o,k} + \phi_{d,k}) n_{n,k} \Delta S_{n,k} \quad (2.59)$$

in which:

- $\phi_{d,k}$ = diffraction potential at k^{th} panel obtained by equation (2.53)
- X_n = wave force in the mode n , with $n = 1, 6$ for the structure
- N_n = number of panels involved in the force in mode n
 - $N_n = 1$ if the force on a cushion panel is to be considered
 - $N_n = N_s$ if the force on the structure is to be considered
- $n_{n,k}$ = generalized directional cosine of panel k related to mode n
- $\Delta S_{n,k}$ = area of panel k related to the force in mode n

N_s is equal to the number of panels that describe the wet surface of the structure.

The added mass and damping coefficients are:

$$\begin{aligned} A_{nj} &= -\mathbf{Re} \left[\rho \sum_{k=1}^{N_n} \phi_{j,k} n_{n,k} \Delta S_{n,k} \right] \\ B_{nj} &= -\mathbf{Im} \left[\rho \omega \sum_{k=1}^{N_n} \phi_{j,k} n_{n,k} \Delta S_{n,k} \right] \end{aligned} \quad (2.60)$$

in which $\phi_{j,k}$ is the motion potential value on panel k obtained from equation (2.53).

The restoring coefficients in general consist of two contributions; an aerostatic spring term and a hydrostatic spring term. The hydrostatic restoring term is equal to the product of the waterline area, specific mass of the water and acceleration of gravity. The aerostatic restoring terms are related to the change in air pressure within an aircushion due to, for instance, unit vertical displacement of a free surface panel. The vertical displacement of a cushion panel is the result of the forces on all panels belonging to the same cushion and the forces on the rigid structure. The

coupling of the restoring terms C_{nj} between the cushion panels of the same cushion can be derived from equation (2.5):

$$\begin{cases} C_{nj} = -\kappa P_0 \frac{A_{c,n} A_{c,j}}{V_0} & \text{for: } n \neq j \\ C_{nj} = -\kappa P_0 \frac{A_{c,n} A_{c,j}}{V_0} + \rho g A_{c,j} & \text{for: } n = j \end{cases} \quad (2.61)$$

in which C_{nj} is the heave restoring coefficient of cushion panel n due to motion mode j , with $n = 7, 8, \dots, D.O.F.$ and $j = 7, 8, \dots, D.O.F.$. Displacing the structure in any of the three vertical modes heave, roll or pitch may change the volume of the aircushion thus inducing pressure changes which results in forces on all free surface panels and the structure itself.

Motions and force modes of the rigid part of the structure are considered in case $n=1,6$ and $j=1,6$. When $n > 6$ and $j > 6$, the coupling between the panels of the free surfaces in the aircushions is described. The case of $n > 6$ and $j=1,6$ represents the coupling between the rigid part of the floater and the vertical forces of the free surface panels in the cushions. If $n=1,6$ and $j > 6$, the coupling between vertical motions of the free surface panels in the aircushions and the six force modes on the rigid part of the structure are considered.

For each wave frequency the displacement \mathbf{x} of the body may be written as:

$$\mathbf{x}(t) = \tilde{\mathbf{x}} e^{-i\omega t} \quad (2.62)$$

The motions of the rigid body and the cushion panels may be determined by solving the equation of motion by using the above mentioned wave forces, added mass, damping and restoring coefficients:

$$\sum_{j=1}^{D.O.F.} \{-\omega^2 (M_{nj} + A_{nj}(\omega)) - i\omega B_{nj}(\omega) + C_{nj}\} \tilde{x}_j(\omega) = X_n(\omega) \quad \text{for: } n=1, D.O.F. \quad (2.63)$$

In which M_{nj} is the mass coupling coefficient for the force in mode n due to an acceleration in mode j . In general, the following relationships are true:

$$\begin{aligned} M_{nj} &= \rho \nabla & \text{for: } n = j = 1, 2, 3 \\ M_{nj} &= I_{nj} & \text{for: } n = j = 4, 5, 6 \\ M_{nj} &= 0 & \text{for: } n \neq j \vee n = j > 6 \end{aligned} \quad (2.64)$$

In which ∇ is the displaced volume of the structure and I_{nj} represents the mass moment of inertia.

Equation (2.60) provides the added mass and damping coupling coefficients for all degrees of freedom described by (2.39). A different approach should be followed in order to determine the added mass and damping of an oscillating aircushion supported structure (with 6 D.O.F.) in still water. In this case, the forces on the cushion panels are the result of the oscillations of the rigid structure.

$$X_{n,p}(\omega) = -\omega^2 A_{nj}(\omega) - i\omega B_{nj}(\omega) + C_{nj} \quad \text{for: } j = 1, 6 \wedge n = 7, 8, \dots, D.O.F. \quad (2.65)$$

in which the already defined added mass coefficients, damping coefficients, and aero- and hydrostatic restoring coefficients may be used. $X_{n,p}$ represents the force on cushion element n due to the p - mode of motion of the rigid structure. Based on the total forces on the cushion panels, added mass, damping, and the aero- and hydrostatic restoring coefficients, the motions of the cushion elements may be solved for each of the rigid body motions:

$$\sum_{j=7}^{D.O.F.} \{-\omega^2 A_{nj}(\omega) - i\omega B_{nj}(\omega) + C_{nj}\} \tilde{x}_{j,p}(\omega) = X_{n,p}(\omega) \quad (2.66)$$

for: $n = 7, 8, \dots, D.O.F. \wedge p = 1, 6$

where $x_{j,p}$ are the motions of cushion element j due to rigid body mode p . The coefficients and wave forces in this equation are again in accordance with equation (2.59) and (2.60). Next, the additional hydrodynamic forces, aerodynamic forces, added mass and damping coefficients are obtained by the associated equations of motions.

Based on the obtained added mass, damping and wave forces, the wave frequency motions of the structure may be solved from the normal six degrees of freedom equations of motion:

$$\sum_{j=1}^6 \{-\omega^2 (M_{nj} + A_{nj}^*(\omega)) - i\omega B_{nj}^*(\omega) + C_{nj}^*\} \tilde{x}_j(\omega) = X_n^*(\omega) \quad \text{for: } n = 1, 6 \quad (2.67)$$

in which the added mass A_{nj}^* , damping B_{nj}^* and wave forces X_n^* apply to the structure only and include the effect of the aircushions.

2.6 Validation of the numerical approach

Several model tests with aircushion supported structures were performed at Delft University of Technology in the past. Pinkster et. al. [55] carried out free-floating tests in regular waves and Tabeta [64] performed forced oscillation and captive model tests in towing tank No.1 of the Ship Hydrodynamics Laboratory. This towing tank measures 140 m x 4.25 m x 2.50 m and is

equipped with a hydraulically operated flap-type wave maker, by means of which regular or irregular waves can be generated.

This section describes the model tests and numerical model which are not extrapolated to any full scale concept. Extrapolation to full scale entails discussion with respect to the influence of the model and stiffness of the aircushion as described by Kaplan [35], Moulijn [45] and Thiagarajan [66].

This section describes three different model tests with an aircushion supported structure. First, the forced oscillation tests will be described. Next, a description of captive model tests will be given, followed by a discussion of the free-floating tests.

2.6.1 Oscillation tests

A rectangular barge model measuring 2.50 m x 0.70 m x 0.50 m was used in the forced oscillation tests. The model was constructed out of wood and consisted of a horizontal deck surrounded by vertical side walls. A vertical wall was added amidship to support the structure by two aircushions instead of one in some of the model tests.

The draft of the barge measured to the lower edge of the side walls was 0.30 m. The thickness of the walls surrounding the aircushions and the deck plate was 2.0 cm. Prior to all tests, the static pressure within the cushions was increased relative to the ambient air pressure to bring the mean water level inside the cushions 0.15 m below the mean waterline of the barge. The main particulars of the model are presented in table 2.1. In case of the single cushion arrangement, 87% of the buoyancy is provided by air, for the two-cushion arrangement this is 85%.

Table 2.1: Main particulars of the aircushion models in the forced oscillation tests and captive tests

		1 Cushion	2 Cushions
Length	m	2.50	2.50
Breadth	m	0.70	0.70
Depth	m	0.50	0.50
Draught (structure)	m	0.30	0.30
Draught (cushion)	m	0.15	0.15
Area of Water Line	m ²	1.75	1.75
Displacement	m ³	0.282	0.283

Forced heave oscillations with amplitudes of 1 cm and 2 cm were carried out in the basin. During these oscillations, the forces on the structure, cushion pressure variations and the water elevation inside the cushion were measured. Figure 2.10 shows the test set-up and location of

the measuring devices. The cushion pressure variations are measured at locations P_1 and P_2 and the water elevation (ζ_b) is measured at $(x, y) = (0.1 \text{ m}, 0.0 \text{ m})$. The heave added mass and damping coefficients were computed from the forces on the structure.

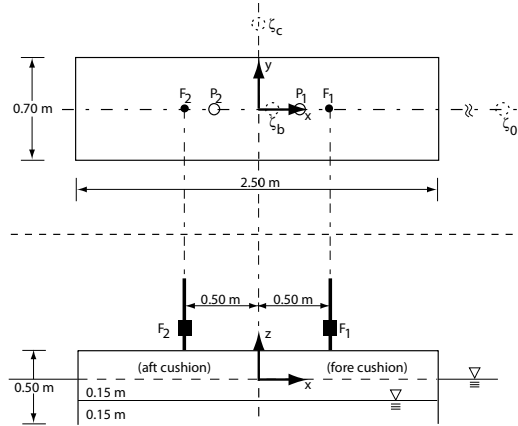


Figure 2.10: Model used in the forced oscillation and captive model tests

Numerical model

The numerical method described in the previous paragraph is used to compute the cushion pressure variations, heave added mass, heave damping and the wave elevations underneath the structure. For this purpose different panel models are used for the one cushion and two-cushion arrangement as shown in figures 2.11 and 2.12. In addition, two different panel distributions for each configuration are constructed to show the influence of the panel size on the results.

The rigid body of the first single aircushion configuration is modeled by 364 panels and the free surface inside the cushion is modeled by 120 panels in the first computations. In the second set of computations the number of cushion elements was increased to 480 panels.

In case of the two-cushion arrangement, the rigid structure is modeled by 400 panels. The two cushions of the first structure are modeled by 60 panels each, 120 panels in total. In the second configuration a refined mesh is used and the aircushions are described by 480 panels in total while the number of elements on the structure remains unchanged.

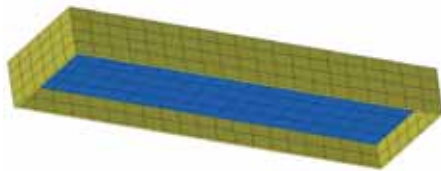


Figure 2.11: Panel model of the structure with 1 aircushion

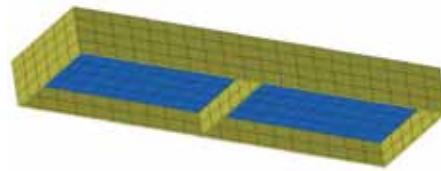


Figure 2.12: Panel model of the structure with 2 aircushions

Discussion of results

The experimental and numerical results of the oscillation tests are presented in figures 2.13 to 2.16. The aircushion pressure variations of the one and two-cushion arrangements are shown in the first figure. These results show a good agreement between the numerical method and the experiments. However sharp peaks are exhibited in the potential computations around 6.0 rad/s and 7.6 rad/s. These peaks are due to resonance frequencies of the cushion elements in the numerical method. Although these elements have no mass, the radiation force of the elements results in an added mass which together with the aero- and hydrostatic restoring coefficients results in sharp peaks at particular (natural) frequencies.

These peaks may be efficiently suppressed by adding a small amount of damping to the cushion elements. The red line in the figures shows results of the computations in which 3% of the critical damping (of each element) was added to the cushion elements. The element model in this case corresponds to the initial element model in which the rigid body is discretized by 364 panels and the aircushion is described by 120 panels.

The implementation of additional damping to the cushion elements was the result of another study about the resonance frequencies of aircushions. In order to further investigate these resonances, CFD computations were performed for the one-cushion arrangement as described by Van Kessel and Fathi [75]. The obtained results confirmed the fact the sharp peaks in the potential method are the outcome of aircushion resonance, rather than irregular frequencies. Changes in the phase and amplitudes of the cushion pressure variations were also noticed at these frequencies during the experiments. However sharp peaks are lacking in the experimental results shown in figure 2.13.

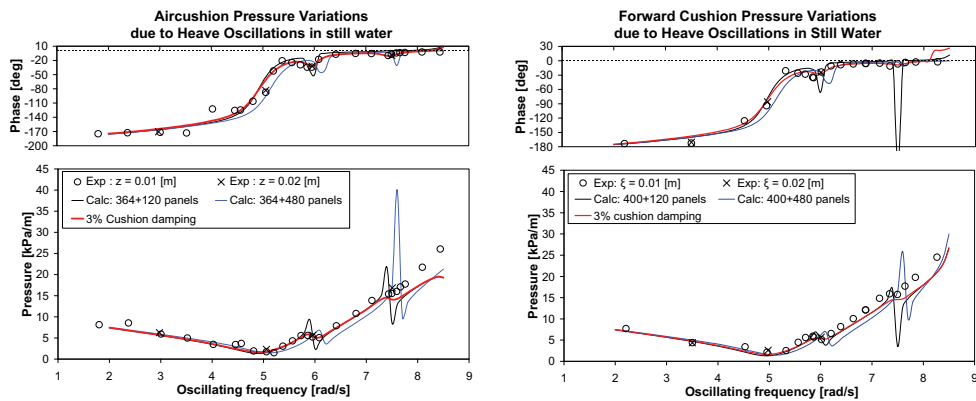


Figure 2.13: Aircushion pressure variations due to heave oscillations of the structure with one cushion (left) and two cushions (right)

Figure 2.13 shows that numerical results of the cushion pressure variations are in good agreement with model tests. All data points are close together and the oscillation amplitude has no effect on the RAOs of the pressure variations. In other words, this illustrates that there is a linear relation between the air pressure variations and the oscillation amplitude.

The introduction of additional damping to the cushion elements, equal to 3% of the critical damping, does not affect the general trend while the peaks are suppressed. This leads to a better agreement with model tests.

Added mass and damping may be retrieved from the amplitudes and phase differences of the total pressure on the structure. The total pressure on the structure is almost equal to the pressure within the cushion since the major part of the buoyancy is provided by the aircushion. Added mass and damping are presented in 2.14 and 2.15. These values are mainly related to the difference in phase angle between the oscillation and aircushion pressure.

Especially at small phase angles, a small difference in the measured data may lead to an important divergence in damping and added mass values. This explains why the agreement between experiments and computations is in some cases less accurate than a direct comparison of the pressure amplitude and corresponding phase.

As a result, the general conclusions with respect to added mass and damping are the same as for the cushion pressure variations. In addition, unphysical peaks predicted by the initial potential calculations may be efficiently suppressed by adding a small amount of damping to the cushion elements.

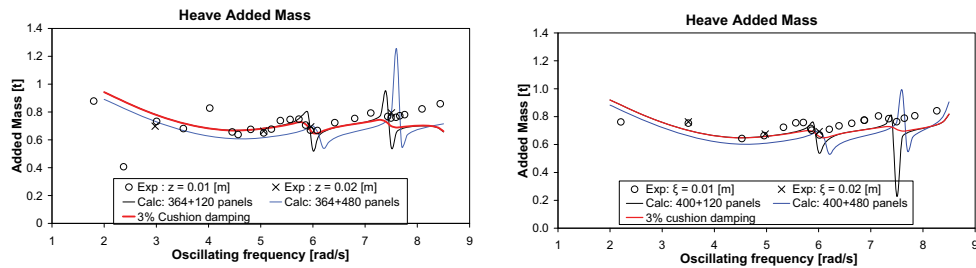


Figure 2.14: Heave added mass of the structure with one cushion (left) and two cushions (right)

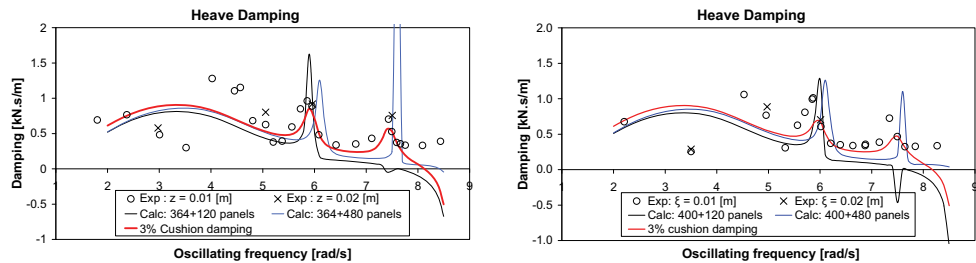


Figure 2.15: Heave damping of the structure with one cushion (left) and two cushions (right)

It will be clear that cushion pressure variations are the result of the oscillations of the structure and water elevations underneath the structure. During model tests, wave elevations were also measured inside the aircushion near the centre of the structure. Figure 2.10 shows the location of these measurements.

The RAOs of the wave elevations underneath the structure arising from the forced heave oscillations of the structure are presented in figure 2.16. Experimental results show relatively high wave elevations around 6.0 and 7.6 rad/s, which are closely related to the increase of heave damping as indicated in figure 2.15.

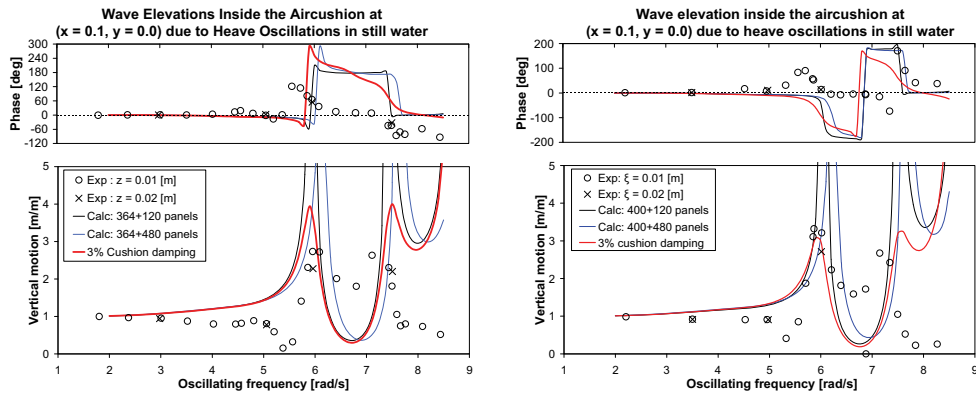


Figure 2.16: Wave elevations inside the aircushion due to heave oscillations of the structure with one cushion (left) and two cushions (right)

Figure 2.16 indicates that there is a fair agreement between both numerical methods and experimental results at frequencies up to 5.0 rad/s. Although the numerical results show approximately the same trend as the measurements at higher frequencies, there is a significant difference in the results.

In general the differences in aircushion pressure variations between the one and two-cushion arrangement are small. This is also the case for the wave elevations underneath the structure. As a consequence, there is a good resemblance in added mass and damping between both aircushion configurations.

2.6.2 Captive tests

The same aircushion configurations from the oscillation tests are also used in the captive model tests. For this reason identical panel models are used to compute the heave forces, cushion pressure variations and wave elevations inside the cushion.

Figures 2.17 to 2.22 show the numerical and experimental results of the captive structures in regular head waves. The first figure shows the heave forces on the one-cushion arrangement and two-cushion arrangement. The heave forces on both structures are nearly zero if the wave length λ is equal to the cushion length. Since the thickness of the vertical walls is small, the aircushion length is approximately equal to the length of the structure L . In this situation the cushion pressure variations of the one-cushion arrangement are zero since the mean waterline level inside the aircushion will not change, see figure 2.18. This is also the case if $L/\lambda = 2, 3, \dots$. In other words the aircushion volume of a captive structure in head waves is constant if the structure length is equal to a multiple of the cushion length.

If $L/\lambda = 1, 2, \dots$, the heave forces of the two-cushion arrangement are nearly zero since the cushion pressure variations of both cushions are approximately equal and out of phase as shown in figures 2.19 and 2.20. The difference in cushion pressure between the front and aft cushion is small if $L/\lambda = 1.5$. This results in a peak in the heave forces on the structure since the cushion pressure variations are relatively large in this situation. These peaks are well predicted by the numerical method, although extreme values are under-predicted in case a small amount of damping is added to the cushion elements. Nevertheless the resonance effects of the aircushion elements are well suppressed, and additional damping is an excellent means to compute the cushion pressures and heave forces at relatively high wave frequencies.

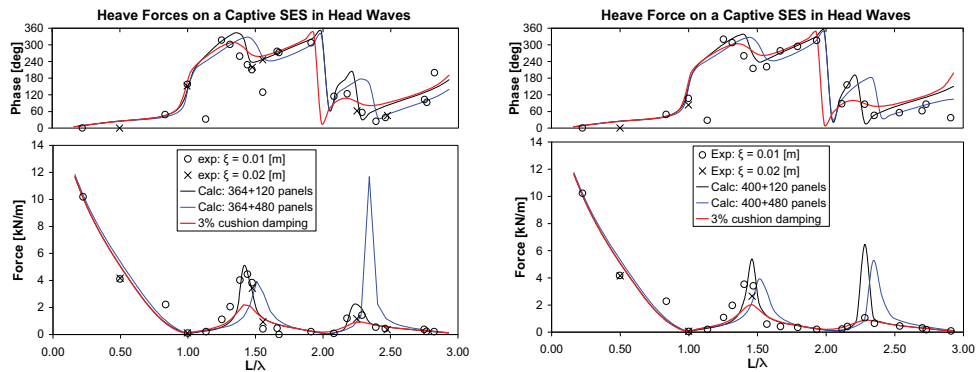


Figure 2.17: Heave forces of the captive structure with one aircushion (left) and two aircushions (right)

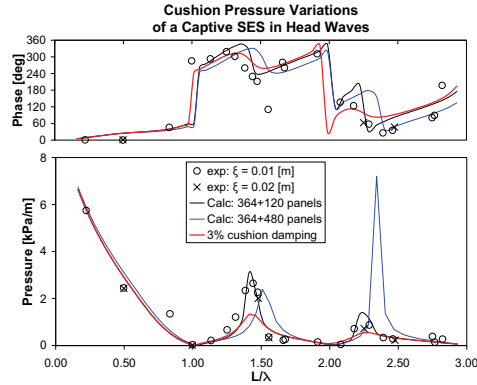


Figure 2.18: Aircushion pressure variations of the captive structure with one aircushion

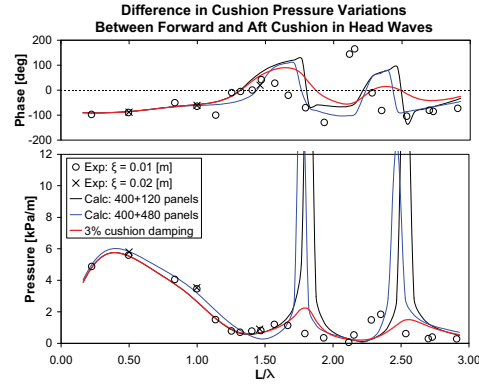


Figure 2.19: Difference in air pressure between the forward and aft cushion of the captive structure with two aircushion

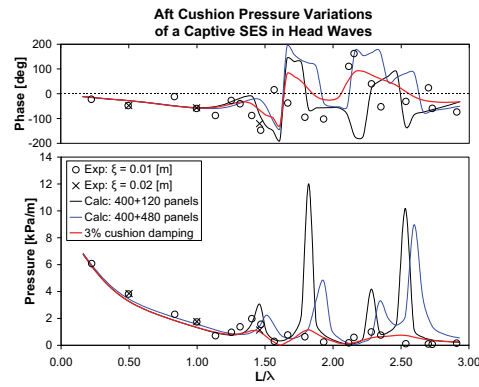
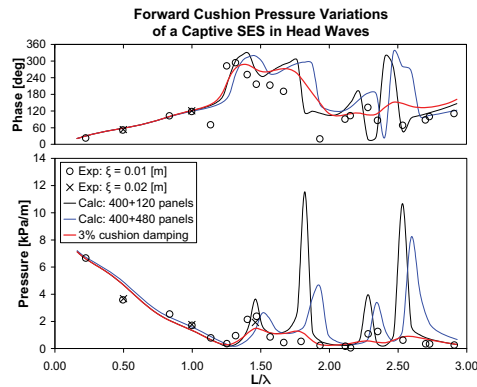


Figure 2.20: Forward cushion pressure variations (left) and aft cushion pressure variations (right) of the captive structure with two aircushions

The pitch moments of the two-cushion arrangement are larger than those of the one-cushion arrangement, this is especially the case at relatively long wave lengths as shown in figure 2.21. In general there is a bad agreement between the computed pitch moments and the measured results. Normally one would say that the program does not accurately predict the pitch moments. However in this case the experiments show some remarkable results which are normally considered to be unlikely.

For instance, relatively large pitch moments are to be expected for the two-cushion arrangement when the air pressures within the front and aft cushion are out of phase, which is the case if $L/\lambda = 1.0$. However in this case the pitch moment of the two-cushion arrangement is equal to zero. Contrary the difference in cushion pressure is small around $L/\lambda = 1.5$ as shown in figure

2.19, nevertheless figure 2.21 shows an increase in the experimental pitch moments. These unlikely results question the experimental data of the pitch moments.

On the other hand, there is a fair agreement between the measured wave elevations and the computed values in the centre underneath the structure as shown in figure 2.22. Without the modification of the cushion elements it was not possible to accurately compute these wave heights.

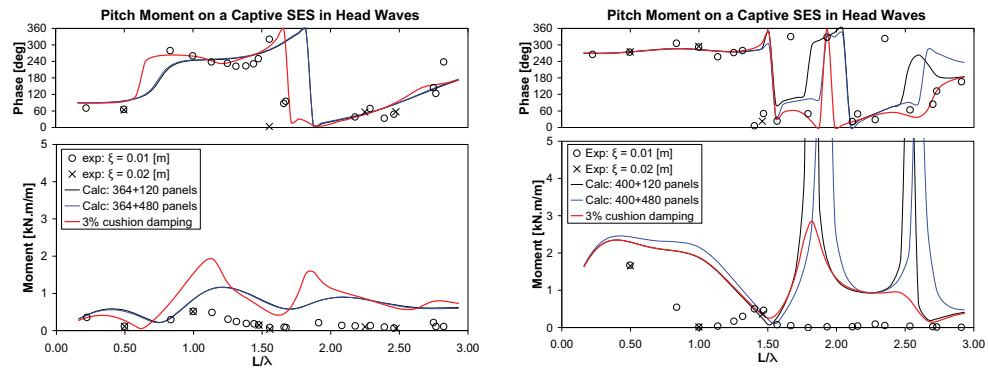


Figure 2.21: Pitch moments of the captive structure with one aircushion (left) and two aircushions (right)

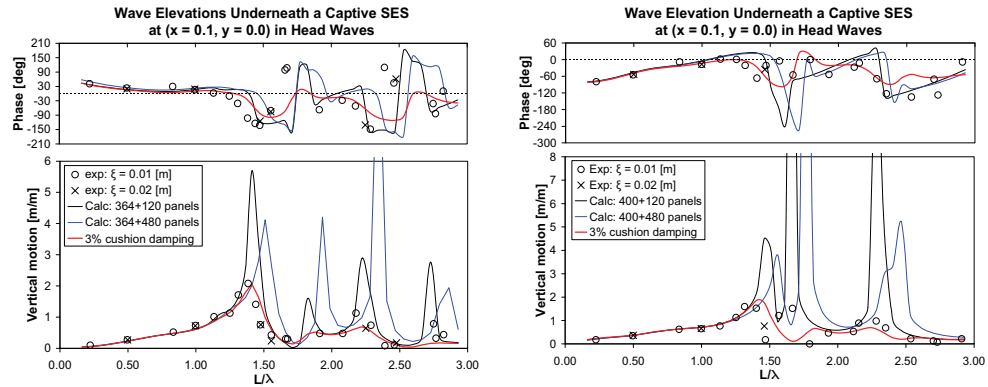


Figure 2.22: Wave elevations inside the cushion of the captive structure with one aircushion (left) and two aircushions (right)

2.6.3 Free-floating tests

Free-floating model tests of two aircushion configurations were described by Pinkster et. al. [55]. For these experiments the aircushion arrangements of the oscillation and captive tests were modified in order to obtain sufficient stability. The depth of the structure was reduced to 0.30 m, and the thickness of the side walls was increased to 6 cm. The thickness of the front and aft wall remained unchanged at 2 cm. The main particulars and associated natural frequencies of the new aircushion arrangements are shown in tables 2.2 and 2.3.

Prior to all tests, the static air pressure within the cushions was increased relatively to the ambient air pressure to bring the mean water level inside the aircushions 5 cm below the outside water level. Finally, 62% of the buoyancy was provided by the aircushions. The height of the air chamber between the free surface in the aircushions and the horizontal deck amounted to 0.18 m.

Table 2.2: Main particulars of the aircushion models in the free-floating tests

		1 Cushion	2 Cushions
Length	m	2.50	2.50
Breadth	m	0.78	0.78
Draught of structure	m	0.15	0.15
Draught of cushion	m	0.05	0.05
Area of Water Line	m ²	1.95	1.95
Displacement	m ³	0.13	0.13
KG	m	0.30	0.30
GM _T	m	0.10	0.10
GM _L	m	1.31	5.94
K _{xx}	m	0.22	0.22
K _{yy}	m	0.75	0.75
K _{zz}	m	0.73	0.73

Table 2.3: Natural frequencies of the aircushion arrangements

		1 Cushion	2 Cushions
Natural heave frequency	rad/s	4.93	4.93
Natural roll frequency	rad/s	2.74	2.75
Natural pitch frequency	rad/s	4.28	4.85

The main difference between the one- and two-cushion arrangement lies in the longitudinal GM-value, this value is significantly larger for the two-cushion arrangement. As a result the natural pitch frequencies will be different as well. However, the difference in natural frequency is limited due to a significant increase of added mass in case the structure is supported by two cushions. A difference in air pressure between the forward and aft aircushion arises if the structure is subjected to a pitch angle. This difference results in a restoring moment which is not present in the one-cushion arrangement.

Model tests were carried out in regular head waves in which the model was moored by means of a linear soft spring mooring system. The forward and aft mooring lines were connected at deck level to force transducers which measured the surge drift force. The mean surge drift force was obtained by summing the mean values of the surge force transducers [55]. In addition the aircushion pressures together with surge, heave and pitch motions were measured. The location of the pressure sensors corresponds to the oscillating tests as illustrated in figure 2.10.

New panel models were constructed in order to compute the quantities during the free-floating tests. These element models are shown in figure 2.23. The one-cushion arrangement was modeled by 1116 elements and the two-cushion arrangement by 1188 elements; this corresponds to the models used by Pinkster et. al. [55]. Table 2.4 shows the distribution of the elements over the rigid body and aircushions, which are indicated by yellow and blue colors respectively in figure 2.23.

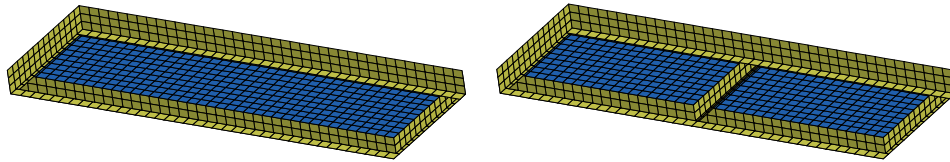


Figure 2.23: Panel models of aircushion structures used in the free-floating tests

Table 2.4: Number of panels of the discretized models

	1 Cushion	2 Cushions
Panels on structure	636	708
Panels on cushion(s)	480	480
Total number of panels	1116	1188

The experimental results of the free-floating models are shown in figures 2.24 to 2.30. These figures also show the results of the new numerical method in which 3% of the critical damping was added to the cushion elements. In addition results of the method presented by Pinkster [55] were added to the figures in order to show the differences.

Figures 2.24 to 2.26 show that the motions of the structure can be well predicted by the numerical methods. Although the maximum pitch motions of the two-cushion arrangement computed by the new program are lower, the differences between the numerical methods are generally small. Figure 2.24 shows a fair agreement between the experimental surge motions and the computed values. However the peak values are under-predicted by the computations.

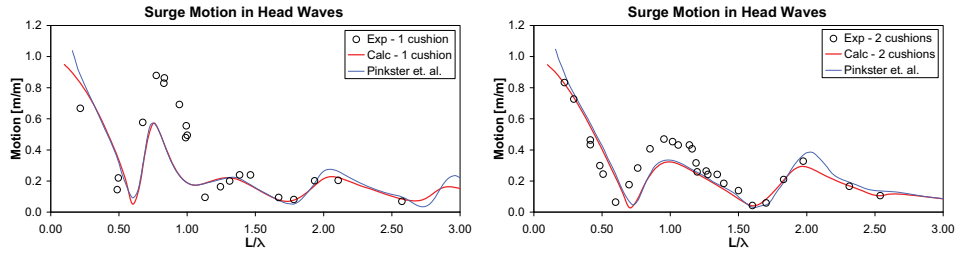


Figure 2.24: Surge RAOs of the free-floating structure with one cushion (left) and two cushions (right)

The heave motions agree well with the computations and are nearly zero in case the wave length corresponds to a multiple of the cushion length (L_c). For the two-cushion arrangement this is the case if $L_c / \lambda = 0.5$. In this case the air pressure in both cushions is approximately equal but out of phase as shown in figures 2.28 and 2.29. As a consequence the total heave force will be zero resulting in minimal heave motions.

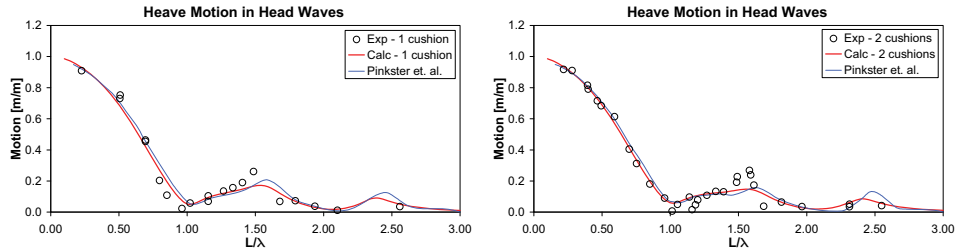


Figure 2.25: Heave RAOs of the free-floating structure with one cushion (left) and two cushions (right)

Although the natural pitch frequencies are approximately equal for both structures, there is a significant difference in the pitch amplitude. In general the pitch damping will be small if a structure is supported by a large single aircushion. In this case the aircushion volume will not change if the structure is subjected to a (small) pitch angle. As a consequence the water surface underneath the structure will not deform and few radiation waves are propagated by the structure. However, this does not explain the large difference between numerical and experimental results

of the pitch amplitude at the natural frequency. It is likely that the pitch motions of the model are reduced by viscous effects which are not taken into account in the computations. Apparently these effects are smaller for the two-cushion arrangement.

Pitch motions of the two cushion configuration will result in pressure changes in the cushions as shown in figure 2.29. These pressure changes will deform the water surface underneath the structure and eventually result in radiation waves propagating away from the structure. This effect is more pronounced than other non-linear effects. For this reason the peak pitch responses can be well predicted by the numerical diffraction methods.

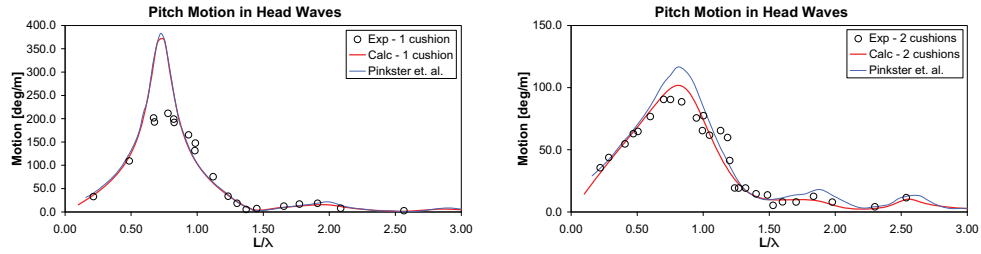


Figure 2.26: Pitch RAOs of the free-floating structure with one cushion (left) and two cushions (right)

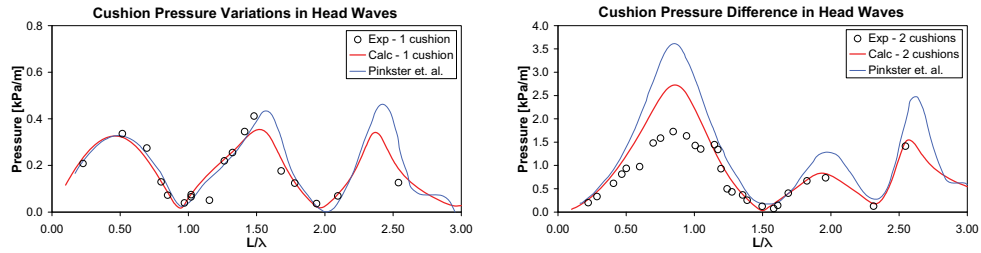


Figure 2.27: Cushion pressure variations of the free-floating structure with one air cushion

Figure 2.28: Difference in air pressure between the forward and aft cushion of the free-floating structure with two air cushions

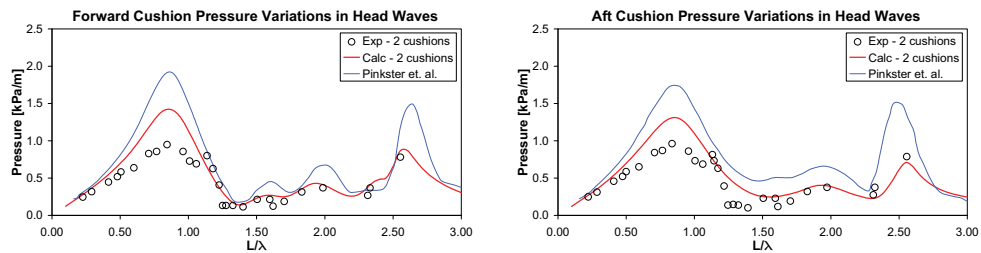


Figure 2.29: Forward cushion pressure variations (left) and aft cushion pressure variations (right) of the free-floating structure with two air cushions

An over-prediction of the pitch motions of the one-cushion arrangement at the natural pitch frequency, results in an over-prediction of the maximum draft at the bow and stern. As a consequence the mean second order surge drift force is also over-predicted at this frequency as indicated in figure 2.30.

The difference between the new computational method, in which 3% of the critical damping was added to the cushion elements, and results of Pinkster et. al. [55] is remarkable. The peaks which were present in Pinkster's method are efficiently suppressed by the new method. Moreover, the new computations of the two-cushion arrangement show a fair agreement with the experiments.

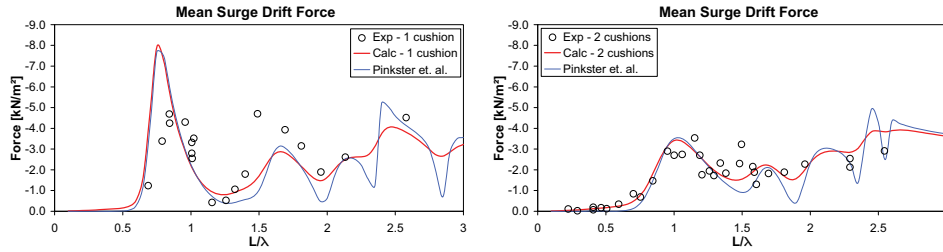


Figure 2.30: RAOs of the mean second order surge wave drift forces of the free-floating structure with one cushion (left) and two cushions (right)

2.7 Comparison with a conventional barge

The previous sections showed the validation of the numerical method and indicated that dynamic behavior of a rigid aircushion supported structure can be well predicted by a linear potential method. This section shows the effect of an aircushion on the behavior of the structure by comparing the numerical results with a conventional barge.

A change in the characteristics of the aircushion may result in a significant change of the dynamic behavior of the structure as will be shown in the next paragraph. In addition the behavior of the structure will significantly change if the aircushion is divided in compartments. Paragraphs 2.7.2 and 2.7.3 describe a full-scale structure and the effect of different aircushion configurations on the motions, drift forces, wave field and structural loads.

2.7.1 Tuning the aircushion characteristics

The aircushion pressure is the result of the vertical difference between the mean water level inside the aircushion and the mean waterline outside the structure. The water level of the cushion is referred to as the draft of the aircushion (T_c) in the remainder of this chapter. If the

air pressure inside the cushion is increased, the draft of the aircushion will increase accordingly. As a consequence the draft of the structure decreases since the mass of the body will not change. In reality the draft of the structure may be changed by pumping air underneath the structure or by venting air from the cushion. In addition air may also escape from the cushion in extreme sea conditions, which is the case if a wave trough is deeper than the draft of the vertical walls around the aircushion, i.e. the draft of the structure. This effect was observed during the model tests of an aircushion supported MOB in high sea states which were performed by Pinkster et. al. [56].

This chapter discusses the effect of the cushion pressure on the dynamic behavior of the structure. The dynamic behavior of the free-floating single cushion arrangement is computed at different drafts. The structure is equal to the one presented in paragraph 2.6.3, and the main particulars may be found in table 2.2.

The results for a conventional barge are also presented to show the effect of the aircushions on the dynamic behavior. With the exception of the draft, all other main particulars of the conventional barge are equal to those of the aircushion supported structure. The draft of the barge is set to 7 cm in order to obtain the same displacement as the aircushion supported structure.

Results from model experiments are only available for the structure at a draft of 15 cm, see paragraph 2.6.3. In this case the draft of the aircushions (T_c) is 5 cm. Numerical computations are performed for the Air-Cushion Supported Structure (ACSS) at different drafts, i.e. $T_c = 0$ cm, $T_c = 3$ cm, $T_c = 4$ cm, $T_c = 5$ cm, $T_c = 6$ cm. In the remainder of this section these results will be referred to as ACSS 1, ACSS 2, ACSS 3, ACSS 4 and ACSS 5 respectively. Different panel models are constructed to compute the dynamic behavior of the structure at different drafts. Since the size of the elements is approximately equal, the number of elements changes with the draft of the structure. In case all air is vented from the aircushion, all elements are associated to the rigid body as shown in table 2.5. Figure 2.31 shows the element model of ACSS 1. The panel model of ACSS 4 was shown before in figure 2.23.

Table 2.5: Number of panels of the models

	Panels on structure	Panels on cushions	Total panels
Barge	1496	n/a	1496
ACSS 1	1784	n/a	1784
ACSS 2	1064	480	1544
ACSS 3	928	480	1408
ACSS 4	636	480	1116
ACSS 5	480	480	960

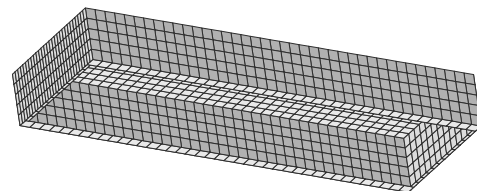


Figure 2.31: Panel model of the aircushion arrangement at a draft of 0.32 m (ACSS 1)

The stability of the aircushion supported structure changes with the aircushion pressure. Table 2.6 shows that the stability increases after air is vented from the aircushion. This has an effect on the natural frequencies of roll and pitch, which are shifted to higher frequencies.

On the other hand the natural heave frequency decreases if air is vented from the cushion. This is due to the fact that the increase of the heave restoring coefficient is smaller than the increase in added mass.

In general the GM-values of a conventional barge are significantly larger than those of an aircushion supported structure. The difference in stability between the conventional barge and ACSS 1 is mainly due to a difference in the BG-value, i.e. the distance between the centre of buoyancy and the centre of gravity, as indicated in equation (2.19).

Table 2.6: Stability characteristics and natural frequencies of the conventional barge and the aircushion supported structure

	Draft		Buoyancy		Stability Char.		Natural Frequencies		
	T_c [m]	T_s [m]	Air [-]	Skirt [-]	GM_T [m]	GM_L [m]	Heave [rad/s]	Roll [rad/s]	Pitch [rad/s]
Barge	-	0.07	-	-	0.49	7.51	5.61	5.81	5.78
ACSS 1	0.00	0.32	0%	100%	0.61	7.31	4.37	4.51	4.70
ACSS 2	0.03	0.25	37%	63%	0.17	1.38	4.39	3.04	4.27
ACSS 3	0.04	0.20	50%	50%	0.14	1.34	4.64	2.91	4.30
ACSS 4	0.05	0.15	62%	38%	0.10	1.31	4.92	2.74	4.28
ACSS 5	0.06	0.10	75%	25%	0.05	1.26	5.25	2.35	4.27
Exp. ACSS 4	0.05	0.15	62%	38%	0.11	1.32	5.00	2.96	4.33

The heave motions of the aircushion supported structure at different drafts and the conventional barge are shown in figure 2.32. The shift of the natural heave frequency in beam waves is clearly visible. The heave motion at the natural frequency can be decreased by increasing the aircushion volume. The reason for this can be found in figure 2.33 which shows that an increase of the mean waterline inside the aircushion results in an increase of the heave damping.

If the draft of the structure is minimized, i.e. $T_c = 6$ cm, the maximum heave motions correspond to those of a conventional barge. In this case the heave motions are increased by a factor 2.2 compared to the situation in which all air is vented from the cushion. This shows that the heave motions are sensitive to a change of the aircushion pressure in beam waves. Contrary, the effect in head waves is less pronounced.

The main difference in heave motions between the aircushion supported structure and the conventional barge occurs in head waves when the wave length is equal to the cushion length. In

this case the cushion pressure is fairly constant as indicated in figure 2.34. As a result the heave forces on the structure are small and the heave motions are nearly zero. This is the case for all drafts, except when $T_c = 0$ cm.

Obviously, a smaller cushion height results in smaller cushion pressure variations. These pressure variations are largest at the natural heave frequency. For this reason the natural heave frequencies at different drafts can be clearly distinguished in figure 2.34.

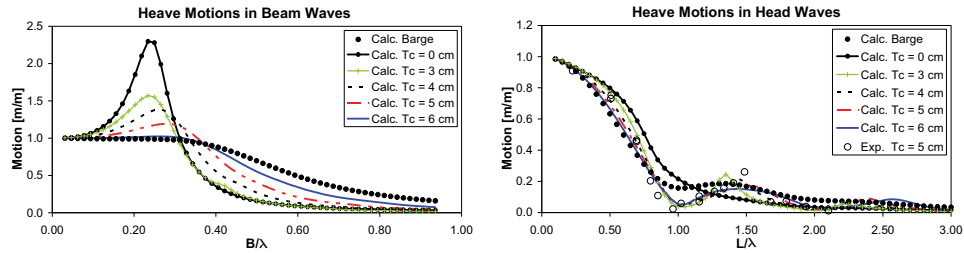


Figure 2.32: Heave motions in beam waves (left) and head waves (right) of a conventional barge and an aircushion supported structure at different drafts

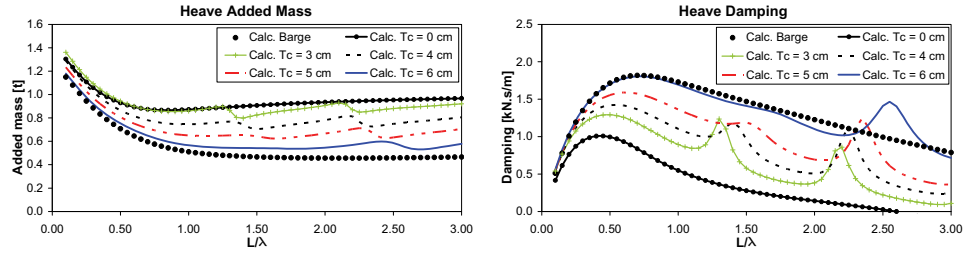


Figure 2.33: Heave added mass (left) and damping (right) of a conventional barge and an aircushion supported structure at different drafts

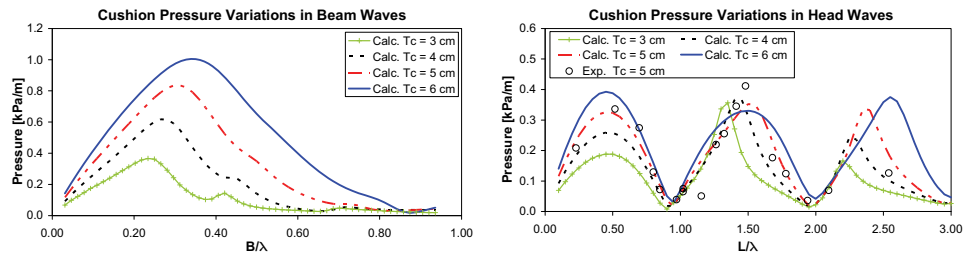


Figure 2.34: Aircushion pressure variations in beam waves (left) and head waves (right) of a conventional barge and an aircushion supported structure at different drafts

The roll and pitch motions at all drafts of the aircushion supported structure are larger than those of the conventional barge. This is mainly due to a lack of rotational damping of aircushion supported structures in general. The effect of the draft of the floater on the natural roll frequency is clearly shown in figure 2.35. The shift of the natural pitch frequency is small. The reduction of the maximum pitch motion is also small if the air pressure within the cushion is reduced. A significant reduction of the pitch motions will only occur if all air is vented from the cushion. In this case the pitch motions approximately correspond to those of the conventional barge.

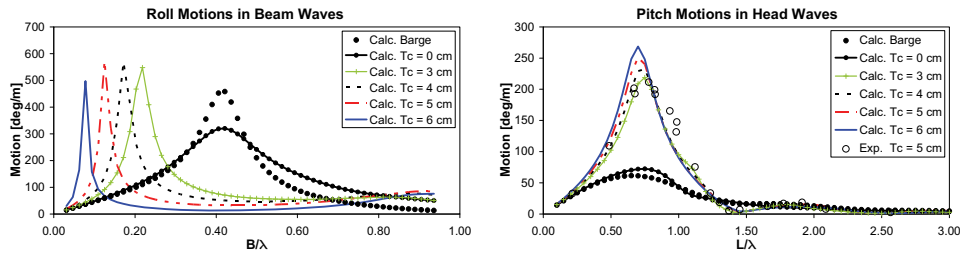


Figure 2.35: Roll motions in beam waves (left) and pitch motions in head waves (right) of a conventional barge and an aircushion supported structure at different drafts

2.7.2 Drift forces and wave field

The previous section showed the effect of an aircushion on the dynamic behavior of a structure at model scale. In the remainder of this chapter the behavior of large aircushion supported structures will be discussed. This section describes the physical differences in the wave field around different aircushion configurations and a conventional barge. The main particulars are equal for all structures and are shown in table 2.7.

Table 2.7: Main particulars of the structures

Length	150.0	m	Displacement	38437.5	t
Breadth	50.0	m	KG	15.0	m
Depth	20	m	k_{xx}	15.0	m
Draught structure	10.0	m	k_{yy}	42.0	m
Draught cushion	5.0	m	k_{zz}	42.0	m

Four different aircushion configurations are considered, i.e. a structure supported by one large aircushion (1AC), three aircushions (3AC), four aircushions (4AC) and 75 aircushions (75AC). All configurations are completely supported by air, i.e. the thickness of the vertical wall is equal to zero. In addition an aircushion supported structure (ACSS 1) with a wall thickness of 10 m

will be considered. In this case 75% of the buoyancy is supported by air and 25% is supported by the vertical walls around the cushion.

The dimensions of the cushions, natural frequencies and stability characteristics of the structures are shown in table 2.8. Figure 2.41 shows the configuration of these structures in a wave field. The height of the air chambers is 5 m and the ambient air pressure is 100 kPa.

Table 2.8: Dimensions of the cushions, natural frequencies and stability

Structure type / name		Cushion size		ω_{n3}	ω_{n4}	ω_{n5}	GM_T	GM_L
		Length	Breadth					
		[m]	[m]	[rad/s]	[rad/s]	[rad/s]	[m]	[m]
1 cushion	(1AC)	150.0	50.0	0.68	-	-	-2.5	-2.5
3 cushions	(3AC)	50.0	50.0	0.68	-	0.68	-2.5	266.5
4 cushions	(4AC)	75.0	25.0	0.68	0.73	0.65	22.7	224.5
75 cushions	(75AC)	10.0	10.0	0.69	0.80	0.74	29.8	298.8
Barge		-	-	0.69	0.80	0.74	39.2	372.5
ACSS 1		140.0	40.0	0.69	0.77	0.82	19.3	128.6

The negative GM-values of the 1AC and 3AC configurations are due to the fact that a single cushion covers the whole waterline area. Since the wall thickness of these configurations is zero, the centre of buoyancy will not shift if the body is subjected to a small heeling angle. Accordingly, the buoyancy force acts through a fixed point at half draught of the structure and the GM-value corresponds to the distance between the centre of buoyancy and the centre of gravity.

The bodies with a negative GM-value are unstable, but nevertheless have been included to show the effect of different aircushion configurations on the behavior of the structure. In these cases additional stability can be gained by increasing the thickness of the skirts as is the case for ACSS 1.

The motions in regular head waves of the structures are presented in figure 2.36. Heave motions in regular head waves are approximately equal for all structures. The pitch motions are nearly zero for the 1AC configuration. In this case a single cushion covers the total length of the structure and as a result no natural pitch frequency will be present. If the structure is supported by many small cushions like the 75AC, the motions fairly correspond to those of the conventional barge as shown in figure 2.36.

The heave motions in beam waves decrease if the structure is supported by a large aircushion. Figure 2.37 shows that the largest aircushion results in the smallest heave response. On the other hand, the roll motions increase if the structure is supported by fewer aircushions, which is the

result of an increased roll moment and reduced roll damping. The roll motions of 1AC and 3AC configurations are zero due to their negative GM-values as shown in table 2.8.

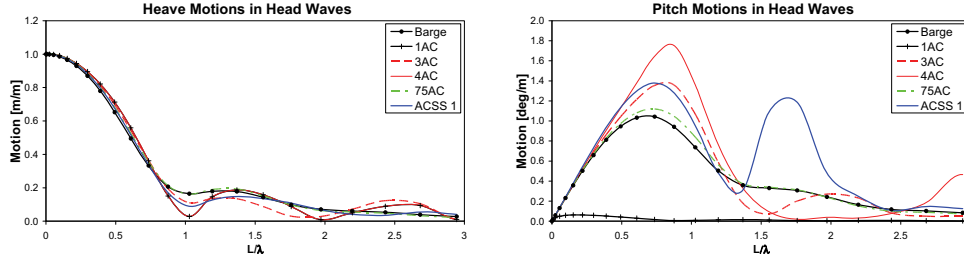


Figure 2.36: RAOs of heave motions (left) and pitch motions (right) in head waves for different aircushion configurations and a conventional barge

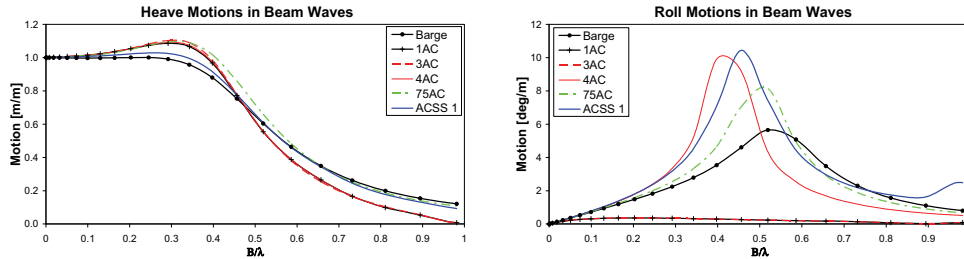


Figure 2.37: RAOs of heave motions (left) and roll motions (right) in beam waves for different aircushion configurations and a conventional barge

The mean drift forces of the structure in head and beam waves are shown in figure 2.38. Since the main dimensions of the structures are equal and the motions of the 75AC in head waves correspond to those of the conventional barge, the drift forces of both structures are approximately equal as well.

The small heave responses and nearly zero pitch motions of the 1AC configuration result in relatively small mean drift forces particularly in head waves. The pitch motions and accordingly the drift forces increase if the skirt thicknesses of the bow and stern increase. The maximum mean surge drift force of the ACSS 1 configuration occurs around the same frequency as the peak of the pitch motions, i.e. at $L/\lambda = 1.8$. This is not the case for the other structures in head waves where the maximum mean surge drift forces occur at higher frequencies than the peak pitch responses.

The mean sway drift forces of the cushion configurations in beam waves occur at the natural roll frequency. The mean sway drift forces of the conventional barge and 75AC are fairly constant at high wave frequencies and approximately equal to 750 kN/m^2 . This value corresponds to $1/2 \rho g \zeta_a^2 L$, which means that all waves are reflected by the structure. The same consideration

holds for the mean drift forces in head waves, however in this case the beam of the structure shall be considered.

The mean surge and sway drift forces in oblique waves of 135 deg are shown in figure 2.39. In this case the structure is not symmetric with respect to the wave direction and therefore the drift forces will result in a moment as shown in figure 2.40.

The figures show that the mean drift forces of the 1AC configuration are smallest. However, it should be noted that the presented results are response amplitude operators (RAOs); this implies that the final drift forces depend on the environmental conditions. In other words, these transfer functions should be multiplied with an appropriate wave spectrum in order to assess the mooring loads.

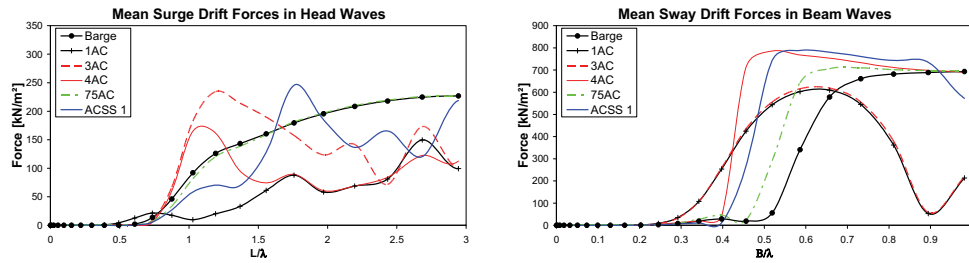


Figure 2.38: RAOs of mean drift forces in head and beam waves for different air cushion configurations and a conventional barge

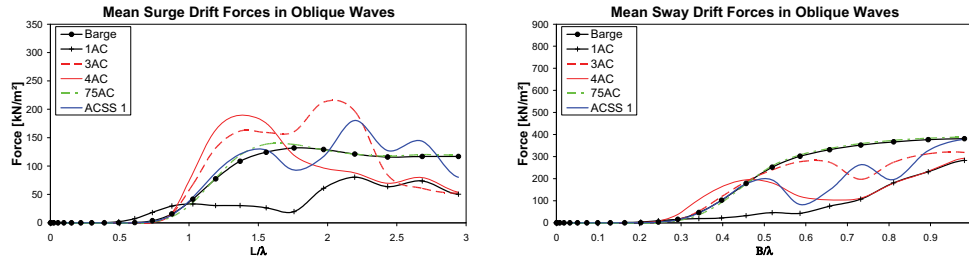


Figure 2.39: RAOs of mean surge and sway drift forces in oblique waves of 135 deg for different air cushion configurations and a conventional barge

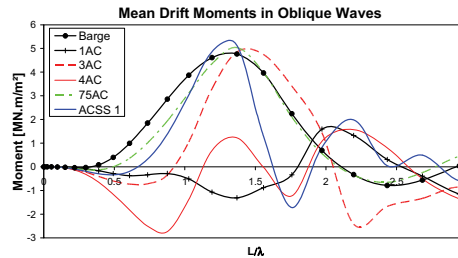


Figure 2.40: RAOs of mean drift moments in oblique waves of 135 deg for different air cushion configurations and a conventional barge

In general the drift forces are highly related to the wave field around the structure. If the drift forces are large, most wave energy is reflected by the floater. Basically the wave field around the structure is a superposition of the incident waves, radiation waves and diffraction waves. Figure 2.41 shows the wave field around the different aircushion configurations and the conventional barge in regular head waves of 0.90 rad/s ($L/\lambda = 2$). The wave height values are normalized and presented in terms of non-dimensional response amplitude operators (RAOs). The wave fields in regular beam seas and oblique seas can be found in appendix B.

The distortion of the wave field is especially small for the 1AC structure. In this case, the waves can travel freely underneath the floating body resulting in a small wake behind the structure. Few waves are reflected in front of the structure and accordingly the drift forces are small. Less wave energy is transmitted underneath the cushion if the thickness of the front skirt increases, which is the case for ACSS 1. Due to the increase of the thickness of the skirts, the waves underneath and behind the structure are attenuated.

Since the motions and drift forces of the 4AC and 1AC configurations are approximately equal, the differences in the wave fields are also small. The same consideration holds for the 75AC and the conventional barge. The drift forces in figure 2.38 indicated that the wave field around the 3AC structure is more distorted than that around the 1AC and 4AC at $L/\lambda = 2$. This is confirmed by figure 2.41, which shows that the 3AC structure attenuates the waves as the wave heights in the aft cushion are smaller than those in the forward cushion.

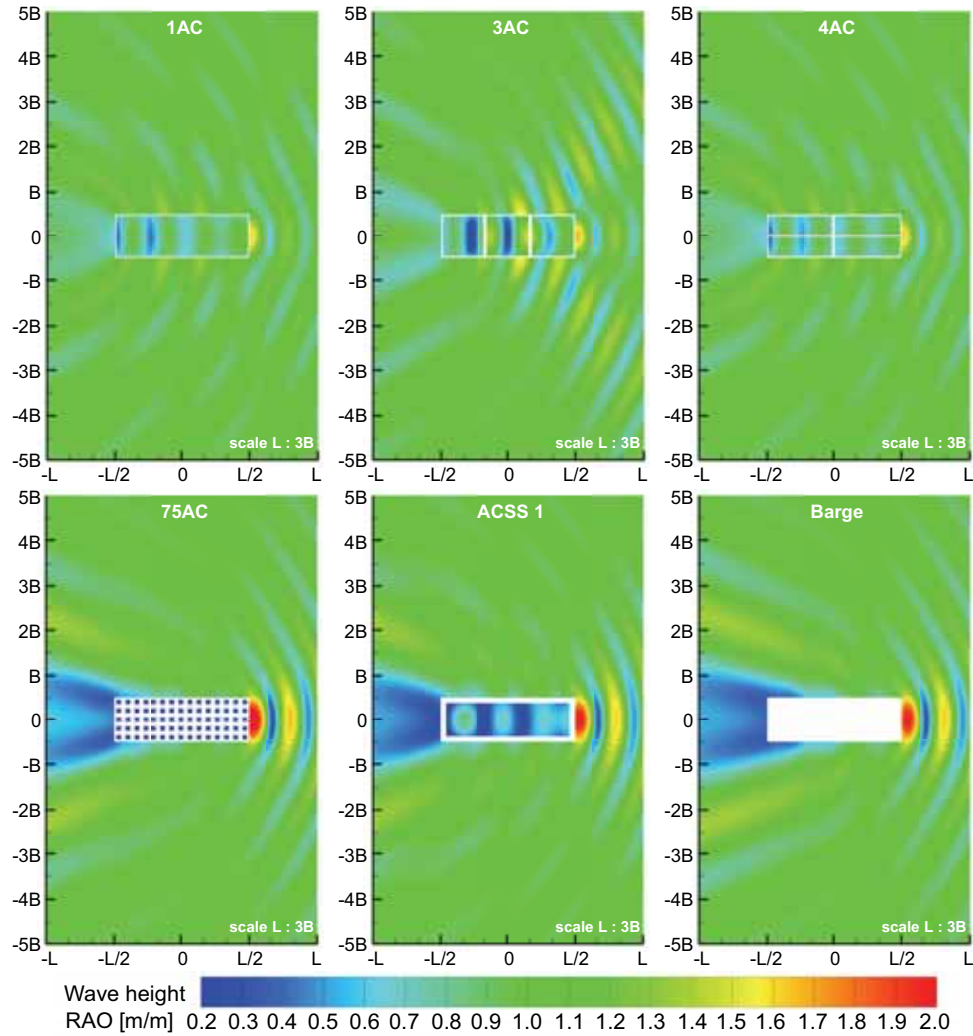


Figure 2.41: Wave field around different air cushion configurations and a conventional barge in case of regular head waves with a frequency of 0.90 rad/s ($L/\lambda = 2$).

2.7.3 Wave induced shear forces and bending moments

Aircushions may significantly reduce the internal loads of large floating structures. The effect on these structural loads is largest for the 1AC configuration when the body is supported by one large air cushion. In this case the maximum shear forces and bending moments in the complete frequency range are reduced by 98% and 96% respectively. However, it should be noted that the

1AC configuration is a theoretical example because the vertical skirts underneath the structure have no thickness and the structure is completely supported by air.

The maximum wave induced shear forces and bending moments of the aircushion configurations and conventional barge are shown in table 2.9, which illustrates that the structural loads increase with the number of cushions. If the body is supported by many small cushions, like the 75AC configuration, the maximum wave induced shear forces and bending moments approach those of the conventional barge. On the other hand, the loads decrease if more buoyancy is provided by the vertical skirts, but they are significantly larger than those of the 1AC configuration, which was completely supported by air. In case of ACSS 1, 25% of the buoyancy is provided by the skirts and the maximum wave induced bending moments are, compared to the conventional barge, reduced by 43%.

Table 2.9: Maximum wave induced structural loads

	Shear Force		Bending Moment	
	[kN/m]	[-]	[MN]	[-]
1AC	107	2%	8	4%
3AC	3741	78%	129	61%
4AC	2396	50%	49	23%
75AC	4297	90%	186	89%
ACSS 1	3357	70%	119	57%
Barge	4783	100%	210	100%

The distribution of the structural loads along the length of the structure may change if the body is supported by aircushions. Figures 2.42 and 2.43 show the RAO distributions of the vertical wave induced shear forces and bending moments along the length of the conventional barge and the aircushion configurations at different wave lengths. The aircushions underneath the structure distribute the wave pressure equally over a large area. If the structure is completely supported by one large cushion, the pressure is constant along the bottom of the structure and the wave induced shear forces and bending moments are significantly reduced.

The maximum shear forces of the 4AC configuration occur in the centre of the structure at the boundary between the forward and aft cushions. This is also the case for the 3AC configuration, but in this case the boundaries between the cushions are located at $-L/3$ and $L/3$. The location of the vertical walls is indicated by the white lines in figures 2.42 and 2.43. For the 3AC and 4AC configuration, the air pressure variation within the forward cushions is larger than in the aft cushions. As a result the distribution of the structural loads will not be completely symmetrical.

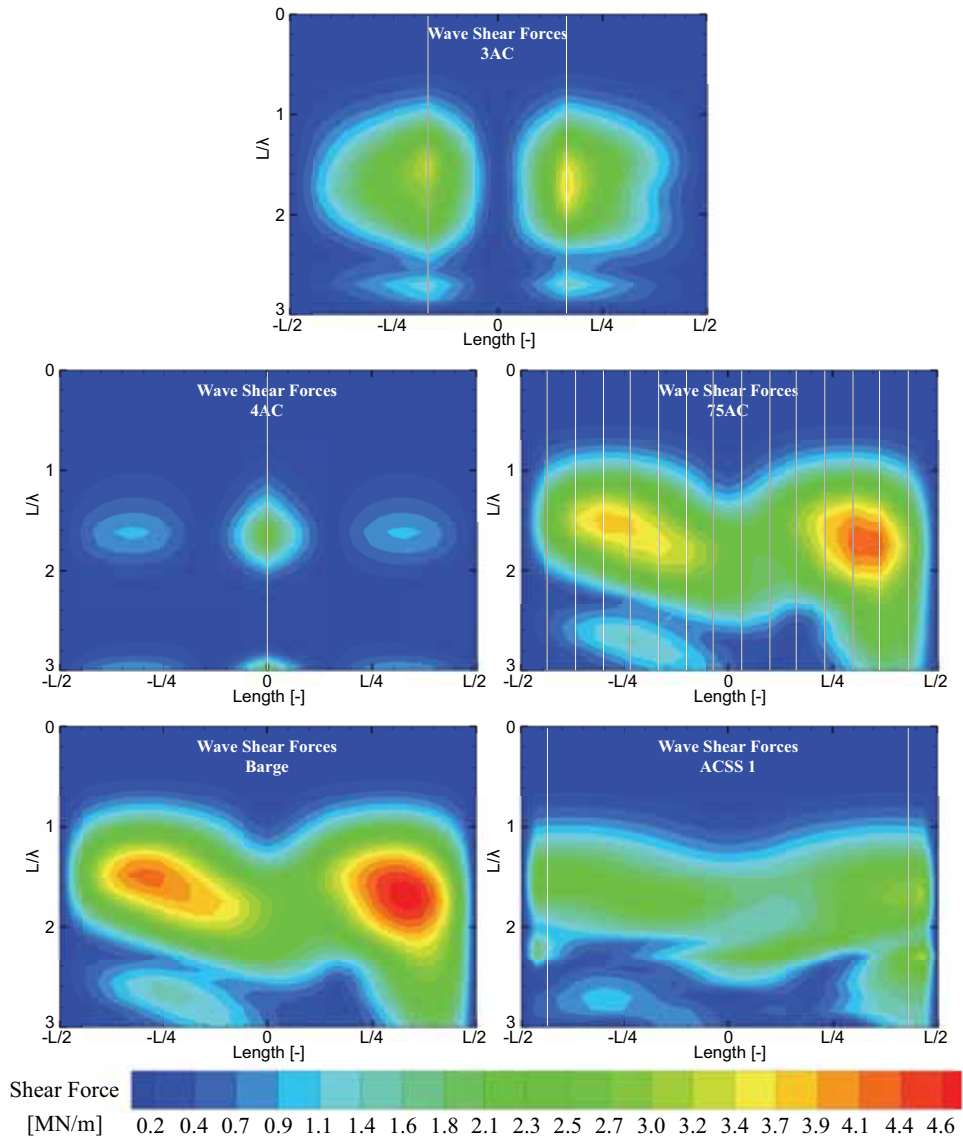


Figure 2.42: RAOs of wave induced shear forces of the aircushion configurations and the conventional barge in regular head waves

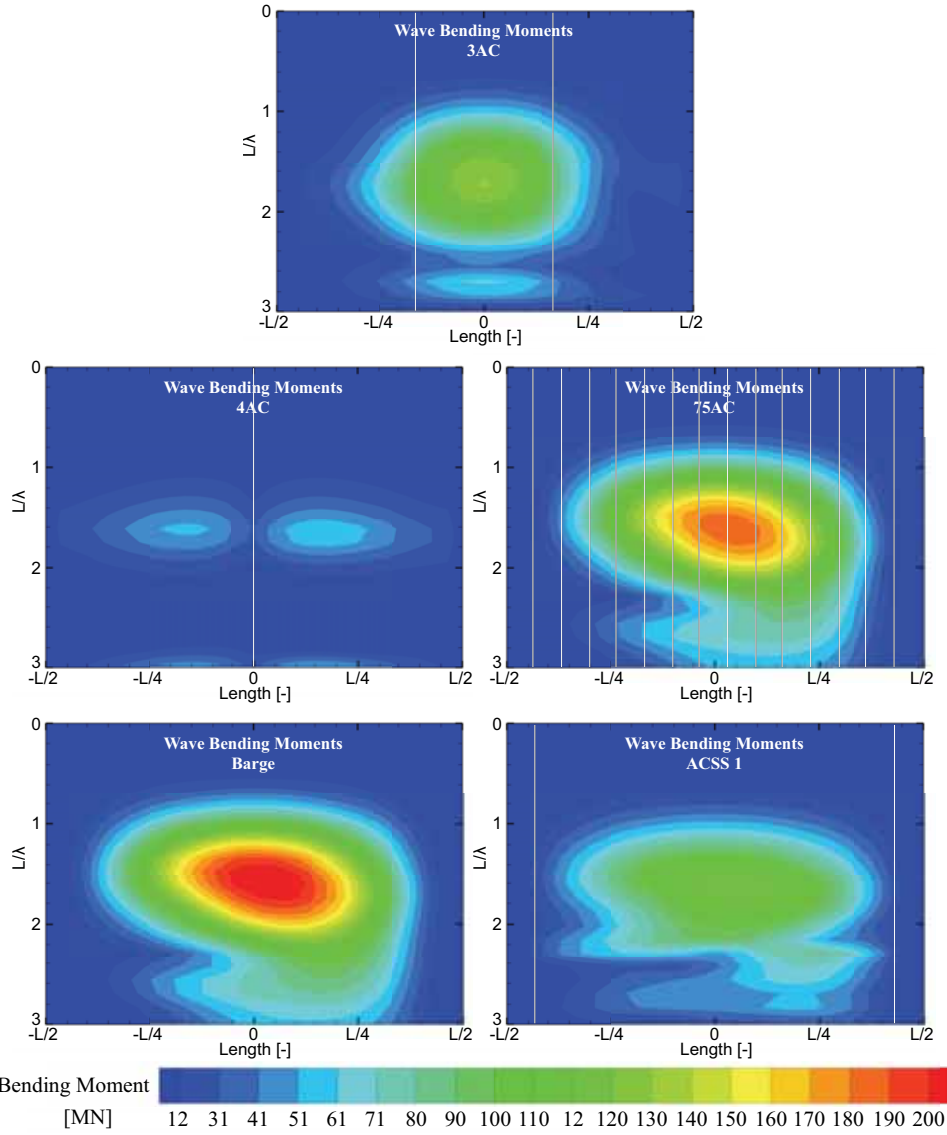


Figure 2.43: RAOs of wave induced bending moments of the aircushion configurations and the conventional barge in regular head waves

Even though the structural loads are small if the structure is supported by one aircushion, they can be further reduced. A disadvantage of the ACSS1 and 1AC configuration is the lack of pitch damping. As a result the pitch motions and pitch accelerations are relatively large and these may result in relatively large wave induced bending moments. The cushion configuration and

dimensions of the skirts may be changed to further reduce the structural loads. For example, the maximum pitch motions of ACSS 1 will decrease if the structure is supported by two cushions (ACSS 2) as described by Van Kessel et. al. [73].

The wave induced structural loads may also be reduced by interconnecting the aircushions. Figure 2.44 shows an example in which 28 equally sized aircushions are pairwise connected in a way that air can flow freely between each pair of cushions. Basically this structure consists of 14 individual cushions since the mean waterline and air pressure are equal in the connected cushions. In the remainder of this chapter this structure will be referred to as ACSS 3. The dimensions of the cushions of this configuration, as well as those of ACSS 1 and ACSS 2, are given in table 2.10. The dimensions and particulars of all structures remain unchanged and 75% of the buoyancy is provided by air.

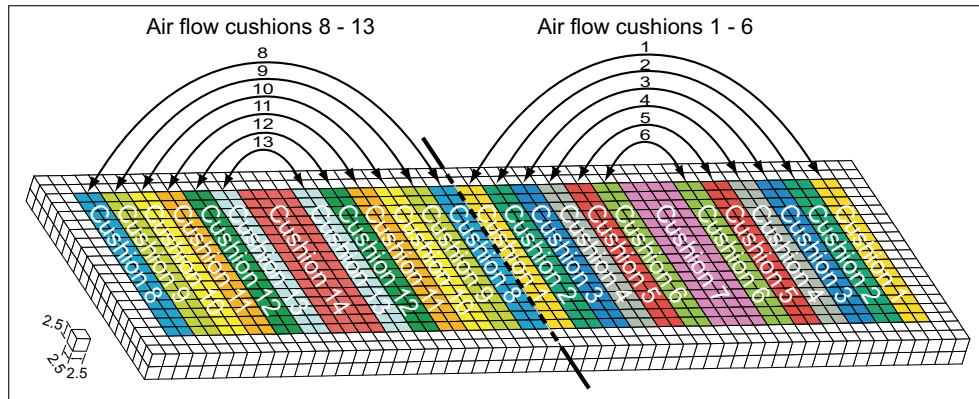


Figure 2.44: Aircushion supported structure with 14 interconnected cushions (ACSS 3)

Table 2.10: Dimensions of cushions

Structure type / name	No. of Cushions (N x M)	Length of 1st Cushion [m]	Length of 2nd Cushion [m]	Length of N th Cushion [m]	
1 cushion (ACSS 1)	1 x 1	140	-	-	
2 cushions (ACSS 2)	2 x 1	70	70	-	
14 cushions (ACSS 3)*	14 x 1	2 x 5	2 x 5	2 x 5	

* Cushions connected

The RAOs of the maximum wave induced shear forces and bending moments in regular heads waves are presented in table 2.11. This table shows that use of one large aircushion does not necessarily result in the largest reduction of the wave induced shear forces and bending moments.

A large single cushion shows good results, but the largest reduction of the wave induced shear forces and bending moments will be obtained if the structure is supported by two cushions in longitudinal direction.

Good results with respect to vertical shear forces and bending moments can be obtained when the structure is supported by multiple cushions which are interconnected in a way that air can freely flow from one aircushion to another. This structure is more complex, but table 2.11 shows that the wave induced shear forces and bending moments are smaller than those of the one-cushion arrangement (ACSS 1).

Table 2.11: Maximum wave induced structural loads

Structure type / name		Maximum Wave Shear Force		Maximum Wave Bending Moment	
		[kN/m]	[-]	[MN]	[-]
1 cushion	(ACSS 1)	3357	70%	119	57%
2 cushions	(ACSS 2)	2832	59%	117	56%
14 cushions	(ACSS 3)*	3175	66%	118	56%
Barge		4783	100%	210	100%

* Cushions connected

2.8 Conclusions

The results of model tests show that the behavior of aircushion supported structures can be well predicted by means of a three-dimensional linear potential method. The computations have shown that aircushions may significantly influence the behavior of floating structures.

The merits of an aircushion supported structure are significant if the structure is supported by a single aircushion. In this case the roll and pitch motions are small and the mean second order drift forces may be smaller than those of a conventional barge. This results in a less distorted wave field, which is due to the fact that the waves can travel more freely underneath the structure.

In addition, it is possible to alter the dynamic behavior of aircushion supported structures by changing the air pressure within the cushions. Especially the heave motions and natural roll frequencies are sensitive to a change in aircushion characteristics.

Moreover, aircushions may significantly reduce the wave induced bending moments of the structure. An example in this chapter shows that aircushions can theoretically reduce the RAO of the wave induced bending moment by 96%. However, in practice a reduction of 44% is more realistic.

Although a large single cushion shows good results, the largest reduction of the wave induced structural loads is obtained if the structure is supported by two aircushions in longitudinal direction. On the other hand, a significant reduction of the wave induced shear forces and bending moments may also be obtained by interconnecting the aircushions.

Overall the results have shown that an aircushion supported structure can be a good alternative for large floating structures. In addition, the computational method proves to be a suitable tool to optimize cushion configurations for a particular application.

Chapter 3

Flexible aircushion supported structures

3.1 Introduction

It is common practice in seakeeping theory to describe the displacements of a floating body in the six rigid-body modes surge, sway, heave, roll, pitch and yaw. This approach is appropriate when the structure is considered to be stiff, i.e. when the eigenfrequencies of the elastic deflections are substantially higher than the frequency of the wave loads. On the other hand, the structure is considered to be elastic when the eigenfrequencies of the flexible modes fall within the spectrum of the wave loads. In case of an elastic structure, the structural analysis and hydrodynamic analysis should be coupled, this is called hydroelastic analysis.

Several examples of floating structures are described in the literature in which elastic deflections play a significant role in the dynamic behavior. Often these structures are relatively long and slender, resulting in a low bending stiffness. Examples of floating structures in which the elastic behavior may be significant are floating airports [43], large containerhips [44], FPSOs [38], large aircushion supported structures [73] and the Mobile Offshore Base [40].

In general, the hydroelastic behavior of floating bodies consists of a hydromechanical and a structural component. The hydromechanical component describes the fluid induced forces on the floating body, while the structural component describes the deformations of the structure in the absence of the fluid. There are many different approaches to solve the fluid-structure interaction between the floating body and surface water waves. Two commonly used basic methods are the modal expansion method and the direct method.

The modal expansion method combines the hydrodynamic analysis of the wet body with the dynamic analysis of the dry body in vacuum. Since the mode shapes are affected by the hydrodynamic pressure field, they cannot be specified in advance. Therefore the distortion of the

dry body is decomposed in an arbitrary number of vibration modes, which are then used in the hydromechanical analysis. The final distortion of the body is the sum of an arbitrary number of principal modes. This method was developed by Bishop and Price in 1979 [5]. Since this date adjustments and extensions to this theory have been made by various authors [43, 49]. Nevertheless, the first general theory is still valid and widely accepted for its practical use and numerical efficiency.

The direct method solves the deflections of the body directly without expanding the body motions into eigenmodes. Several direct methods are presented by Ohkusu and Namba [51], Kashiwagi [36], Hermans [22], Gueret [21] and Andrianov [3].

Different techniques have to be used to compute the hydroelastic behavior of aircushion supported structures. Tsubogo and Okada [70] modeled the structure as an elastic plate with finite breadth and infinite length. The air inside the cushion was assumed to be incompressible and was described by potential theory. Shallow water approximations were used to describe the fluid around the structure and the air inside the cushion.

Ikoma et. al. [23, 28, 31] use a linear potential method to compute the wave forces and wave elevations inside the aircushion. A two-dimensional modal expansion method is used to compute the vertical distortions of the body. Distortions in the horizontal plane are not taken into account in this approach.

The next two paragraphs describe a new three-dimensional method to compute the hydroelastic behavior of large aircushion supported structures in the frequency domain. The time domain is not considered since wave loads acting on large floating structures are generally non-impulsive, continuous and of first order. The last sections of this chapter describe the validation and verification of the new numerical method by making use of experimental results and analytical computations. The effect of aircushions on the dynamic behavior and structural loads of flexible floating structures will be discussed as well.

3.2 Structural model

The first part of the analysis of the hydroelastic behavior of a floating body starts with the structural model. In outlining the hydroelastic theory, a flexible body of arbitrary shape will be considered which possesses rigid-body modes as well as modes of distortion. The body will also be free to float without any restraints. If the body is fixed in some way or another, there are no rigid-body modes and modifications of the boundary conditions are needed.

A Finite Element Method (FEM) is a convenient way to model the structural properties of a dry three-dimensional body and to obtain the natural frequencies and modes shapes in vacuum. In line with this method the structure is modeled by a finite number of elements each having constant mass and stiffness properties (m , E , G , I). The nodes of the elements will be subjected

to generalized displacements $\mathbf{U} = \{U_1, U_2, \dots, U_n\}$ where n denotes the number of nodes of each element concerned. The matrix equation of motion for an element may be replaced by a general equation of motion which may be expressed as follows:

$$\mathbf{M}\ddot{\mathbf{U}} + \mathbf{B}^*\dot{\mathbf{U}} + \mathbf{K}\mathbf{U} = \mathbf{F} + \mathbf{Q} \quad (3.1)$$

where:

- \mathbf{M} = structural mass matrix
- \mathbf{B}^* = structural damping matrix
- \mathbf{K} = structural stiffness matrix
- \mathbf{U} = vector of nodal displacements
- \mathbf{F} = vector of external forces
- \mathbf{Q} = vector of concentrated nodal loads

The matrices $\mathbf{M}, \mathbf{B}^*, \mathbf{K}$ contain $n \times n$ submatrices, each of which contains 6×6 elements. These matrices are real and symmetric since they are associated with the dry structure. The nodal displacements are harmonic and may be written as:

$$\mathbf{U} = \mathbf{D}e^{-i\omega t} \quad (3.2)$$

If the damping term is ignored the previous equations result in the following characteristic equation:

$$(\mathbf{K} - \omega^2 \mathbf{M}) \mathbf{D} = 0 \quad (3.3)$$

The real and positive eigenvalues ω_r ($r = 1, 2, \dots, N$) are the dry natural frequencies, each associated with a characteristic dry eigenvector $\mathbf{D}_r = \{D_{r1}, D_{r2}, \dots, D_{rN}\}$, in which r is the principal mode and N represents the number of degrees of freedom of the dry structure. The generalized displacement vector at node j due to the r^{th} principal mode may be expressed as $\mathbf{D}_{rj} = \{u_r, v_r, w_r, \theta_{x_r}, \theta_{y_r}, \theta_{z_r}\}$. Physically, if one excites the structure with a harmonic oscillation at the natural frequency, the structure will oscillate at the same frequency and its spatial distribution will be given by the corresponding eigenvector.

3.2.1 Principal coordinates

The total deflection and distortion of the structure may be expressed as the sum of displacements in the principal modes. It follows that the matrix of nodal displacements may be expressed as:

$$\mathbf{U} = \sum_{r=1}^m p_r(t) \mathbf{D}_r \quad (3.4)$$

and the displacement at any point may then be expressed as:

$$\mathbf{u} = \{u, v, w\} = \sum_{r=1}^m p_r(t) \mathbf{u}_r \quad (3.5)$$

where the discretized structure is assumed to have m degrees of freedom and $p_r(t)$ is a set of principal coordinates. If $\mathbf{p} = \{p_1(t), p_2(t), \dots, p_m(t)\}$ then equation (3.4) may be rewritten as:

$$\mathbf{U} = \mathbf{D} \mathbf{p} \quad (3.6)$$

It is convenient to introduce a matrix of principal modes:

$$\mathbf{D} = [\mathbf{D}_1, \mathbf{D}_2, \dots, \mathbf{D}_m] \quad (3.7)$$

in which each column represents a principal mode. Making use of the orthogonality of the structural mass and stiffness matrices as presented in appendix C, the following relations are true:

$$\begin{aligned} \mathbf{D}^T \mathbf{M} \mathbf{D} &= \mathbf{a} \\ \mathbf{D}^T \mathbf{K} \mathbf{D} &= \mathbf{c} \end{aligned} \quad (3.8)$$

where \mathbf{a} and \mathbf{c} are the generalized mass and stiffness matrix respectively. Both matrices are diagonal such that $c_{ss} = \omega_s^2 a_{ss}$ in accordance with equation (3.3).

3.2.2 Equation of motion

If the expression for \mathbf{U} in equation (3.6) is substituted in the general equation of motion (3.1) and pre-multiplied by \mathbf{D}^T , it is found that:

$$\mathbf{a} \ddot{\mathbf{p}} + \mathbf{b} \dot{\mathbf{p}} + \mathbf{c} \mathbf{p} = \mathbf{f} + \mathbf{q} \quad (3.9)$$

with $\mathbf{f} = \mathbf{D}^T \mathbf{F}$, $\mathbf{q} = \mathbf{D}^T \mathbf{Q}$ and $\mathbf{b} = \mathbf{D}^T \mathbf{B} \mathbf{D}$ in accordance with equation (C.4). The principal coordinates may naturally be subdivided into two groups \mathbf{p}_R and \mathbf{p}_D associated with rigid-

body modes and distortion modes. The effect of the aircushion on the structure is not present in the structural analysis in vacuum since the stiffness coefficients are zero and aircushion elements have no mass. As such the matrix equation of motion may be partitioned:

$$\begin{bmatrix} \mathbf{a}_R & 0 \\ 0 & \mathbf{a}_D \end{bmatrix} \begin{bmatrix} \ddot{\mathbf{p}}_R \\ \ddot{\mathbf{p}}_D \end{bmatrix} + \begin{bmatrix} \mathbf{b}_R & 0 \\ 0 & \mathbf{b}_D \end{bmatrix} \begin{bmatrix} \dot{\mathbf{p}}_R \\ \dot{\mathbf{p}}_D \end{bmatrix} + \begin{bmatrix} \mathbf{c}_R & 0 \\ 0 & \mathbf{c}_D \end{bmatrix} \begin{bmatrix} \mathbf{p}_R \\ \mathbf{p}_D \end{bmatrix} = \begin{bmatrix} \mathbf{f}_R \\ \mathbf{f}_D \end{bmatrix} + \begin{bmatrix} \mathbf{q}_R \\ \mathbf{q}_D \end{bmatrix} \quad (3.10)$$

with $\mathbf{p} = \{\mathbf{p}_R, \mathbf{p}_D\}$, $\mathbf{p}_R = \{p_1, p_2, \dots, p_6\}$ and $\mathbf{p}_D = \{p_7, p_8, \dots, p_m\}$.

3.3 Hydromechanical model

The difference between hydroelastic and conventional hydromechanical computations lies in the fact that the latter approach only includes rigid-body modes. The fluid loading caused by the waves results in deflections of the flexible structure. These deflections are a combination of rigid-body motions and distortions. In this chapter it is assumed that the fluid is ideal (i.e. inviscid and incompressible) and its flow is irrotational. The rigid-body boundary conditions discussed in chapter 2.5 are still valid, but need to be extended with flexible modes. As such the complex potential ϕ may be decomposed in an undisturbed wave potential ϕ_0 , diffraction potential ϕ_d , radiation potentials ϕ_j of the body, and radiation potentials ϕ_c associated with the free surface of each aircushion:

$$\phi = -i\omega \left\{ (\phi_0 + \phi_d)\zeta_0 + \sum_{j=1}^{N_m} \phi_j x_j + \sum_{c=1}^{N_{AC}} \frac{1}{S_C} \iint_{S_C} \phi_c \zeta_c dS_C \right\} \quad (3.11)$$

where:

- x_j = body motion in the j -mode
- ζ_c = vertical motion of the free surface in cushion c
- S_C = free surface area of cushion c
- N_m = number of mode shapes, with $m \geq 6$
- N_{AC} = number of independent non-connected cushions

The number of mode shapes (N_m) corresponds to the sum of the six rigid-body modes and an arbitrary number of distortion modes (N_D):

$$N_m = 6 + N_D \quad (3.12)$$

Subsequently, the number of degrees of freedom of a flexible aircushion supported structure may be expressed as:

$$D.O.F. = N_m + \sum_{c=1}^{N_{AC}} N_c \quad (3.13)$$

in which N_c is the number of elements laying at the free water surface inside cushion c , N_{AC} is the number of aircushions.

The next step is to deduce the boundary conditions for each potential. If the source strengths for the diffraction potential are required, the normal velocity vector becomes:

$$n_{m(D.O.F. + 1)} = \frac{\partial \phi_d}{\partial n_m} = - \frac{\partial \phi_0}{\partial n_m} \quad (3.14)$$

where the panel index m covers the panels on the structure and n_m is the outward unit normal vector with respect to wetted surface of element m . The added mass and damping coupling coefficients are found by applying the following normal velocity requirement:

$$n_{mj} = \frac{\partial \phi_j}{\partial n_m} = \mathbf{n}^T \mathbf{u}_j \quad (3.15)$$

The vector \mathbf{n} contains the directional cosines n_{mj} and \mathbf{u}_j describes the distortion modes of the j^{th} modal shape. The normal velocities on the wetted elements of the structure are considered if $j = 1, 2, \dots, N_m$. On the other hand, the normal velocities associated with the cushion panels are considered if $j = N_m, N_m + 1, \dots, D.O.F.$, in this case $\mathbf{n} = \{n_1, n_2, n_3\} = \{0, 0, 1\}$ and $\mathbf{u}_j = \{u, v, w\} = \{0, 0, -1\}$ for one cushion element at each mode shape.

The generalized fluid force X_r may be expressed in terms of the pressure p on the wetted surface S of the structure as follows:

$$X_r = - \int_S \mathbf{n}^T \mathbf{u}_r p dS \quad (3.16)$$

The total linearized pressure may be found from Bernoulli's equation:

$$p = i\omega\rho\phi - \rho g z \quad (3.17)$$

The part associated with the potential ϕ may be subdivided into the following diffraction and radiation components:

$$X_r^d = i\omega \iint_S (\phi_0 + \phi_d) \mathbf{n}^T \mathbf{u}_r dS \quad (3.18)$$

$$X_r^r = i\omega \iint_S \phi_j \mathbf{n}^T \mathbf{u}_r dS \quad (3.19)$$

Accordingly the added mass and damping coefficients are:

$$A_{rj} = -\rho \operatorname{Re} \iint_S \phi_j \mathbf{n}^T \mathbf{u}_r dS \quad (3.20)$$

$$B_{rj} = -\rho \omega \operatorname{Im} \iint_S \phi_j \mathbf{n}^T \mathbf{u}_r dS \quad (3.21)$$

These restoring coefficients are associated with rigid-body modes C_R , distortion modes C_D and aircushion contributions C_C :

$$\mathbf{C} = \begin{bmatrix} \mathbf{C}_R & \mathbf{C}_{DR} & \mathbf{C}_{CR} \\ \mathbf{C}_{RD} & \mathbf{C}_D & \mathbf{C}_{CD} \\ \mathbf{C}_{RC} & \mathbf{C}_{DC} & \mathbf{C}_C \end{bmatrix} \quad (3.22)$$

Each restoring term may be subdivided into a hydrostatic C_{rj}^H and an aerostatic C_{rj}^A part:

$$C_{rj} = C_{rj}^H + C_{rj}^A \quad (3.23)$$

The restoring coefficients of the rigid-body modes C_R and aircushion contributions C_C are equal to those of the rigid-body approach as described by equations (2.40) to (2.52). The hydrostatic and aerostatic coefficients of the distortion modes (C_D) are expressed as:

$$C_{rj}^H = -\rho g \iint_S \mathbf{n}^T \mathbf{u}_r w_j dS, \quad r = j = 7, 8, \dots, m \quad (3.24)$$

$$C_{rj}^A = \frac{\kappa P_0}{V_c} \iint_{S_C} \mathbf{n}^T \mathbf{u}_r dS_C \iint_{S_C} \mathbf{n}^T \mathbf{u}_j dS_C, \quad r = j = 7, 8, \dots, m \quad (3.25)$$

with w_j being the vertical displacement of element j and S_c is associated with the dry elements of the structure laying at the edge of the aircushion.

Figure 3.1 shows the direction of the normal vectors of the elements in a transverse cross-section of an aircushion supported structure. The yellow section corresponds to the dry elements of the structure at the edge of the aircushion; these elements should be used in equation (3.25). The red panels are cushion elements at the free water surface inside the aircushion. Blue panels are located underneath the waterline and represent diffraction elements. White elements are located above the waterline and are not included in the linear diffraction computations. In addition, the figure shows that the normal vectors of the wet structural elements are directed outwards. Conversely, the (dry structural) elements associated with the aircushion are directed outward from the centre of the aircushion.

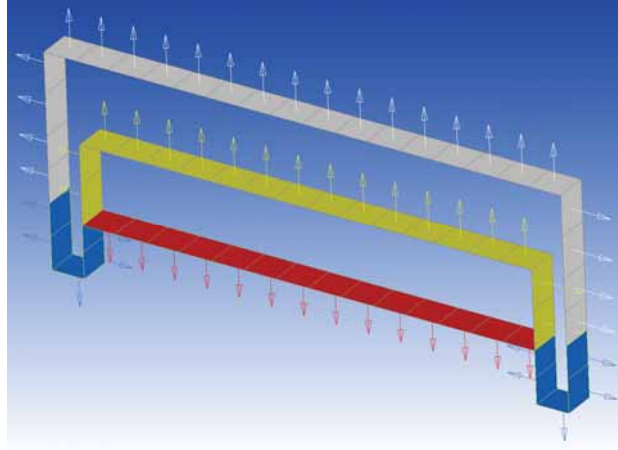


Figure 3.1: Normal vectors of the elements on the structure and free water surface within the aircushion

The hydrostatic coupling terms between the rigid-body and distortion modes (C_{RD}, C_{DR}) are:

$$C_{rj}^H = -\rho g \iint_S n_r w_j dS, \quad r = 1, 2, 3; j = 7, 8, \dots, m \quad (3.26)$$

$$C_{4j}^H = -\rho g \iint_S [n_3(y - y_G) - n_2(z - z_G)] w_j dS, \quad j = 7, 8, \dots, m \quad (3.27)$$

$$C_{5j}^H = -\rho g \iint_S [n_1(z - z_G) - n_3(x - x_G)] w_j dS, \quad j = 7, 8, \dots, m \quad (3.28)$$

$$C_{6j}^H = -\rho g \iint_S [n_2(x - x_G) - n_1(y - y_G)] w_j dS, \quad j = 7, 8, \dots, m \quad (3.29)$$

$$C_{rj}^H = 0, \quad j = 1, 2, 6; r = 7, 8, \dots, m \quad (3.30)$$

$$C_{r3}^H = -\rho g \iint_S \mathbf{n}^T \mathbf{u}_r dS, \quad r = 7, 8, \dots, m \quad (3.31)$$

$$C_{r4}^H = -\rho g \iint_S \mathbf{n}^T \mathbf{u}_r (y - y_G) dS, \quad r = 7, 8, \dots, m \quad (3.32)$$

$$C_{r5}^H = -\rho g \iint_S \mathbf{n}^T \mathbf{u}_r (x - x_G) dS, \quad r = 7, 8, \dots, m \quad (3.33)$$

The aerostatic coupling terms between the rigid-body and distortion modes (C_{RD}, C_{DR}) may be expressed as:

$$C_{rj}^A = \frac{\kappa P_0}{V_c} \iint_{A_c} \delta_r dS \iint_{S_c} \mathbf{n}^T \mathbf{u}_r dS_c \quad r = 1, 2, \dots, 6; j = 7, 8, \dots, m \quad (3.34)$$

$$C_{rj}^A = C_{jr}^A \quad j = 1, 2, \dots, 6; r = 7, 8, \dots, m \quad (3.35)$$

in which A_c is the aircushion area, $\delta_1 = \delta_2 = \delta_6 = 0$, $\delta_3 = 1$, $\delta_4 = y - y_G$ and $\delta_5 = x - x_G$. It is interesting to note that the hydrostatic coupling terms not necessarily result in a symmetric restoring matrix.

If the coupling between distortion modes and cushion elements is considered, the dry elements of the structure at the aircushion boundary (the yellow elements) should be included as well. The coupling coefficients between distortion modes and cushion elements (C_{DC}, C_{CD}) are:

$$C_{rj} = -\kappa P_0 \frac{A_j}{V_c} \iint_{S_C} \mathbf{n}^T \mathbf{u}_r dS_C, \quad r = 7, 8, \dots, m; j = m+1, m+2, \dots, m+N_c \quad (3.36)$$

$$C_{ij}^A = C_{jr}^A, \quad r = 7, 8, \dots, m; j = m+1, m+2, \dots, m+N_c \quad (3.37)$$

3.3.1 Equation of motion

For each wave frequency the displacement \mathbf{p} of the body may be written as:

$$\mathbf{p}(t) = \tilde{\mathbf{P}} e^{-i\omega t} \quad (3.38)$$

If the wave forces \mathbf{X} , added mass \mathbf{A} , damping \mathbf{B} and restoring coefficients \mathbf{C} of the freely floating structure in waves are known, the equation of motion may be written in the form:

$$\{-\omega^2 (\mathbf{a} + \mathbf{A}(\omega)) - i\omega \mathbf{B}(\omega) + (\mathbf{c} + \mathbf{C})\} \tilde{\mathbf{P}}(\omega) = \mathbf{X}(\omega) \quad (3.39)$$

In which \mathbf{a} and \mathbf{c} are the generalized mass and stiffness matrices of equation (3.8) respectively. Equation (3.39) may be subdivided into rigid-body modes, distortion modes and aircushion modes:

$$\left\{ -\omega^2 \begin{bmatrix} \mathbf{a}_R + \mathbf{A}_R & \mathbf{A}_{RD} & \mathbf{A}_{RC} \\ \mathbf{A}_{DR} & \mathbf{a}_D + \mathbf{A}_D & \mathbf{A}_{DC} \\ \mathbf{A}_{CR} & \mathbf{A}_{CD} & \mathbf{A}_C \end{bmatrix} - i\omega \begin{bmatrix} \mathbf{B}_R & \mathbf{B}_{RD} & \mathbf{B}_{RC} \\ \mathbf{B}_{DR} & \mathbf{B}_D & \mathbf{B}_{DC} \\ \mathbf{B}_{CR} & \mathbf{B}_{CD} & \mathbf{B}_C \end{bmatrix} + \begin{bmatrix} \mathbf{c}_R + \mathbf{C}_R & \mathbf{C}_{RD} & \mathbf{C}_{RC} \\ \mathbf{C}_{DR} & \mathbf{c}_D + \mathbf{C}_D & \mathbf{C}_{DC} \\ \mathbf{C}_{CR} & \mathbf{C}_{CD} & \mathbf{C}_C \end{bmatrix} \right\} \begin{bmatrix} \tilde{\mathbf{P}}_R \\ \tilde{\mathbf{P}}_D \\ \tilde{\mathbf{P}}_C \end{bmatrix} = \begin{bmatrix} \mathbf{X}_R \\ \mathbf{X}_D \\ \mathbf{X}_C \end{bmatrix} \quad (3.40)$$

It should be noted that the added mass coefficients, damping coefficients, displacement and wave forces in this matrix equation are frequency dependent as indicated in equation (3.39). Knowing the principal modes of the dry structure and having determined the principal coordinates, one may find the displacement at any point in the structure by:

$$\mathbf{u}(x, y, z, t) = \sum_{r=1}^m \mathbf{u}_r(x, y, z) p_r e^{-i \omega t} \quad (3.41)$$

Other quantities like bending moments, shear forces, stresses, etc. may be determined in a similar manner by using the appropriate characteristic function of the dry structure.

3.4 Numerical results and discussion

This section describes the results of the new hydroelastic method for flexible aircushion supported structures. First, the natural frequencies of a large flexible floating body with and without aircushions will be discussed. Next, the numerical and experimental results of a flexible barge will be discussed. Finally the dynamic behavior and internal loads of different flexible aircushion supported structures will be discussed and compared with those of a conventional flexible structure.

3.4.1 Natural frequencies

The first step in the validation process of the new hydroelastic model for aircushion supported structures concerns the natural frequencies of a long slender floating body. If the mass is equally distributed over the length of the body, it is appropriate to simplify the structure by a beam model. In this case beam theory may be applied and the dry natural frequencies ω_{di} associated with the i^{th} distortion mode of a dry structure in vacuum are:

$$\omega_{di} = \frac{\lambda_i^2}{L^2} \sqrt{EI/m}, \quad i = 1, 2, 3 \dots \quad (3.42)$$

in which L is the length of the beam, E the modulus of elasticity, m the mass per unit length and I the area moment of inertia about the neutral axis. λ_i is a non-dimensional parameter depending on the distortion mode and boundary conditions applied to the beam. If the beam is free to oscillate without restraints, $\lambda_1 = 4.73$, $\lambda_2 = 7.85$, $\lambda_3 = 11.00$, $\lambda_4 = 14.14$, $\lambda_5 = 17.28$ and $\lambda_i = \frac{1}{2}(2i+1)\pi$ for $i > 5$ [6].

In order to calculate the natural frequencies of the distortion modes of the wet structure, the fluid underneath the structure may be modeled as vertical springs and masses. In this case the general theory for a *beam on elastic foundation* may be applied and the natural frequencies ω_{ni} are:

$$\omega_{ni} = \sqrt{\omega_{di}^2 + \frac{c}{m}}, \quad i = 1, 2, 3 \dots \quad (3.43)$$

in which $c = \rho g A_w / L$ being the hydrostatic stiffness per unit length. If the wet natural frequencies are to be considered, the mass of the system is equal to $m = (\Delta + A_{rr}) / L$ with Δ being the mass of the structure. The sway added mass A_{22} should be used for distortion modes in the horizontal plane, and the heave added mass A_{33} for vertical bending modes.

In the remainder of this section a flexible floating beam with a length of 500 m will be considered. The inner and outer core are made of different materials as shown in figure 3.2. The inner core is made of solid steel with a height of 0.5 m, a width of 1.3 m, a Poisson ratio of 0.30, density of 7850 kg/m³ and modulus of elasticity of 2.10E+11 Pa. This core was modeled by 200 beam elements in the finite element program *NX Nastran*. The material around the core has a total weight of 11,250 kg and was modeled as non-structural mass equally distributed over the beam elements of the inner core.

The body is freely floating at a draft of 0.5 m in a fluid with a density of 1,025 kg/m³. As a result the wet natural frequencies will change with respect to the dry structure according to equation (3.43). The first five natural frequencies of the horizontal and vertical bending modes are presented in tables 3.1 and 3.2 respectively. It should be noted that damping is omitted in the computations of the natural frequencies. The second column shows the dry results of the structure in vacuum according to equation (3.42). The third column shows the semi-analytical eigenfrequencies based on equation (3.43) with use of added mass and restoring coefficients as computed by the new program *DelAir*. The fourth column shows the results of the program *HydElast* (developed by J.T. Tuitman) by making use of the output of the diffraction program *PreCal* (developed at MARIN). The eigenfrequencies computed by the new program *DelAir* are presented in the last column.

As the added mass is frequency dependent, several iterations had to be performed by both hydroelastic programs *DelAir* and *HydElast* before the computed eigenvalue corresponded to the frequency of the added mass. The results of all methods presented in tables 3.1 and 3.2 correspond well, which shows that the wet natural frequencies can be well predicted by the new program.

Table 3.1: *Natural frequencies (rad/s) of horizontal bending modes of a flexible (floating) beam*

Mode	Analytical Dry	Semi-Analytical Wet	HydElast / PreCal	DelAir
1	0.173	0.156	0.160	0.156
2	0.478	0.428	0.432	0.429
3	0.937	0.826	0.835	0.827
4	1.548	1.383	1.387	1.380
5	2.313	2.194	2.154	2.188

Table 3.2: Natural frequencies (rad/s) of vertical bending modes of a flexible (floating) beam

Mode	Analytical	Semi-Analytical	HydElast /	DelAir
	Dry	Wet	PreCal	
1	0.067	1.607	1.588	1.605
2	0.184	1.608	1.591	1.606
3	0.360	1.612	1.601	1.607
4	0.596	1.621	1.618	1.612
5	0.890	1.639	1.642	1.621

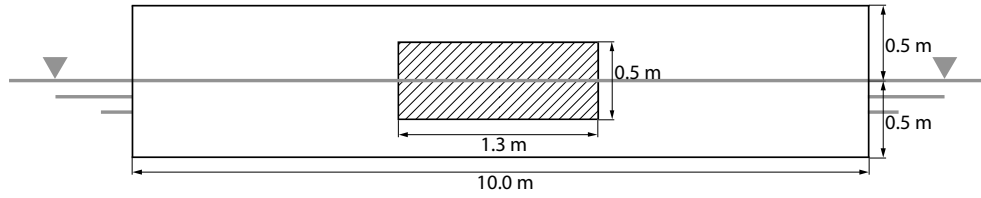


Figure 3.2: Cross-section of the floating rectangular beam

The next step is to subdivide the rectangular beam in several aircushion compartments in order to show the effect of the air chambers on the natural frequency of the structure. The main dimensions of the beam remain the same and the draft of the free-surface within the aircushions is equal to the draft of the beam. As such, the displacement of the beam will not change. Since the aircushion compartments have no effect on the natural frequencies of horizontal bending modes, only vertical bending modes will be discussed in the remainder of this section.

If the structure is completely supported by one aircushion, the natural frequencies of the vertical bending modes are almost equal to those of the dry structure in vacuum. This is illustrated in the third column of table 3.3 and can be explained by the fact that the volume variation of the aircushion due to the deflection of the structure is nearly zero. In other words, the mean water level inside the cushion does not change and added mass and hydrostatic restoring coefficients are approximately zero. As a consequence, the wet eigenvalue problem of a single aircushion supported structure is equal to the dry eigenvalue problem of the same structure in vacuum.

The first five vertical bending modes of the beam supported by one aircushion are shown in figures 3.3 to 3.7. The nodes of the different bending modes are located on the thin red horizontal line where the displacement is zero. The volume of the aircushion underneath the body does not change if the average deflection is zero. In this case the following expression is true:

$$\sum_{i=1}^{n+2} A_i = 0 \quad (3.44)$$

with n being the n^{th} vertical bending mode.

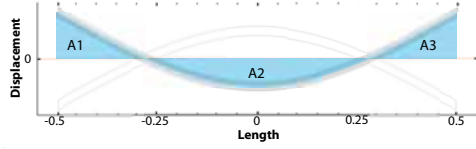


Figure 3.3: First vertical bending mode

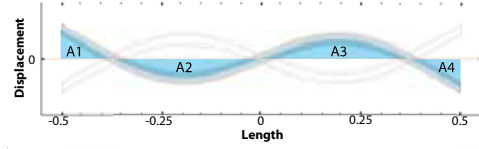


Figure 3.4: Second vertical bending mode

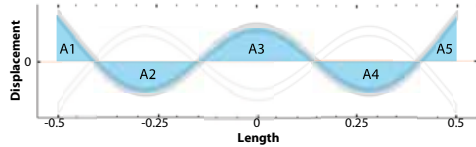


Figure 3.5: Third vertical bending mode

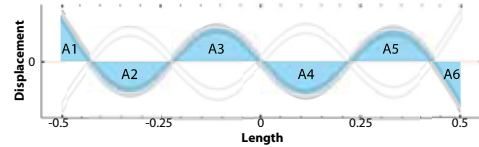


Figure 3.6: Fourth vertical bending mode

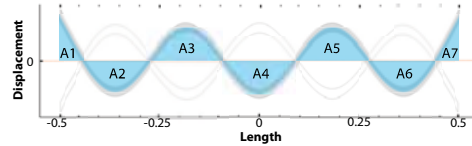


Figure 3.7: Fifth vertical bending mode

Table 3.3: Natural frequencies (rad/s) of the vertical bending modes of a rectangular beam supported by one aircushion

Mode	Analytical	DelAir
	Dry	Wet
1	0.067	0.062
2	0.184	0.181
3	0.360	0.359
4	0.596	0.594
5	0.890	0.888

Tables 3.2 and 3.3 show that the effect of an aircushion on the eigenfrequencies of a flexible floating structure is significant in this example. To show the effect of aircushions on the natural modes of the structure, two other cushion configurations will be discussed.

The first additional example consists of a configuration in which four cushions of 125 m long are equally distributed over the length of the body. The second additional configuration consists of fifty cushions in longitudinal direction, each having a length of 10 m. Both configurations are completely supported by air, i.e. 100% of the buoyancy is provided by the aircushions, this was also the case for the single aircushion supported structure. The height of all cushions is 1 m, the ambient air pressure is 1000 hPa and the main dimensions of all structures are equal.

The deflections of the vertical bending modes significantly change when the structure is supported by four aircushions. The first bending mode, associated with the smallest eigenvalue, is dominated by the volume variations of the aircushions. These volume variations are smallest when the nodes of the distortion mode are located at the centers of the cushions.

If the beam is supported by four aircushions, the cushion volume variations are nearly zero in case the structure is oscillating in its third dry vertical bending mode. As a result this dry mode will be the first wet mode since the volume variations of the first and second dry mode are significantly larger. Figure 3.8 shows the first wet vertical bending mode in which the vertical red lines represent the walls between the aircushion compartments. Figures 3.8 to 3.11 show the volume variations of the cushions in the first four wet vertical bending modes. As a result equation (3.44) will be valid for each of the four aircushions. In these situations the wet natural frequencies correspond to the dry structure in vacuum as shown in table 3.4, which includes the natural frequencies of the body. The second wet mode is a superposition of the second and fourth dry mode, as a result there is a difference between the fourth dry and the second wet eigenfrequency.

The fifth wet principal mode, shown in figure 3.12, is dominated by the first dry mode. For this reason equation (3.44) is not valid and the natural frequency may be computed analytically by equation (3.43). This result is included in the third column of table 3.4 and agrees well with the computed results in column five. The sixth wet eigenfrequency shown in figure 3.13, is mainly dominated by the second dry mode and is accurately predicted by the new program *DelAir*.

Table 3.4: Natural frequencies (rad/s) of the vertical bending modes of a rectangular beam supported by four aircushions

Mode Dry	Analytical Dry	Semi-Analytical Wet	Mode Wet	DelAir Wet
3	0.360		1	0.346
4	0.596		2	0.451
5	0.890		3	0.837
6	1.242		4	1.225
1		1.580	5	1.568
2		1.581	6	1.581

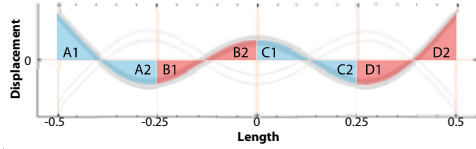


Figure 3.8: first vertical bending mode of a beam supported by four aircushions

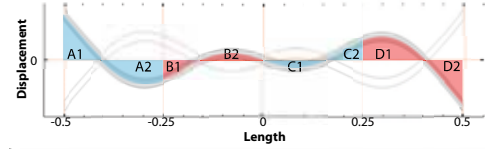


Figure 3.9: second vertical bending mode of a beam supported by four aircushions

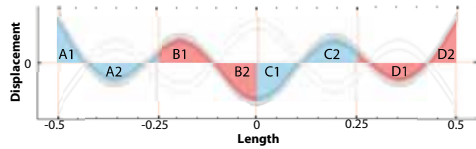


Figure 3.10: third vertical bending mode of a beam supported by four aircushions

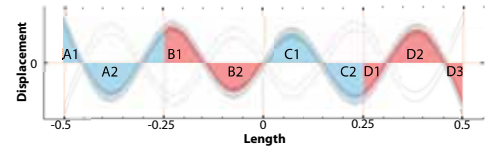


Figure 3.11: fourth vertical bending mode of a beam supported by four aircushions

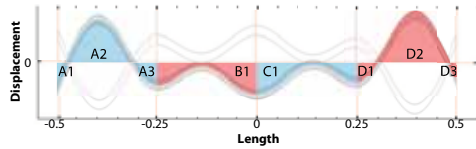


Figure 3.12: fifth vertical bending mode of a beam supported by four aircushions

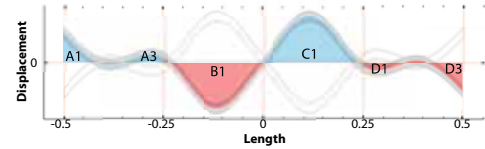


Figure 3.13: sixth vertical bending mode of a beam supported by four aircushions

The natural frequencies of a beam supported by 50 cushions correspond well with those of a conventional floating beam. The size of the cushion compartments is relatively small compared to the length of the body. As a result the effect on the eigenfrequencies of the floating body will be small as well. For this reason the natural frequencies presented in table 3.5 agree well with those of the conventional beam (table 3.2) and may be computed by the semi-analytical equation (3.43). The small difference in natural frequencies is due to the restoring coefficient, which is smaller for a beam supported by fifty aircushions than for a non-air supported beam.

Table 3.5: Natural frequencies (rad/s) of the vertical bending modes of a rectangular beam supported by fifty aircushions

Mode	Analytical	Semi-Analytical	DelAir
Dry	Dry	Wet	Wet
1	0.067	1.575	1.571
2	0.184	1.576	1.571
3	0.360	1.581	1.573
4	0.596	1.590	1.595
5	0.890	1.608	1.613

3.4.2 Fluid-structure interaction

Malenica et. al. [43], Remy et. al. [58], Tomašević [69] and Senjanović et. al. [59] described different series of model tests of an elastic barge in regular and irregular waves. All models in the experiments consisted of twelve caissons which were separated by narrow gaps and connected at deck level by one or two steel beams. These experiments were used to validate the new hydroelastic program. Due to the extensive test program it is not possible to present all data in this dissertation. For this reason a selection of the most relevant results was made.

The first floater of the flexible barge has a beveled shape as shown in figure 3.14. Its mass is 10 kg and the roll radius of gyration (K_{xx}) is 213 mm. The other eleven caissons are rectangular and the main particulars are shown in table 3.6.

Table 3.6: Main particulars of the flexible barge

Length	190	mm	KG	163	mm
Width	600	mm	K_{xx}	225	mm
Depth	250	mm	Mass	13.7	kg
Draft	120	mm			

According to Remy et. al. [58] the centre of gravity of the bow caisson above keel level (KG) is 87 mm. This value seems unrealistic compared to the shape and KG-value of the other caissons. For this reason a KG-value of 163 mm is used for the bow caisson in the new computations, which is similar to the other caissons.

All caissons are separated by gaps of 15 mm which makes the total length of the structure 2.445 m. The beam on top of the caissons is located 307 mm above keel level and has a length of 2.445 m. Its cross section is 1 cm², bending stiffness 175 Nm² and torsional stiffness 135 Nm².

The structural model was made in *NX Nastran* and consisted of 501 beam elements with concentrated loads representing the floaters. The hydromechanical model consists of 1100

diffraction elements. The gaps between the floaters are modeled by 220 elements which are not included in the computations of added mass, damping and wave forces. The panel model is segmented in a way that the translations and rotations of elements associated with a particular caisson are equal. In other words, these elements will not deform, contrary to the elements laying in the gaps between the caissons which are free to move and deform. Figure 3.15 shows the panel model used for the hydroelastic diffraction computations. Obviously, the elements above the waterline are excluded from the diffraction computations.

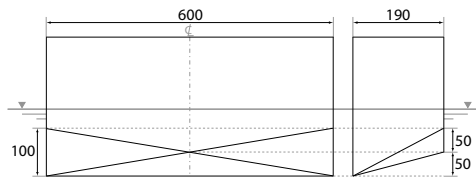


Figure 3.14: Geometry of the bow caisson

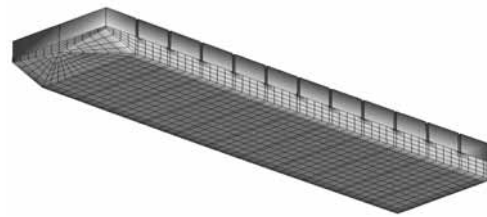


Figure 3.15: Panel model for diffraction computations

Caisson 1 is the bow caisson and the stern corresponds to caisson 12. The motions of the barge were measured in six degrees of freedom at six locations illustrated by red circles in figure 3.16. These measurement points are located at the deck levels of caissons 1, 3, 5, 7, 9 and 12.

Decay tests for different degrees of freedom were performed in order to obtain the natural frequencies, viscous damping and structural damping. These tests included horizontal bending, vertical bending and torsion modes. Vertical bending was the measured difference in pitch angle between the first caisson (C1) and the last caisson (C12). Horizontal bending is the difference in yaw angle between C1 and C12 and torsion the difference in roll angle.

The natural frequencies of the vertical bending (VB), horizontal bending (HB) and torsion mode are shown in table 3.8. It should be noted that damping is not included in the calculations of the eigenfrequencies by the new program. The effect of damping on the eigenfrequencies of the structure is small and may be neglected.

The table shows that the calculated natural frequencies agree well with those of the decay tests. For comparison, the results of Tomašević and Senjanović [69, 59] are included in the same table. A graphical representation of the natural frequencies and the associated principal modes is shown in figures 3.17 to 3.22.

The viscous and structural modal damping in nine degrees of freedom obtained from the decay tests can be found in table 3.7. In addition, this table shows the additional damping that was used by Tomašević and Senjanović [69] and the calculations performed by the new program.

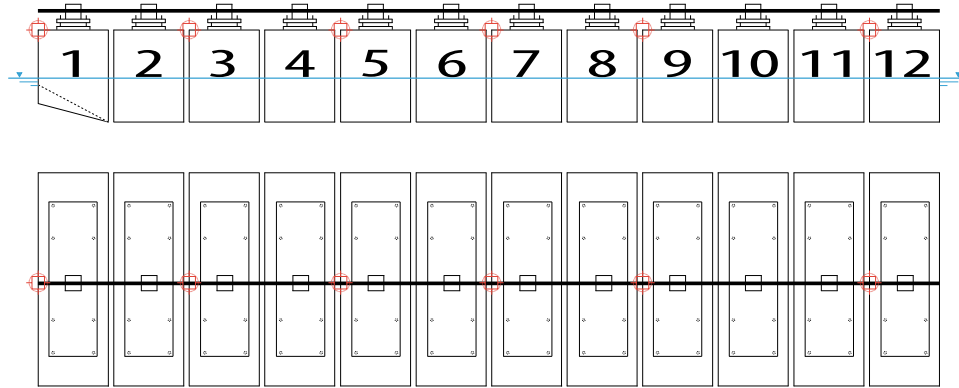


Figure 3.16: General arrangement of the flexible barge

Table 3.7: Additional modal damping as percentage of critical damping

Mode		Decay	Tomašević /	
		Tests	Senjanović	Calc.
1	Surge	2	0	2
2	Sway	4	0	4
3	Heave	6	5	6
4	Roll	4	5	7
5	Pitch	6	5	7
6	Yaw	5	0	5
7	Vertical Bending	7.5	5	7.5
8	Horizontal Bending	2.5	9	8.5
9	Torsion	2.5	7	4.5

Table 3.8: Natural frequencies of principal modes (rad/s)

	Remy et. al. (experiments)	Tomašević / Senjanović (computations)	DelAir (computations)
1st HB mode	4.72	5.32	4.59
1st VB mode	6.68	5.21	7.04
1st Torsion mode	7.48	7.92	7.80
2nd VB mode		12.37	12.08
2nd HB / torsion mode		12.70	13.25
3rd VB mode		21.08	20.38

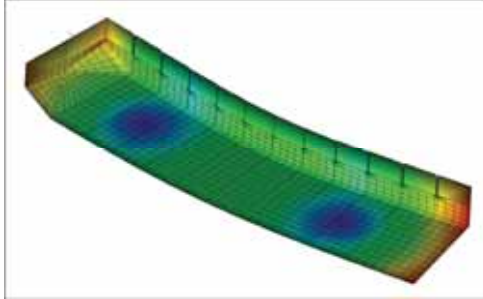


Figure 3.17: 1st HB mode 4.59 rad/s

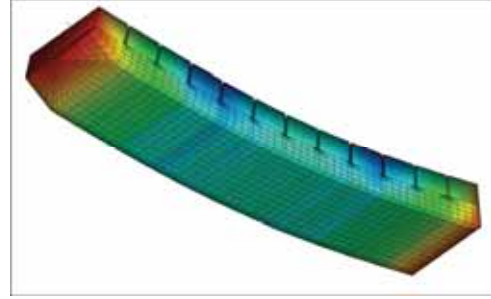


Figure 3.18: 1st VB mode 7.04 rad/s

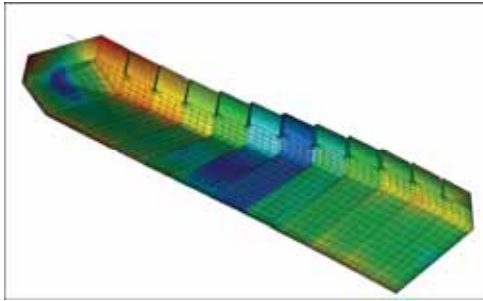


Figure 3.19: 1st torsion mode 7.80 rad/s

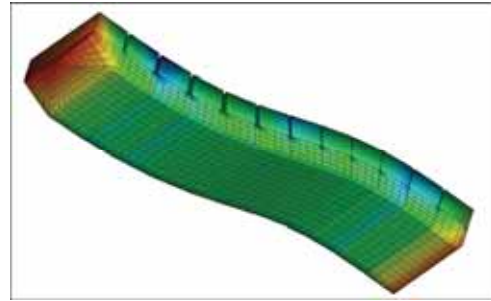


Figure 3.20: 2nd VB mode 12.08 rad/s

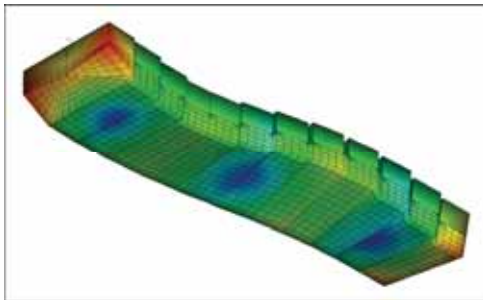


Figure 3.21: 2nd HB/torsion mode 13.25 rad/s

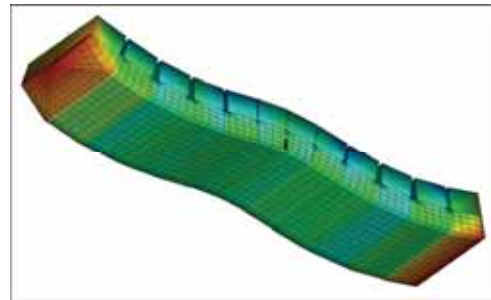


Figure 3.22: 3rd VB mode 20.38 rad/s

The experimental results and numerical Response Amplitude Operators (RAOs) of the freely floating flexible barge in waves from different headings are presented in figures 3.25 to 3.36. The experimental results in regular wave tests, which are illustrated by black dots, are obtained from Tomašević [69]. In addition the figures show the numerical results of Remy et. al. [58], Tomašević [69] and Senjanović et. al. [59].

The experiments were performed at the BGO-first basin in France, which has a length of 30 m and a width of 16 m. The water depth during the model tests was set to 1 m. The experimental results were first published by Remy et. al. [58] in 2006. Afterwards, Tomašević and Senjanović presented their numerical results in several publications in 2007 and 2008 [69, 59].

The experimental results in regular waves together with the numerical results of the above mentioned authors are shown in figures 3.25 to 3.36. These figures also include the results of calculations performed with the new hydroelastic program, which are presented by red lines.

The responses in head waves are shown in figures 3.25 to 3.29. The first figure shows the heave responses at the measurement points of caissons 1, 3, 5, 7, 9 and 12. These heave motions are largest at the bow and stern section and decrease towards the centre of the structure. Heave motions of caisson 7 are over-predicted by the new program, this is mainly due to collisions in the model tests between the centre caissons as indicated by red circles in figure 3.23. This figure shows the distortion of the structure in head waves of 201 mm wave height with a frequency of 4.8 rad/s, this condition was actually tested and the measurements are included in figures 3.25 to 3.29.

As mentioned before, the translations and rotations of the elements associated with each caisson are equal and follow the motions of the connection point at the beam located above the floaters. The elements in the gaps between the caissons are free to move and deform. For this reason it is possible that elements of different caissons coincide in certain situations. Obviously this is not possible in reality. In practice, the clash between the caissons results in non-linearities as illustrated in figure 3.24. In addition the collisions result in reduced heave and pitch responses of caisson 7 as shown in figures 3.25 and 3.27.

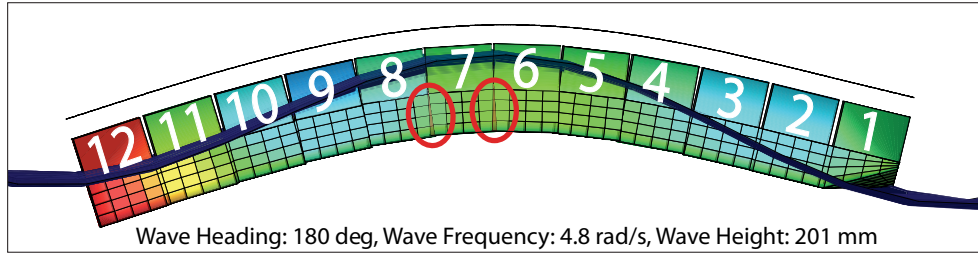


Figure 3.23: Collision between caissons in the centre of the body

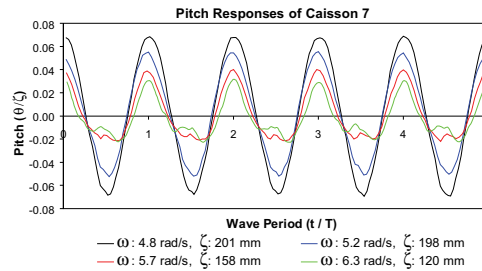


Figure 3.24: Time series of normalized pitch responses of caisson 7 in regular head waves

The collisions between the floaters are clearly visible at high frequencies in the time series, as shown in figure 3.24. On the other hand these effects are less pronounced at low wave frequencies due to the relatively slow distortion of the structure. The time series of caisson 7 were reanalyzed and the results are shown by black crosses in figures 3.25 and 3.27. The black dots are obtained from Tomašević[69].

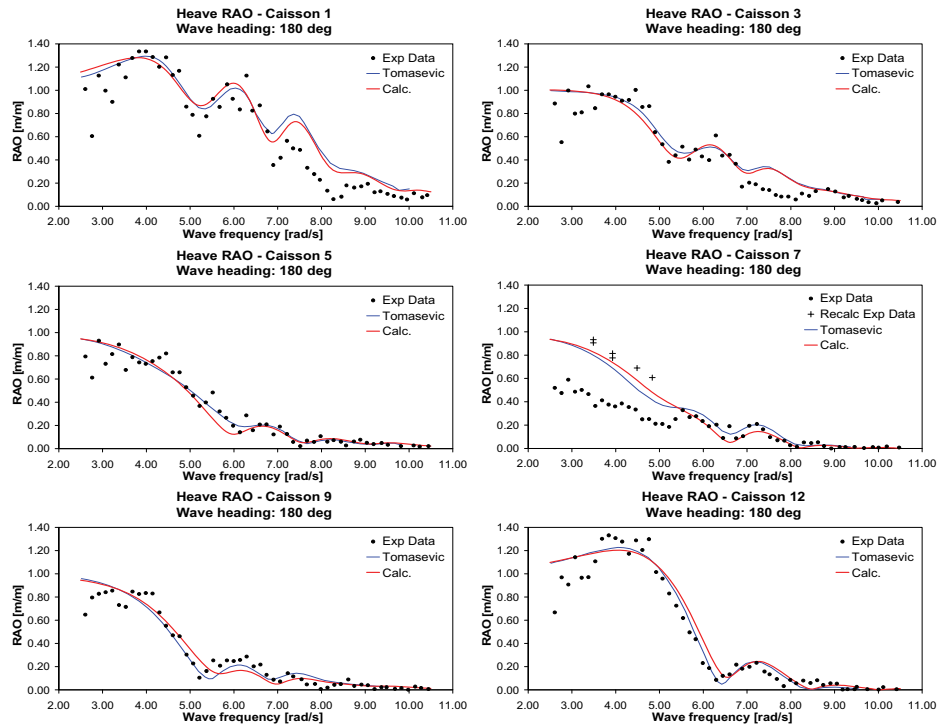


Figure 3.25: Heave RAOs of caissons 1, 3, 5, 7, 9 and 12 in head waves

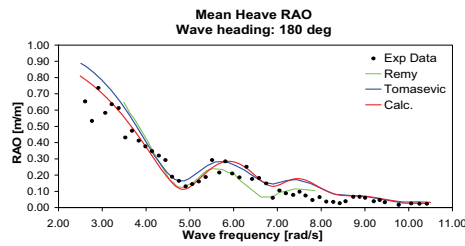


Figure 3.26: Mean heave RAO in head waves

The mean heave RAO, i.e. the average heave response of the six measurement points on caissons 1, 3, 5, 7, 9 and 12, is shown in figure 3.26. Despite the fact that the collisions of caisson 7 influence the heave responses, the experimental results of the mean heave motions show good agreement with numerical results.

Figures 3.27 and 3.28 show the pitch responses and indicate that there is a good agreement between experimental and numerical pitch responses of the floaters. However, there are discrepancies in the results of caisson 7 at the frequencies where collisions occur. Due to the good correlation between numerical and experimental results of caissons 1 and 12, the computed vertical bending of the structure corresponds well with the experimental results in figure 3.29.

In general there is a reasonable agreement between the numerical results of Remy, Tomašević / Senjanović and the new hydroelastic program, although there are some differences. Some of these differences were already presented in table 3.7, which contains the viscous and structural modal damping. In the new computations the additional damping was chosen in a way that the variance with the decay tests was minimized. As a result the additional damping used in the new computations corresponds better to those of the decay tests than the damping used by Tomašević and Senjanović.

Another difference is the variance in the natural frequencies of the distortion modes as shown in table 3.8. This is mainly the result of the difference in coupling between the structural model and hydromechanical model. Tomašević and Senjanović used a completely flexible model, in which the elements of each individual caisson may have different translations and rotations. This approach was not chosen in the new computations as described before. In addition, added mass and restoring coefficients associated with elements in the gaps between the caissons are not included in the iterative eigenvalue solutions of the new computations. The differences in the numerical approach result in differences in the eigenfrequencies as shown in table 3.8. As the assumptions made in the new approach are closer to those of the model tests, the eigenfrequencies computed by the new program are closer to the decay tests as well.

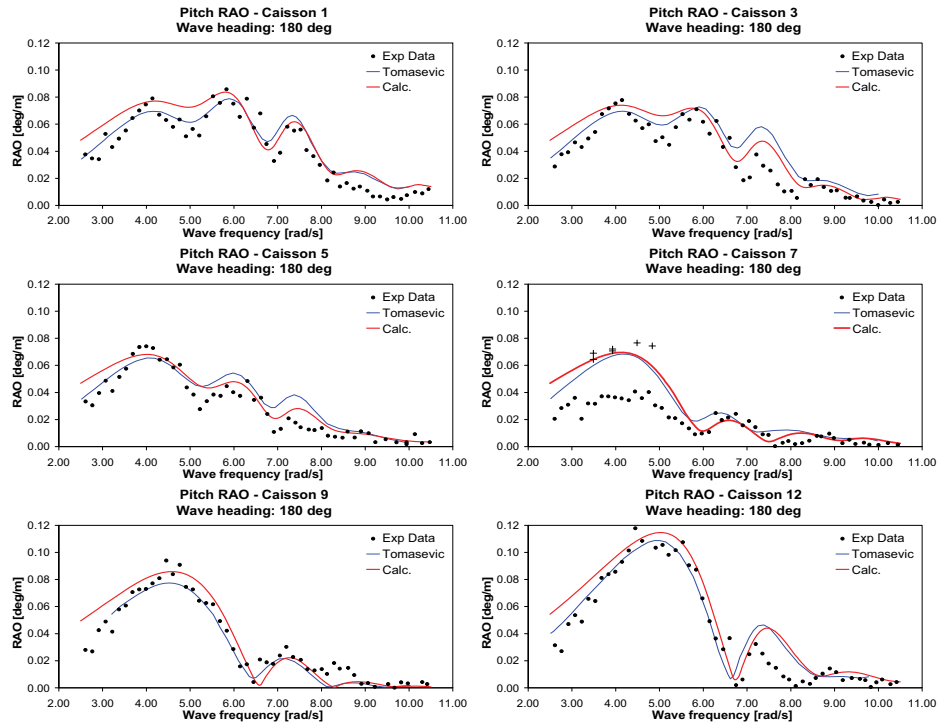


Figure 3.27: Pitch RAOs of caissons 1, 3, 5, 7, 9 and 12 in head waves

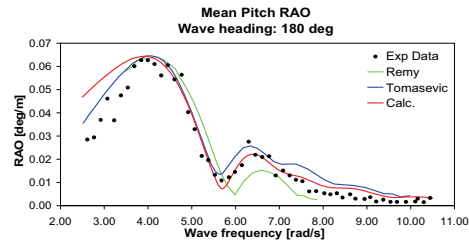


Figure 3.28: Mean pitch RAO in head waves

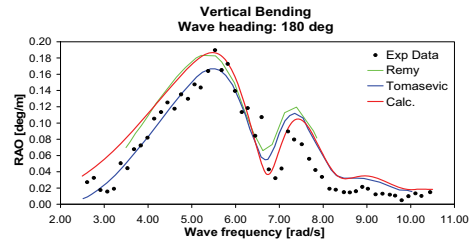


Figure 3.29: Vertical bending RAO in head waves

The RAOs of the flexible barge in quartering waves of 120 deg are presented in figures 3.30 to 3.36. Figures 3.30 and 3.31 show the roll responses of the six caissons and illustrate an excellent agreement between experimental results and the new numerical computations. The same conclusion may be drawn for the heave and pitch responses in figures 3.32 and 3.33. The difference in pitch responses with the results of Remy et. al. [58] at moderate frequencies is remarkable. Compared to other numerical methods, these results show a relatively large difference with model tests.

The distortion modes of vertical bending, horizontal bending and torsion are shown in figures 3.34, 3.35 and 3.36 respectively. The peaks in these figures correspond to the natural frequencies in table 3.8 and show some differences between the numerical methods.

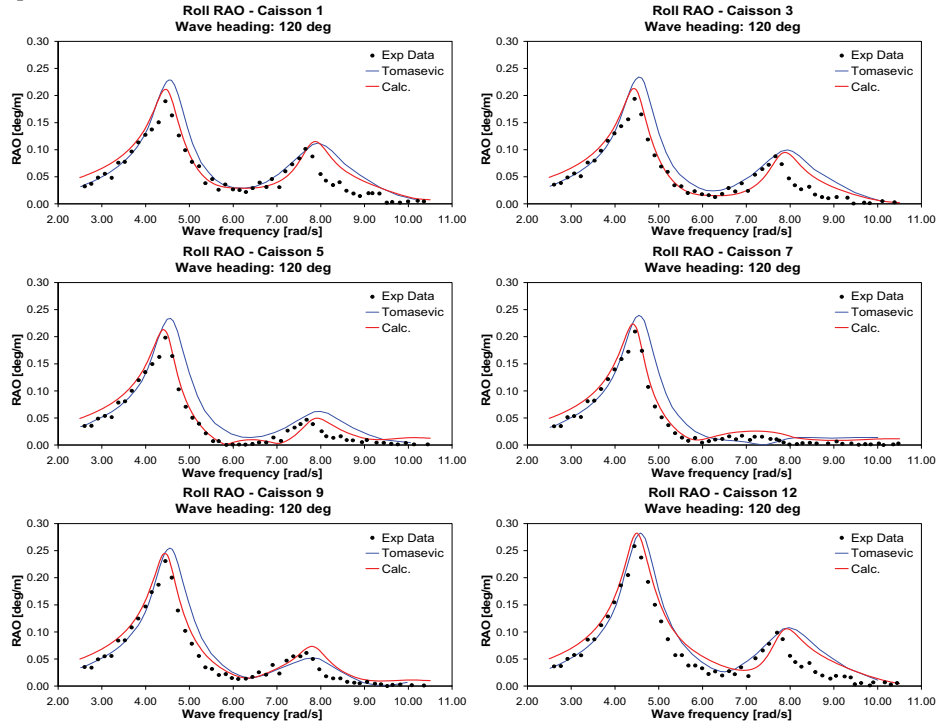


Figure 3.30: Roll RAOs of caissons 1, 3, 5, 7, 9 and 12 in quartering waves of 120 deg

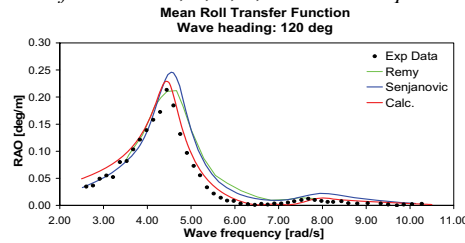


Figure 3.31: Mean roll RAO in quartering waves of 120 deg

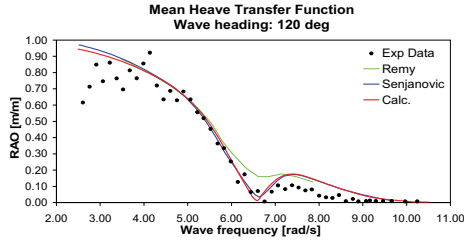


Figure 3.32: Mean heave RAO in quartering waves of 120 deg

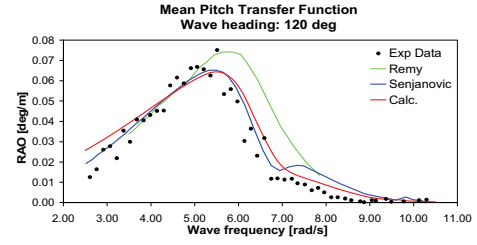


Figure 3.33: Mean pitch RAO in quartering waves of 120 deg

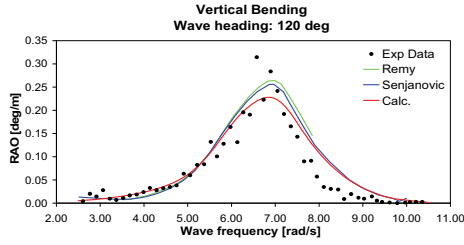


Figure 3.34: Vertical bending RAO in quartering waves of 120 deg

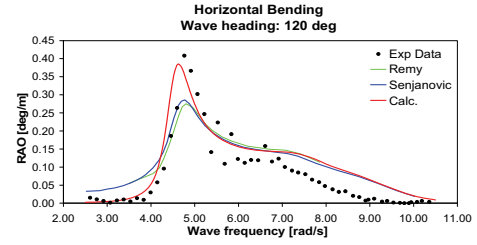


Figure 3.35: Horizontal bending RAO in quartering waves of 120 deg

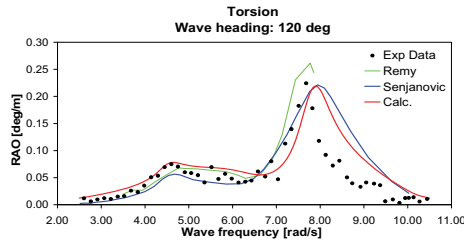


Figure 3.36: Torsion RAO in quartering waves of 120 deg

3.4.3 Fluid-gas-structure interaction

If the flexible barge is supported by aircushions, the interactions between the air underneath the structure, the fluid around the body and the distortion modes of the floater have to be taken into account. The method used to describe these so called fluid-gas-structure interactions in three-dimensions was described in section 3.3. This paragraph elaborates on the effect of aircushions on the dynamic behavior of a flexible floating body.

The flexible barge discussed in the previous section can be supported by aircushions in different ways. Only three possible aircushion configurations will be described in this paragraph, although many other aircushion configurations were analyzed. These three cases were selected since they best show the effect of the aircushions on the dynamic behavior of the floating structure.

The main dimensions of all aircushion configurations are equal to those of the flexible barge in paragraph 3.4.2. Nevertheless, there are some differences with the original flexible barge. In the first place, the bow caisson was replaced by a rectangular shape equal to the other caissons. Secondly, a caisson has no bottom plate in case it is supported by air, i.e. the bottom of the caisson is open to the fluid underneath the structure in a way that the fluid can freely flow in and out the caisson. Figure 3.37 shows the panel model of a flexible barge with twelve aircushion compartments. The figure only shows the elements of the body, the panels representing the free water surface of the aircushions are not included.



Figure 3.37: Bottom view of a panel model of an aircushion supported flexible barge

The first aircushion configuration consists of 24 cushions (24ac). All buoyancy is provided by the air underneath the floater. This means that the wall thickness of the caissons is equal to zero. In order to obtain sufficient transverse stability, each caisson is subdivided into two air chambers laying next to each other in transverse direction.

Figure 3.37 shows only the outer walls of the structure, the inner walls between the aircushions are not modeled. For this reason the coupling between the distortion modes of the body and the aircushions is solely described by the elements in the deck of the caissons. If one would incorrectly include the outer walls of the body in the structure-aircushion coupling without modeling the inner walls, the cushions would not be enclosed in the horizontal plane. This

means that the volume of the aircushion will change in case the considered caisson moves in the horizontal plane. Obviously this is incorrect and there are two ways to model an aircushion supported structure with multiple cushions. Either the complete structure has to be modeled, including the inner walls which compartmentalize the aircushions. In this case all structural elements that enclose the aircushion are included in the structure-air coupling. Or one models only the outer walls of the structure, which means that only the deck elements of the caissons should be included in the structure-air coupling as shown in figure 3.38. The colored elements in this figure correspond to the decks of the floaters and represent the 24 interactions between the structure and the 24 aircushions underneath. The dark color of the outer walls of the structure indicates that there is no coupling between the side walls and the cushions.

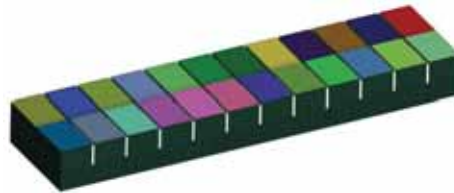


Figure 3.38: Top view of the structure showing the coupling with 24 aircushions

The second aircushion configuration consists of 6 cushions (6ac). These cushions are not equally distributed over the length of the structure as can be seen in figure 3.39 in which each color represents the top of an aircushion. The third configuration consists of 10 conventional caissons and four air chambers (4ac) as shown in figure 3.40. The bow and stern caisson are supported by two cushions in order to reduce the roll motions of the structure in quartering waves. The roll motions of the body will be significantly larger if the bow and stern caisson would be supported by only one caisson.

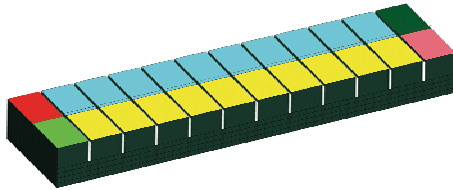


Figure 3.39: Top view of the structure showing the coupling with 6 aircushions

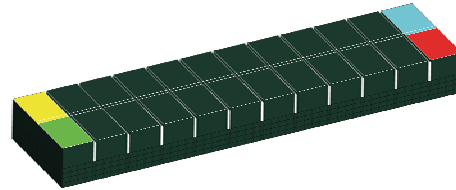


Figure 3.40: Top view of the structure showing the coupling with 4 aircushions

As was indicated before in paragraph 3.4.1, aircushions can significantly change the natural frequencies of the structure. This is also the case in the present situation where aircushions shift the natural frequency of the vertical bending and torsion modes. Table 3.9 shows the natural frequencies of the first order distortion modes of the conventional barge and the three aircushion supported structures.

Table 3.9: Natural frequencies of the first order distortion modes

	Conventional flexible barge	24 cushions	6 cushions	4 cushions + 10 caissons
1st HB mode	4.59	4.42	4.32	4.28
1st VB mode	7.05	6.49	6.39	6.52
1st Torsion mode	7.80	7.35	6.59	7.61

The computed RAOs of the conventional flexible barge and the three aircushion supported structures are presented in figures 3.41 to 3.49. The amount of modal damping added to the computations of these structures corresponds with the conventional barge (table 3.7).

In general, the heave motions of the aircushion supported structures are smaller than those of the conventional barge in head waves, this can be seen in figure 3.41. The mean pitch and vertical bending, presented in figures 3.42 and 3.43, show a significant difference between the conventional flexible barge and a structure supported by six cushions around 5.00 rad/s. This difference is particularly large at the bow and stern of the structure. This is illustrated in appendix D, which includes the heave and pitch responses at different locations at the structures. It should be noted that sloshing and piston modes which may occur in the aircushions of the present model are not included in the numerical analysis. These effects are of minor importance for full-scale aircushion supported mega-floaters.

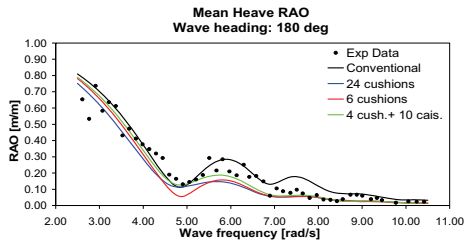


Figure 3.41: Mean heave RAO in head waves

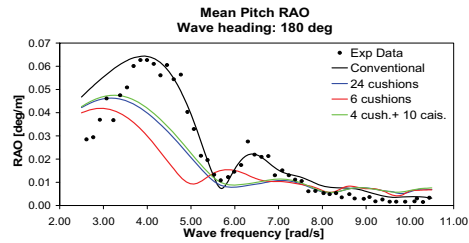


Figure 3.42: Mean pitch RAO in head waves

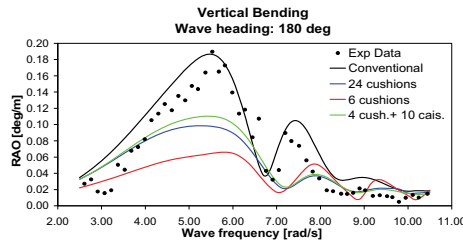


Figure 3.43: Vertical bending RAO in head waves

Figures 3.44 to 4.48 show the effect of the aircushions on the dynamic behavior in quartering waves of 120 deg. The aircushions considerably reduce the maximum roll and pitch motions as shown in figures 3.45 and 3.46

The difference in responses between head waves and quartering waves is remarkable. A structure supported by six cushions shows superior behavior in all degrees of freedom in head seas. Contrary, the torsion of the structure exceeds that of a conventional floating barge in quartering waves as can be seen figure 3.49. The torsion of the other aircushion configurations is relatively small in quartering waves, which is also the case for the vertical bending. However, the maximum vertical bending of these structures in head waves is considerably larger than that of a configuration with six cushions. Nevertheless, vertical bending of the conventional flexible barge in head waves is still significantly larger.

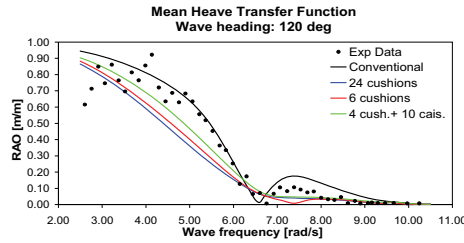


Figure 3.44: Mean heave RAO in quartering waves of 120 deg

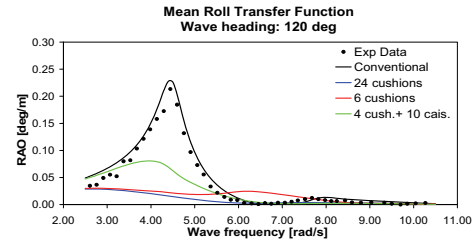


Figure 3.45: Mean roll RAO in quartering waves of 120 deg

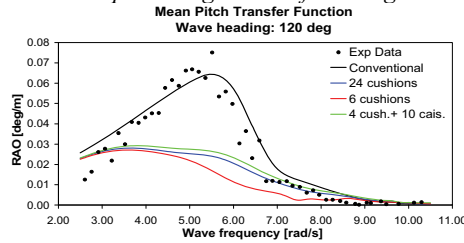


Figure 3.46: Mean pitch RAO in quartering waves of 120 deg

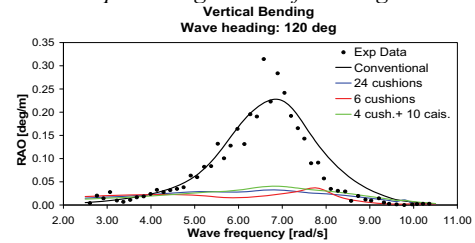


Figure 3.47: Vertical bending RAO in quartering waves of 120 deg

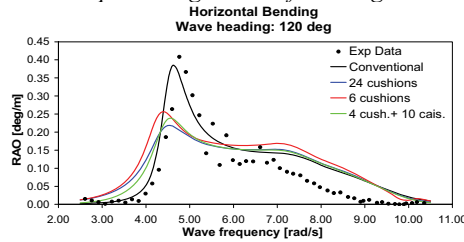


Figure 3.48: Horizontal bending RAO in quartering waves of 120 deg

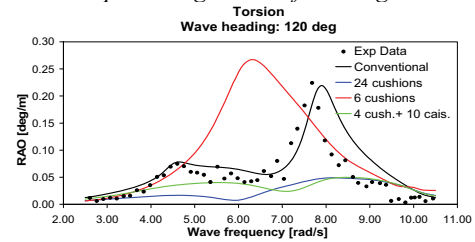


Figure 3.49: Torsion RAO in quartering waves of 120 deg

3.4.4 Structural loads

The structural loads play an important role in the design process of a floating body. The static and wave induced shear forces and bending moments have to be determined in the structural analysis.

This paragraph describes the structural loads of the aircushion configurations and compares the results with those of the conventional flexible barge. Unfortunately, there is no experimental data available to validate the numerical results directly. For that reason different methods were used to verify the numerical results which will be discussed in the next sections. In addition, a direct method will be discussed to compute the wave induced stresses of flexible floating structures.

Wave induced shear Forces and Bending Moments

The beam on top of the floaters will deform elastically when subjected to waves. The structural loads in the beam may be determined in a way that is analogous to the calculation of the displacement as described by equation (3.41). Euler-Bernoulli beam theory may be applied since the beam is uniform and slender. As a result the beam is considered to be a two-dimensional body and the expressions for the displacement (u), wave induced shear forces (V) and bending moments (M) may be reduced to:

$$u(x, t) = \sum_{r=1}^m u_r(x) p_r e^{i \omega t} \quad (3.45)$$

$$V(x, t) = \sum_{r=1}^m V_r(x) p_r e^{i \omega t} \quad (3.46)$$

$$M(x, t) = \sum_{r=1}^m M_r(x) p_r e^{i \omega t} \quad (3.47)$$

Normally it is assumed that the wave induced bending moments are largest in the centre of the structure. The structural loads amidships of the conventional flexible barge and the three aircushion configurations are presented in figures 3.50 to 3.52. These figures clearly show the effect of the aircushions on the structural loads of the floater. The maximum shear forces are approximately equal for the conventional barge and the 4ac and 24ac configurations. Contrary, the vertical shear forces of the configuration with six aircushions (6ac) are significantly smaller. This is especially the case when the length of the structure L corresponds to a multiple of the wave length λ :

$$\lambda = \frac{L}{n}, \quad \text{with } n = 1, 2, \dots \quad (3.48)$$

The frequencies associated with these wave lengths are 4.99, 7.10, 8.70 and 10.04 rad/s. In these situations, the air pressure variations within the two centre cushions are relatively small since they cover 10/12 of the length of the barge. This is graphically shown by the red lines in figure 3.53 which represent the mean waterline level inside the individual cushions. The distortion of the structure is small if equation (3.48) is valid, as a result the mean water level in the centre cushion will not change. On the other hand, the front part of the body deforms in regular waves of 6.00 rad/s due to an increase of the mean water level in the front cushion.

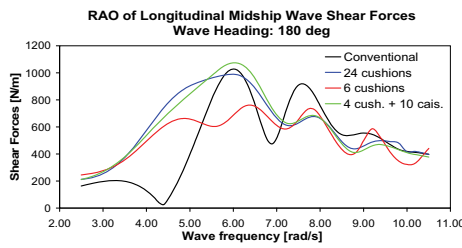


Figure 3.50: Horizontal wave induced shear forces

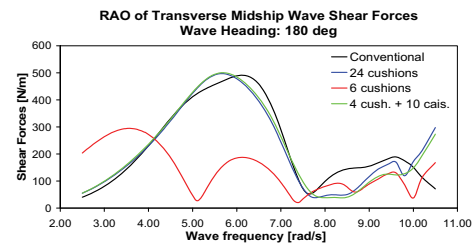


Figure 3.51: Vertical induced wave shear forces

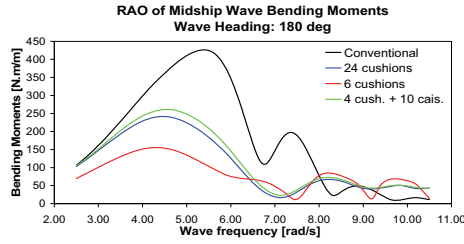


Figure 3.52: Midship wave induced bending moments

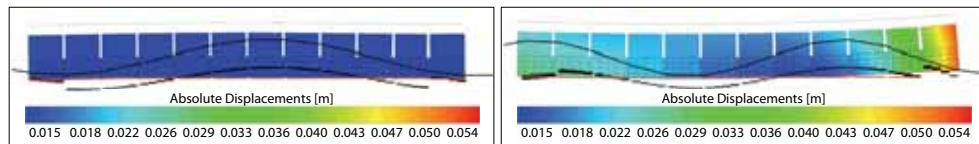


Figure 3.53: The bac structure at the time instant when the vertical shear forces are maximum in regular head waves of 5.10 rad/s (left) and 6.00 rad/s (right)

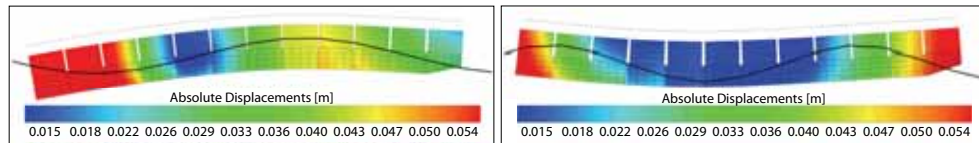


Figure 3.54: The conventional barge at the time instant when the vertical shear forces are maximum in regular head waves of 5.10 rad/s (left) and 6.00 rad/s (right)

For comparison, the deformation of the conventional flexible barge in regular waves of 5.10 and 6.00 rad/s at the instance when the vertical shear forces are largest is shown in figure 3.54. The figure clearly shows that the deformation of the conventional barge is significantly larger than the distortion of the 6ac structure in figure 3.53.

Figures 3.56 to 3.59 show the development of the vertical wave induced shear forces and bending moments over time in the beam on top of the floaters of all structures. If a structure is subjected to head waves, the extreme values of these internal loads move with the wave crests towards the aft of the body. This is clearly the case for the vertical wave induced shear forces and to a lesser extent for the bending moments of the conventional barge. The extreme values of the wave induced bending moments occur around the centre of the structure, which is normally expected for floating bodies in waves. This is also illustrated by figure 3.55 which shows the wave induced bending moment distribution according to the DNV rules for classification of ships [14]. According to these rules, the maximum wave induced bending moment is expected to occur between $-0.1 L$ and $0.15 L$, with a mean value at $0.03 L$ in the front part of the vessel. However, the maximum wave induced bending moments of the flexible barge occur in the aft part of the body as shown in figures 3.56 and 3.60. The latter figure shows the internal loads and distortion of the body in regular head waves at the time and wave frequency when the wave induced bending moments are largest. The maximum bending moment of the flexible barge in head waves occurs at $-0.05 L$ from the centre at 5.50 rad/s.

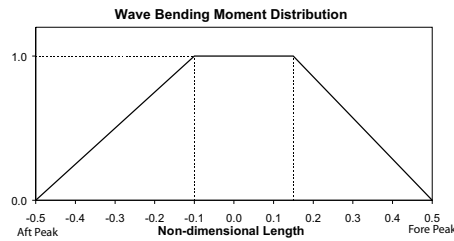


Figure 3.55: Wave induced bending moment distribution according to DNV rules [14]

The difference with the DNV rules increases for aircushion supported structures. The location at which the maximum wave induced bending moment occurs varies from $-0.12 L$ to $0.38 L$ for the 24ac and the 4ac configuration respectively. Figures 3.53 and 3.54 already indicated that the distortion of the aircushion configurations does not correspond to that of a conventional barge. As a result the distribution of the internal loads does not agree with that of the conventional barge.

The maximum wave induced bending moments of the 24ac and 6ac structure occur at the location where the bow caisson is connected to the beam as shown in figures 3.57 and 3.58. An

overview of the maximum wave induced bending moments along the length of the beam, for all wave frequencies from 2.50 to 10.50 rad/s, is shown in appendix D. The maximum wave induced bending moment in the beam on top of the 24ac configuration occurs in waves of 7.60 rad/s. For the 6ac configuration this is the case at a wave frequency of 7.70 rad/s.

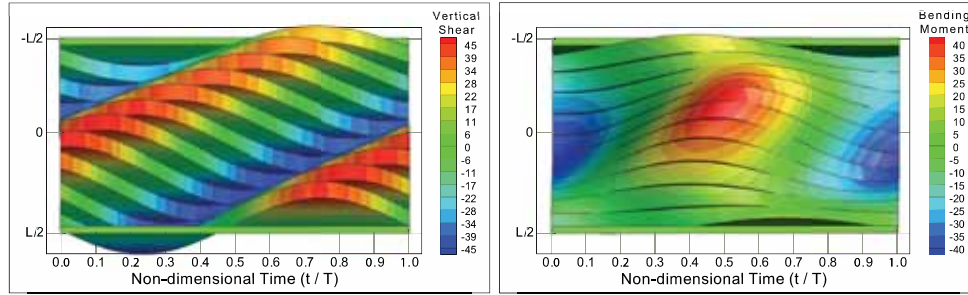


Figure 3.56: Vertical wave induced shear forces and bending moments over time for the conventional flexible barge in regular head waves of 100 mm at 5.50 rad/s

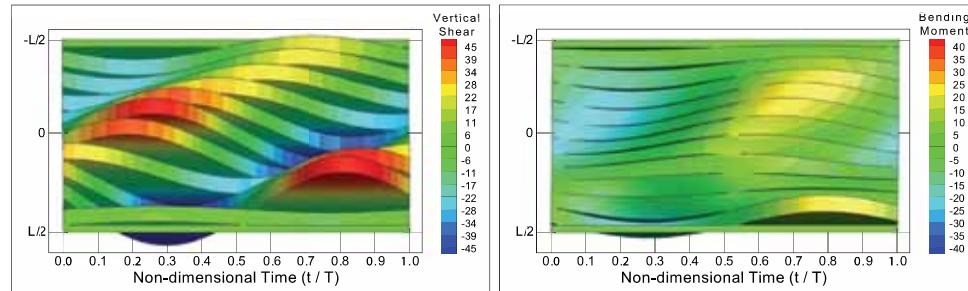


Figure 3.57: Vertical wave induced shear forces and bending moments over time for the flexible barge supported by 24 cushions in regular head waves of 100 mm at 5.50 rad/s

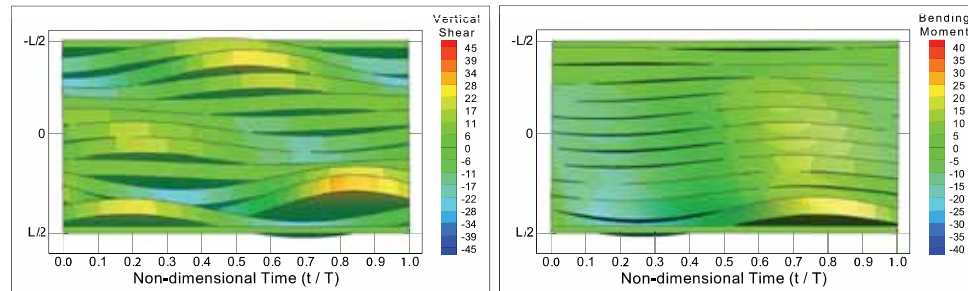


Figure 3.58: Vertical wave induced shear forces and bending moments over time for the flexible barge supported by 6 cushions in regular head waves of 100 mm at 5.50 rad/s

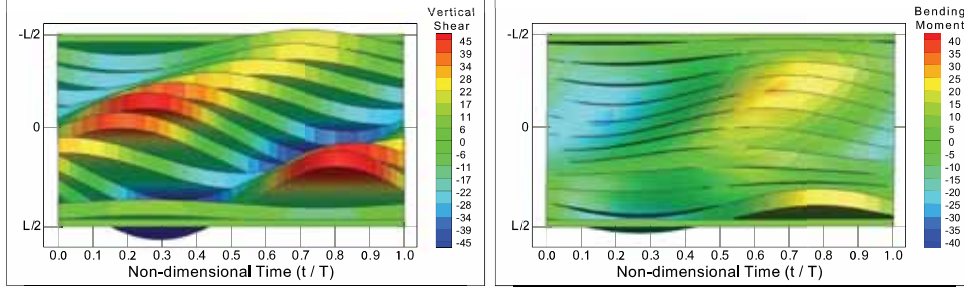


Figure 3.59: Vertical wave induced shear forces and bending moments over time for the flexible barge supported by 4 cushions and 10 caissons in regular head waves of 100 mm at 5.50 rad/s

The effect of the longitudinal shear forces on the bending moments of the 6ac and 24ac configurations are relatively large compared to the conventional barge as shown in figure 3.60. These forces particularly occur in the front part of the floater and are due to relatively large motions of the bow caisson in comparison with the other floaters.

The vertical wave induced shear forces of the 4ac configuration show the same trend as those of the conventional barge. Contrary, the longitudinal shear forces are significantly smaller for the air cushion configuration. As a result, the maximum wave induced bending moments are also reduced.

Obviously the extreme values of the bending moments (M) occur at the locations where the vertical shear forces (V) are zero, which follows from the following equations:

$$V = EI v''' \quad (3.49)$$

$$M = EI v'' \quad (3.50)$$

in which EI is the bending stiffness and v describes the deflection of the beam on top of the floaters. Once the distortion of the beam is known, the internal loads may be computed analytically.

The deflection of the beam in head waves of 5.50 rad/s is fitted by a 6th order polynomial of the form:

$$v(x, t) = (a_0 + a_1 x + a_2 x^2 + a_3 x^3 + a_4 x^4 + a_5 x^5 + a_6 x^6) e^{-i\omega t} \quad (3.51)$$

If the beam on top of the conventional barge is considered:

$$\begin{array}{llll} a_0 = -0.0310 & a_1 = -0.0034 & a_2 = 0.1198 & a_3 = 0.0109 \\ a_4 = -0.0314 & a_5 = -0.0020 & a_6 = 0.0065 & \end{array}$$

There is a good correlation between the polynomial and the deflection of the beam as shown in appendix D. Equation (3.51) accurately describes the deformation of the beam with the

exception of the tail ends of the beam, which will not deform. The vertical shear forces and bending moments, based on the third and fourth derivative, are plotted in figure 3.61 as semi-analytical results. These values show a good agreement with the results computed by the new program (DelAir).

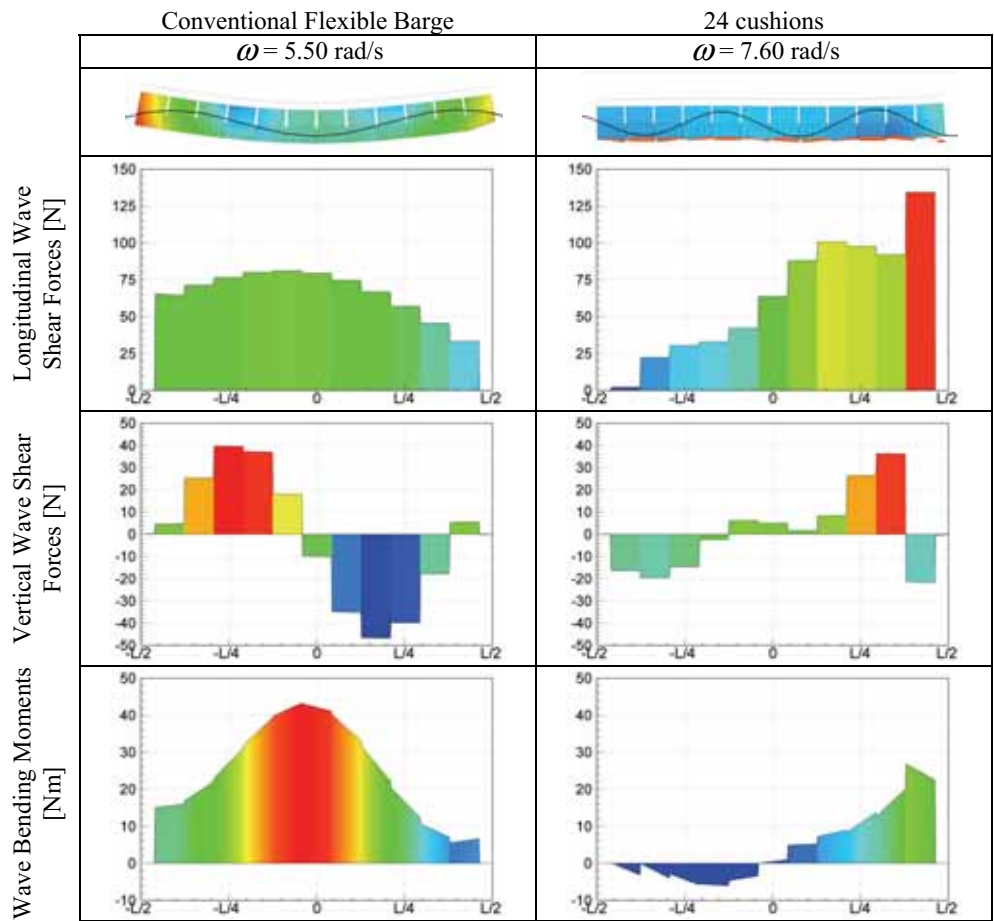


Figure 3.60a: Structural loads in regular head waves

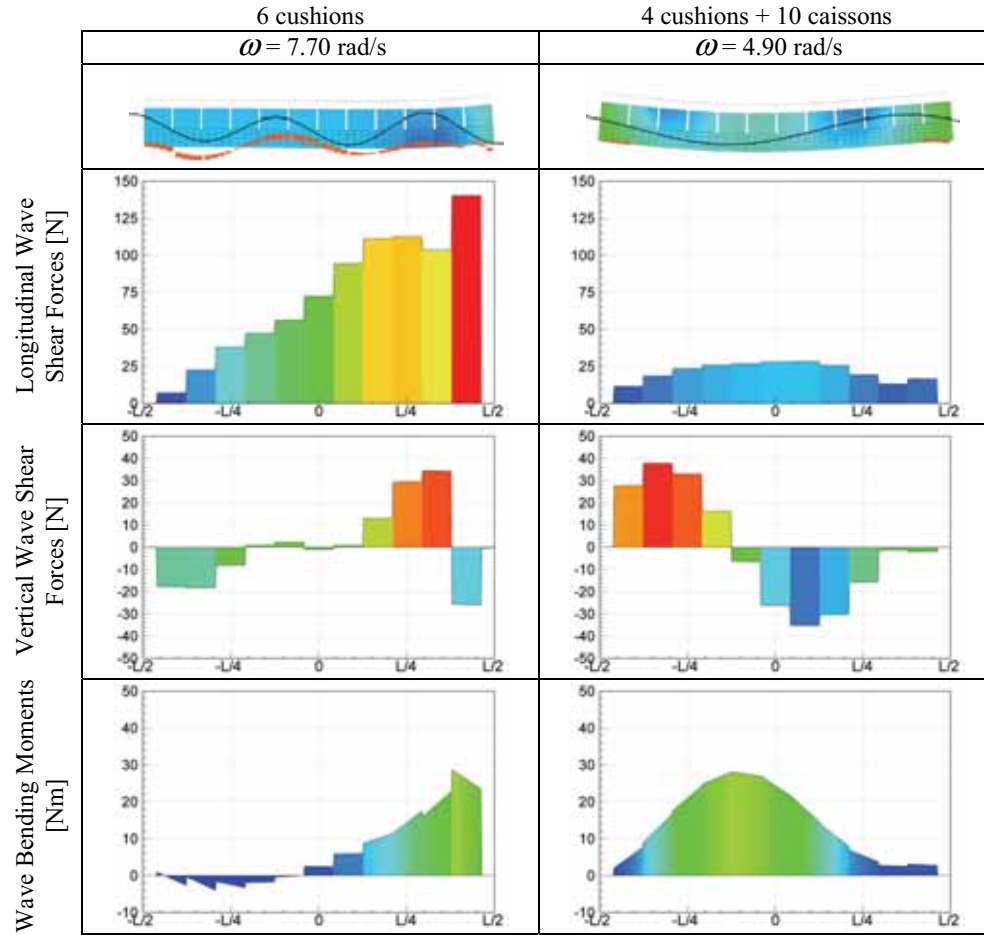


Figure 3.60b: Structural loads in regular head waves

The internal loads computed by the new program may also be verified by direct results from FEM software. In general, the distortion of the beam results in a bending moment. The displacements and rotations at the nodes, which are computed by the new hydroelastic program, may be applied as enforced displacements and rotations in FEM software. The obtained results are included in figure 3.61. In general there is a good agreement between the new hydroelastic program, FEM software and the semi-analytical results based on equation (3.51).

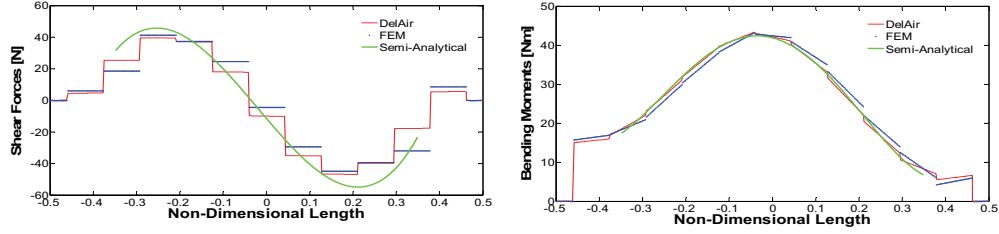


Figure 3.61: Wave induced shear forces and bending moments along the beam on top of the conventional flexible barge in head waves of 100 mm at 5.50 rad/s

Stresses

If the wave induced bending moments M are known, the bending stresses σ may be computed by:

$$\sigma = - \frac{M z}{I} \quad (3.52)$$

in which I is the moment of inertia of the cross section and z the distance from the neutral axis. The stresses may also be computed directly based on the principal coordinates and stresses associated with the eigenfrequencies of the dry structure in vacuum. This latter approach is in analogy with the equations (3.45) to (3.47):

$$\sigma(x, t) = \sum_{r=1}^m \sigma_r(x) p_r e^{i \omega t} \quad (3.53)$$

The behavior of different aircushion configurations of a rigid full-scale structure with dimensions 150 m x 50 m x 20 m was discussed in chapter 2.7.2 and 2.7.3. The body is modeled by plate elements in FEM software and subsequently the distortion of the floating structure is computed. Figure 3.62 shows the distortion of the structure supported by one aircushion in regular waves of 0.95 rad/s with a heading of 135 deg. The (theoretical) thickness of the plates is 500 mm and the associated Von Misses stresses are shown in figure 3.63.

Since the torsion stiffness is relatively small for a structure completely supported by one large aircushion, torsion is the dominating mode. For the present structure this mode is particularly pronounced in regular waves of 0.95 rad/s with a heading of 135 deg. Although the deformation of the structure is significant, the stresses are relatively small and equally distributed. Stress concentrations only occur at the bottom corner points and are approximately equal at the bottom and top of the plates. For this reason only stresses in the top of the plates are shown.

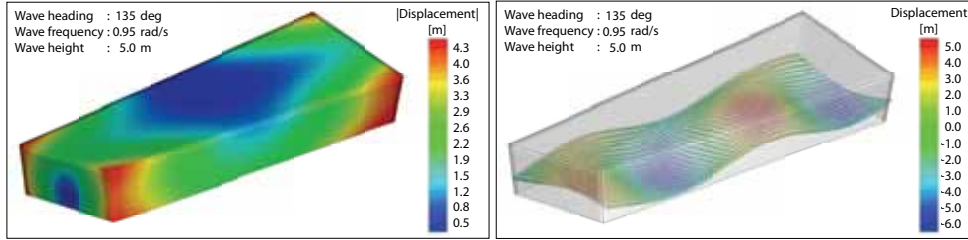


Figure 3.62: Distortion of the structure (left) and wave heights inside the air cushion (right) due to regular waves of 5 m at 0.95 rad/s from a heading of 135 deg

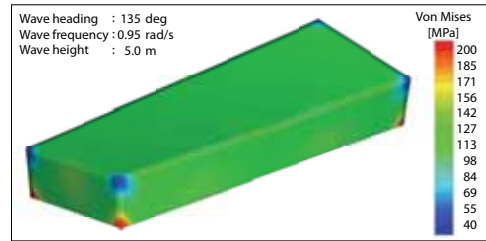


Figure 3.63: Von Mises stresses in the top of the plates due to regular waves of 5 m at 0.95 rad/s from a heading of 135 deg

3.4.5 Number of principal modes required

The number of principal modes required in the hydroelastic analysis highly depends on the chosen analysis. In case the motions of a flexible floating body are considered, few principal modes are required in order to obtain accurate results. On the other hand, the number of principal modes should increase in case the wave induced bending moments have to be computed. In addition, more principal modes are required to accurately predict the shear forces. Figure 3.64 shows the modal contributions of the conventional flexible barge in head waves and illustrates that the contribution of the first vertical bending mode (VB mode) is largest. The effect of the second VB mode is considerably smaller, but still clearly present. The contribution of the third vertical bending mode is small and may be neglected in the computations of the deflections of the body.

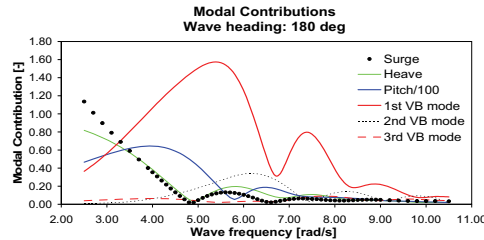


Figure 3.64: Modal contributions in regular head waves

As mentioned before, more principal modes are required if the wave induced bending moments are to be computed. Figure 3.65 shows the modal contributions of the conventional barge in head waves and illustrates the number of modes required in regular waves of 5.50 rad/s. The wave induced bending moment is clearly dominated by principal mode 7, i.e. the first vertical bending mode. The contributions of mode 11 (the second VB mode) and mode 19 (the fourth VB mode) are significantly smaller. The colors that are located further away from the neutral axis in figure 3.65, are associated with higher order modes. Since these contributions are small, the maximum wave induced bending moment in the beam on top of the floaters may be accurately computed when at least thirty principal modes are taken into account.

On the other hand, large distortions of the body along relatively small distances have a significant effect on the vertical shear forces, this is illustrated in figure 3.66. The contribution of high order modes on the shear forces is significant, which is especially the case at the ends of the structure. For this reason at least fifty principal modes are required in order to accurately compute the vertical wave induced shear forces along the total length of the beam on top of the conventional flexible barge. Obviously, the more principal modes are used, the better the approximations of the quantities will be.

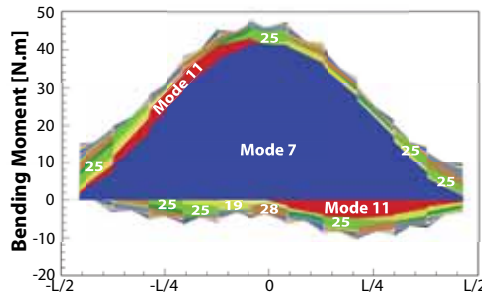


Figure 3.65: Modal contributions to wave induced bending moments in head waves of 5.50 rad/s

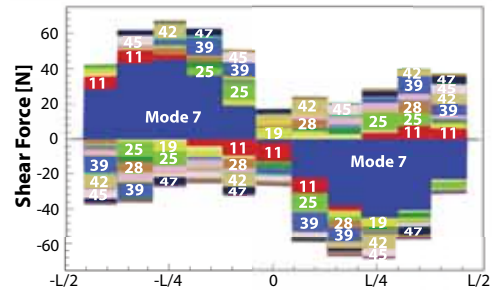


Figure 3.66: Modal contributions to vertical wave induced shear forces in head waves of 5.50 rad/s

3.5 Conclusions

A new method to compute the dynamic behavior of flexible aircushion supported structures at zero speed in waves was presented in this chapter. The approach is based on a linear potential theory and takes into account the interactions between the fluid around the structure, air underneath the floater, rigid-body and distortion modes. The method was incorporated in a new hydroelastic diffraction program, which is able to compute the fluid-air-structure interactions of floating bodies in waves.

Model experiments and analytical computations showed that the hydroelastic behavior of a conventional flexible barge can be well predicted by the new program. Aircushions underneath the structure may significantly change the dynamic behavior. The results showed that the vertical bending of the structure may be efficiently reduced by the aircushions. In addition, the mean roll and pitch responses will be reduced as well. On the other hand, the torsion of an aircushion supported structure may exceed the responses of a conventional floating body in oblique waves.

The results proved that the new program is able to accurately compute the structural loads of a flexible floating structure as well. The computed results were verified with analytical calculations and FEM simulations.

The effect of the aircushions on the structural loads is significant and is particularly pronounced in the wave induced bending moments. In general it was shown that aircushions considerably reduce the bending moments. Normally, the maximum wave induced bending moment of a conventional floating structure occurs amidships. However, the amplitude and location of the maximum moment may significantly change if the structure is supported by aircushions.

The number of principal modes required to accurately compute the hydroelastic behavior of floating bodies highly depends on the required analysis, characteristics of the floating body and the wave conditions. In general it was shown that only a few principal modes are required to compute the motions and deflections of the structure. On the other hand, the number of modes should increase in order to accurately compute the wave induced bending moments. In addition, many principal modes are required if the wave induced shear forces are to be computed.

Chapter 4

Technical feasibility of an aircushion supported mega-floater

4.1 Introduction

So far this dissertation described the dynamic behavior and structural loads of aircushion supported structures from an academic point of view. In this chapter a step will be made from the academic world to a practical application to show how the new program can be used in assessing the technical feasibility of aircushion supported mega-floaters in an early stage of the design process. For this purpose a conventional mega-floater will be used for comparison. The main dimensions will be based on a military study which was performed in the US.

In addition, different locations which are most suitable for mega-float structures will be discussed. After an evaluation of possible locations, the environmental conditions of the most suitable location will be used to compute the maximum wave induced bending moments and stresses in the mega-float structure. Based on these results, together with the geometry and material thicknesses, a conclusion will be drawn whether an aircushion supported mega-floater is technically feasible or not.

4.2 Suitable locations for mega-floaters

Countries like the Netherlands, Japan and Singapore are densely populated and have expanded their land area significantly through aggressive land reclamation programs in the last decades. Due to large land reclamation projects the port of Rotterdam in the Netherlands had been the largest shipping port in the world for 46 years until it was passed by Shanghai and Singapore in

2004 [72]. At present, a large new land reclamation project is being executed to extend the Dutch harbor with 1000 hectares for deep water container throughput, distribution, chemicals and new industry [84].

Japan on the other hand also has a shortage of land since less than 13% of the country is arable while the sea space is approximately 4.5 million km² [2, 76]. The limited land resources, large population, and extensive marine exclusive zone (EEZ) have necessitated an aggressive and innovative pursuit of utilization of the ocean space. Many Japanese papers on this subject have been presented at international conferences (OMAE and ISOPE) in recent years.

Singapore, a center of economic activity in South-East Asia, consists of 63 islands and is one of the smallest countries in the world with a total land area of 680 km². Presently, its population is about 4 million and is expected to grow to 5.5 million in 2040. A land shortage of 40 km² is expected by the Urban Redevelopment Authority when the population reaches this quantity [76]. Seventy-five percent of the population of the US lives in the coastal region [82]. In addition, the West Coast of the US has no deep water shipping port. A floating harbor would therefore be the first deep water shipping port at the West Coast and would provide the country with new logistic possibilities, especially when a shipping port is combined with a floating runway. San Diego, Los Angeles and San Francisco are prime candidates for a large floating structure.

A floating harbor at the East Coast of the US would provide similar opportunities and is basically also a security port for metropolitan cities. Moreover, only 2% of the containers entering the US by ship are inspected [32]. Based on this figure and terrorist actions since 9/11 it becomes clear that it is not inconceivable that a bomb hidden in a container is a serious threat to large cities like New York. At present, it is not possible to check all containers while they are onboard ships as they are mostly stacked cheek to jowl below and above deck. A large floating security port may therefore also serve as a solid core of homeland defense.

4.2.1 Most probable location

The Netherlands is surrounded by relatively shallow waters and Japan has many shallow bays, in most cases this makes land reclamation more attractive than a large floating structure. Apart from water depth, soil conditions also determine the feasibility of land reclamation projects in comparison with floating structures. A good example is Kansai international airport, which was built by the traditional way of land reclamation in a water depth of 20 m. A disadvantage is that the airport was built on soft soil and the complete terminal had to be placed on pneumatic jacks to compensate for the settlement of the soil. By 2005 the airport had already subsided more than 10 m since the project started. As a result the total budget of the project was exceeded by 40% and the total costs amounted to \$15 billion [83].

In case of the US, the East Coast is a potential location for a large floating structure. A floating structure would offer a range of economically attractive applications, particularly in the region of large metropolitan cities. On the other hand, the US has no shortage of land along its shore line as is the case for a country like Singapore.

Singapore copes with a shortage of both land and sand needed for land reclamation projects. Malaysia and Indonesia ended their export of sand to Singapore in 2001 and 2002 respectively [19]. As a result, ongoing land reclamation projects were cancelled. The boundaries of Singapore are shown in figure 4.1, which illustrates the difficulties for land reclamation projects in case the neighboring countries Malaysia and Indonesia do not cooperate. A floating structure would be an ideal solution for both the land and sand problem in Singapore. As such it is most probable that the first mega-float structure will be built in Singapore.



Figure 4.1: Map of Singapore

4.2.2 Environmental conditions

In general, the motions and structural loads of a floating body depend on the environmental conditions and main particulars of the structure itself. The Weibull parameters of the environmental conditions for the Southern part of the South China Sea and the Main Strait of Singapore are provided by DNV [13]. These parameters may be used to statistically determine the significant wave heights and associated wave periods in the waters around Singapore. The obtained significant wave heights (H_s) and associated peak periods (T_p) in design storms are shown in figure 4.2. Each line corresponds to the extreme values of a design storm for a given return period.

A mega-float structure should be able to resist the most severe storms. In the present study, a return period of 100 years will be used. For this reason all combinations of H_s and T_p on the black line in figure 4.2 should be investigated to find the combination of parameters which statistically results in the most extreme responses of the floating structure. In the present study the eleven combinations on the black line in the figure are used to determine the maximum responses of different mega-float structures.

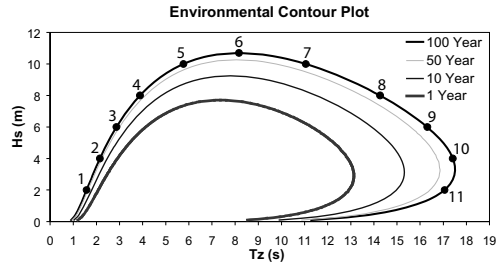


Figure 4.2: Environmental contours of design storms for different return periods

Table 4.1: H_s and T_z values of a design storm with a 100 year return period

#	H_s (m)	T_z (s)	#	H_s (m)	T_z (s)
1	2.00	1.58	7	10.00	11.06
2	4.00	2.15	8	8.00	14.27
3	6.00	2.87	9	6.00	16.31
4	8.00	3.89	10	4.00	17.41
5	10.00	5.77	11	2.00	17.06
6	10.70	8.16			

4.3 Main particulars and numerical settings

Two different aircushion supported mega-floaters and a conventional structure of the same size are evaluated. The length of all structures is 3.8 km, which corresponds to the longest runway of Schiphol International Airport in the Netherlands and is sufficiently large to land the largest airplanes. The remaining main dimensions correspond to those of the Mobile Offshore Base, which was a military study performed in the US between 1993 and 2000 as described in section 1.1. The main particulars of the mega-float structures in this chapter are:

Length : 3800 m
 Breadth : 160 m
 Depth : 65 m
 Draught : 20 m

The first mega-float structure, a conventional barge, has a box shaped body as shown in figure 4.4. The hydromechanical model consists of 3358 diffraction elements and is free to float without restraints. The structural model consists of 237 beam elements of which the properties are presented in table 4.2. It is assumed that the conventional structure, as well as the aircushion supported structures, will be made of steel with the following properties:

Young's modulus : 2.10×10^{11} Pa
 Poisson's ratio : 0.3 -
 Mass density : 7850 kg
 Yield stress : 355 MPa

Table 4.2: Properties of beam elements in the structural analyses

	Unit	Barge	1ac & 10ac
Area	m ²	6.75	7.95
Perimeter	m	450.00	530.00
Neutral axis above keel	m	32.50	41.18
Shear centre above keel	m	32.50	69.99
Y Shear area*	m ²	4.56	4.11
Z Shear area*	m ²	1.31	1.15
Moment of inertia around y-axis	m ⁴	5.75E+03	3.40E+03
Moment of inertia around z-axis	m ⁴	2.27E+04	2.86E+04
Torsional constant	-	1.45E+04	2.62E+03
Non structural mass	kg/m	6.03E+05	8.82E+05
Warping constant	-	2.75E+06	9.97E+06

Figure 4.3 shows the general arrangement of the mega-float structure, which is supported by one large aircushion (1ac). The element model of this structure, used in the hydroelastic diffraction computations, is shown in figure 4.5. The second aircushion supported structure shown in figure 4.6 is supported by ten cushions (10ac). The general arrangement of this latter structure is equal to the 1ac configuration since the walls between the aircushion compartments are not taken into account in the hydrodynamic model. As a result the displacement of both cushion configurations is equal to $3.6 \cdot 10^6$ tons, in which 57% of the buoyancy is provided by air and 43% is provided by the skirts around the cushion(s).

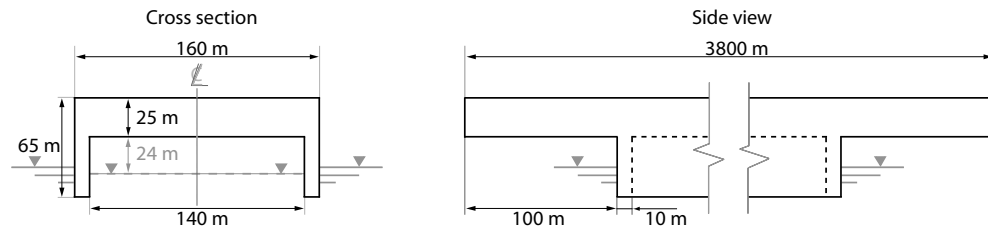


Figure 4.3: General arrangement of structure support by one large aircushion

* The shear area represents the area of the cross section in the FEM computations that is effective in resisting shear deformations.



Figure 4.4: Bottom view of the conventional structure (barge)



Figure 4.5: Bottom view of the structure supported by one aircushion



Figure 4.6: Bottom view of the structure supported by ten aircushions

The colors in figures 4.5 and 4.6 show the elements of the floater which represent a direct coupling between the deflections of the structure and the volume change of the aircushions. All dry elements of the structure laying at the boundary with the aircushion are included in the air-structure interaction. This means that non-symmetric horizontal deflections of the vertical skirts of the 1ac configuration are also included and may result in volume changes of the air chamber and consequently pressure variations on the structure.

On the other hand, the skirts between the cushion compartments of the 10ac are not modeled and only displacements of the dry elements in the bottom of the floater (indicated by colors in figure 4.6) will result in a volume change of the aircushion. In other words, deflections of the skirts of the 10ac configuration have no direct effect on the volume variations of the aircushions.

Both aircushion configurations have the same structural model which consists of 380 beam elements. The properties of the beam elements are presented in table 4.2 and are based on the cross section shown in figure 4.3. In addition, the thickness of the hull plating is assumed to be constant along the length of the structure and equal to 15 mm.

The hydromechanical model of the 1ac structure consists of 3740 diffraction elements, excluding 2550 elements laying at the free water surface inside the aircushion. For the 10ac configuration, the number of cushion elements was limited to 1440 due to physical constraints on the amount of memory (RAM) of a 32 bit computer. However, the effect of the coarser mesh on the responses of the structure is negligible since these are dominated by low wave frequencies.

The structural deflections of all bodies are described by 99 principal coordinates. As a result the conventional structure has 99 degrees of freedom, the 1ac configuration 2649, and the responses of the 10ac are described by 1539 degrees of freedom.

4.4 Wave induced bending moments and stresses

Based on the described main particulars and environmental conditions it is possible to compute the wave induced bending moments and stresses in the structures. The structural properties of these bodies should be taken into account in the computation of the wave induced bending moments since these mega-float structures cannot be considered as rigid bodies anymore. Figures 4.7 to 4.9 show the RAOs of the vertical displacements along the length of the structures in regular head waves. The elastic deflections are significant and particularly pronounced at the bow and stern of the structure. In relatively small waves, i.e. high wave frequencies, the deflections are largest at the bow ($0.5 L$) and decrease towards the stern. Since the structure is free to move at both ends, the vertical responses are relatively large at the bow and stern.

There is a significant difference in the displacements between the conventional structure and the aircushion supported structures. The distortion modes are more pronounced in the aircushion configurations. As a result, the vertical displacements at the bow and stern are larger than those of the conventional barge. Contrary, the vertical displacements of the aircushion configurations are smaller between $-0.35 L$ and $0.35 L$; this is due to the air chamber underneath the structure which equally distributes the wave loads over the area of the cushion. The wave pressures in the crests and troughs are transformed by the air chamber to relatively constant mean pressures on the structure.

Since the behavior of a mega-float structure is dominated by elastic deflections, the rigid-body modes should be extended by distortion modes as described in chapter 3. Figure 4.10 shows the wave induced bending moments of the conventional mega-floater and the difference between a rigid-body and a hydroelastic approach. This difference is significant as a rigid-body method cannot take into account elastic distortions that are present in case of a mega-float structure. As a result, the wave induced bending moments are over-predicted by the rigid-body method.

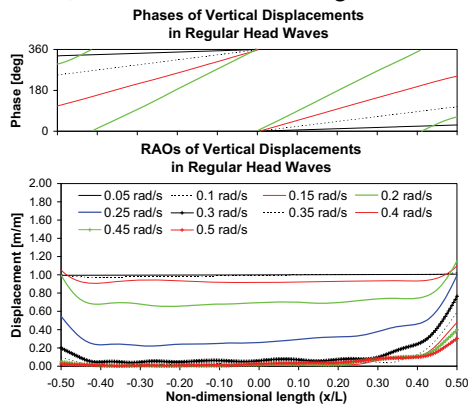


Figure 4.7: Phases and RAOs of vertical displacements of the conventional mega-float structure in regular head waves

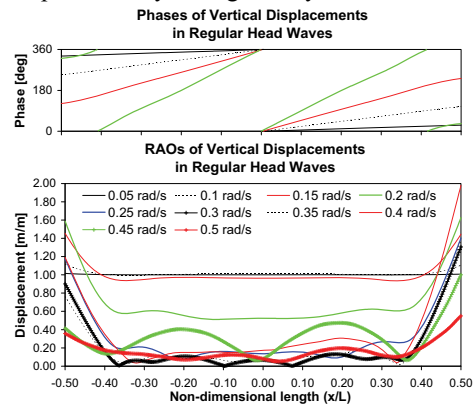


Figure 4.8: Phases and RAOs of vertical displacements of the lac configuration in regular head waves

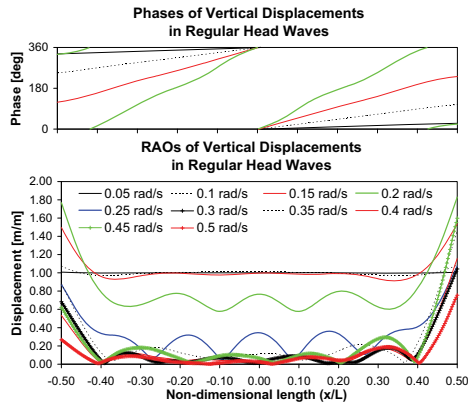


Figure 4.9: Phases and RAOs of vertical displacements of the 10ac configuration in regular head waves

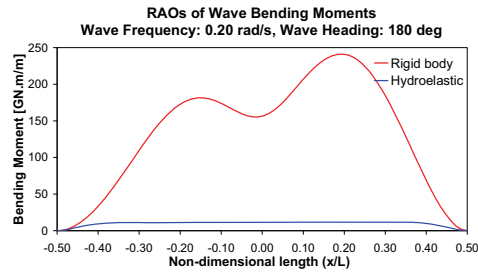


Figure 4.10: RAOs of wave induced bending moments of the conventional structure based on rigid-body and hydroelastic analysis

In order to assess the technical feasibility of the aircushion supported mega-floaters, the transfer functions of the structural loads should be multiplied by the wave spectrum. This results in a statistical maximum wave induced bending moment that may occur during a specified return period. Eventually these bending moments will result in stresses with maximum values in either the bottom or deck of the structure.

Although the structure will be located in fetch limited seas (near the shore of Singapore), JONSWAP and Bretschneider (Pierson-Moskowitz) wave spectra will give similar results since the responses of mega-float structures are dominated by low wave frequencies. Figure 4.11 shows the Pierson-Moskowitz wave spectra of the eleven data points presented in table 4.1; these data points are located on the wave contour with a return period of 100 years in figure 4.2.

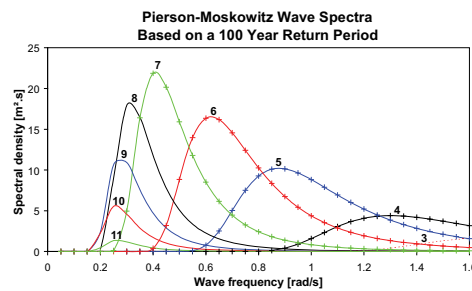


Figure 4.11: Pierson-Moskowitz wave spectra based on a 100 year return period

In order to compute the maximum statistical wave induced bending moment in a 100 years storm, the transfer functions (at any point on the neutral axis) should be multiplied by the wave spectra of figure 4.11. Figures 4.12 to 4.14 show the RAOs of the wave induced bending moments and the computed response spectrum in head seas for a range of wave frequencies along the length of the structure. The presented response spectra are related to the wave spectrum which results in the highest wave induced bending moment. In case of the conventional structure and the 1ac configuration, wave spectrum 8 ($H_s = 8.00$ m, $T_z = 14.27$ s) results in the largest wave induced bending moment. For the 10ac configuration, the maximum wave induced bending moment occurs in wave spectrum 7 ($H_s = 10.00$ m, $T_z = 11.06$ s).

Since the displacements of the conventional structure and the aircushion configurations are different in the frequency domain, the associated wave induced bending moments are different as well. The wave induced bending moments of the conventional structure are significantly larger than those of the aircushion supported structures. Although the RAOs of the wave induced bending moments of the aircushion supported structures can be significant at high wave frequencies, the response spectra are dominated by low wave frequencies.

The wave induced bending moments along the length of the structure may be computed by integrating the associated spectral density over the frequency range as discussed in appendix E. The thus obtained bending moments at the neutral axis are significant values and may be multiplied by 1.86 to obtain the maximum wave induced bending moments, which is discussed in appendix E.

All eleven response spectra specified in table 4.1 should be analyzed in order to get the maximum statistical wave bending moment along the length of the structure. Figure 4.15 shows these maximum values in head seas, in a design storm with a return period of 100 years.

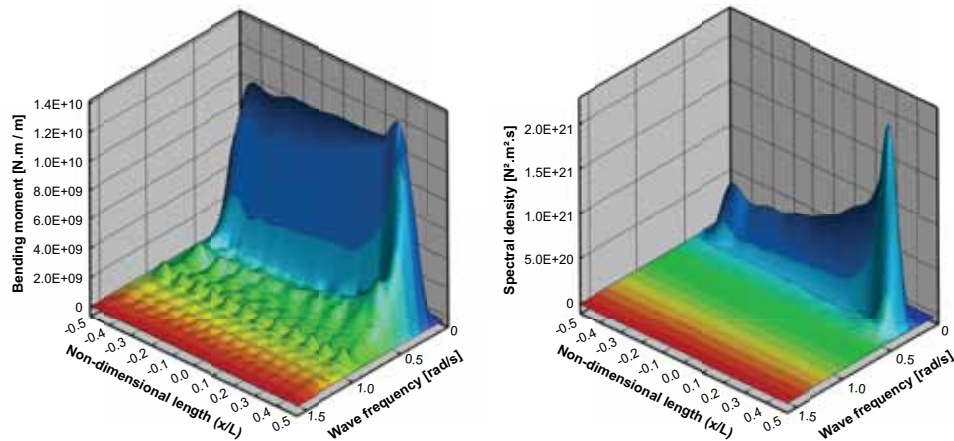


Figure 4.12: Transfer function (left) and response spectrum (right) of the wave induced bending moments of the conventional mega-floater in head seas ($H_s = 8.00$ m, $T_z = 14.27$ s)

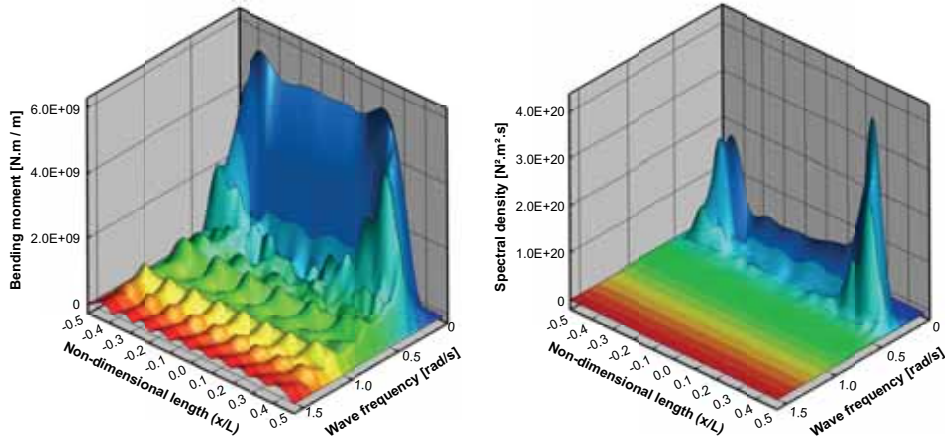


Figure 4.13: Transfer function (left) and response spectrum (right) of the wave induced bending moments of the 1ac configuration in head seas ($H_s = 8.00$ m, $T_z = 14.27$ s)

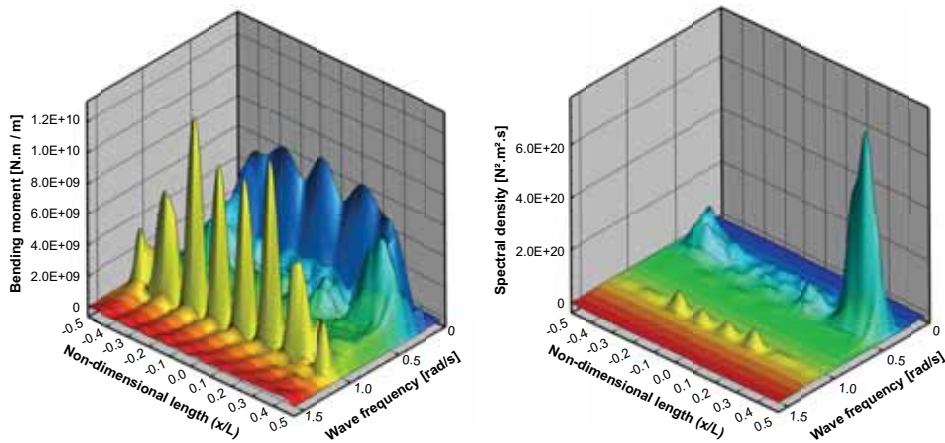


Figure 4.14: Transfer function (left) and response spectrum (right) of the wave induced bending moments of the 10ac configuration in head seas ($H_s = 10.00$ m, $T_z = 11.06$ s)

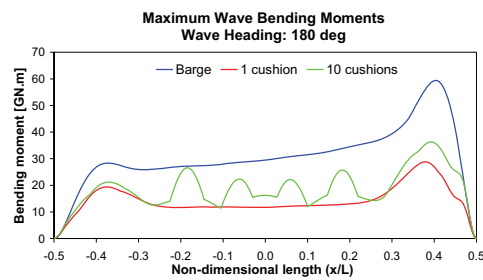


Figure 4.15: Maximum wave induced bending moments (in GN.m) in head seas based on 11 data points on the contour of extreme waves with a return period of 100 years

Since the structure may be subjected to waves from different directions, the above described procedure should be extended to other wave directions as well. Figure 4.16 shows the maximum wave induced bending moments of all structures and all wave directions. The wave induced bending moments of the aircushion supported structures are significantly smaller than those of the conventional structure in all wave directions except 90 degrees. Conversely, wave induced bending moments are in generally small in beam waves of 90 degrees. The loads are remarkably high in case the structure is subjected to waves from 100 degrees; this result is due a coupling between torsional modes, horizontal and vertical bending modes. The maximum wave induced bending moment of the conventional barge is 59.4 GN.m in head waves. This value is reduced by 64% in case the structure is supported by one large aircushion. In case the structure is supported by 10 cushions, the wave induced bending moment increases to 28.8 GN.m, i.e. 49% of the conventional barge.

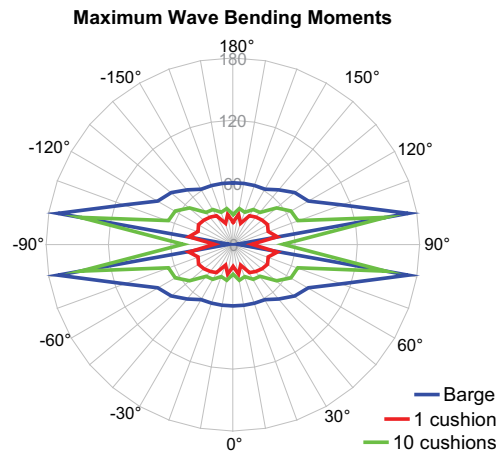


Figure 4.16: Maximum wave induced bending moments (in GN.m) based on a 100 year return period

Even though the wave induced bending moments are significantly reduced by the aircushions, more information is required to assess the technical feasibility of the aircushion supported structures. The wave induced bending moments should be translated to plate stresses in order to assess the technical feasibility of the present structures. Figure 4.17 shows the maximum stresses in the deck and bottom plating of the floaters, which are calculated according to equation (3.52). Since the distance from the deck to the neutral axis is smaller than the distance from the bottom to the neutral axis, the stresses in the deck will be smaller as well. According to shipbuilding regulations the stresses should not exceed 243 MPa for high tensile steel with a yield stress of 355 MPa [14]. This value is called the allowable stress and is included in figure 4.17.

The stresses in the deck of the 1ac configuration stay within the allowable range for most wave directions. However, they exceed the allowable stress in the bottom plating. In order to comply with the regulations, higher steel grades should be used in the bottom of the 1ac structure. Another option to reduce the stresses may be achieved by adding more steel in the bottom of the floater. A consequence of this action is an increase of the stresses in the deck since the neutral axis will shift downwards. However, the hydroelastic behavior of the structure may also be affected since a change of the structural properties of the body may result in a change of the natural frequencies of the distortion modes.

Another possibility to reduce the wave induced stresses, is to change the dimensions and shape of the structure. Together with an increase of the plate thickness in the bottom, it is likely that the stresses will decrease to allowable values.

Dividing the aircushion in multiple compartments will also change the wave induced bending moments as shown in figure 4.16. As a result, the stresses in the bottom decrease when the structure is supported by ten aircushions. The only exceptions are beam seas with a heading between 70 and 110 degrees. In this case the coupling between torsion, horizontal bending and vertical bending results in relatively high stresses in both the bottom and deck of the structure.

The large wave induced bending moments of the conventional barge result in relatively large stresses compared to the aircushion configurations, this is especially the case in the deck plating. On the other hand, the stresses in the deck and bottom of the conventional barge are equal since the neutral axis is located at the centre of the structure.

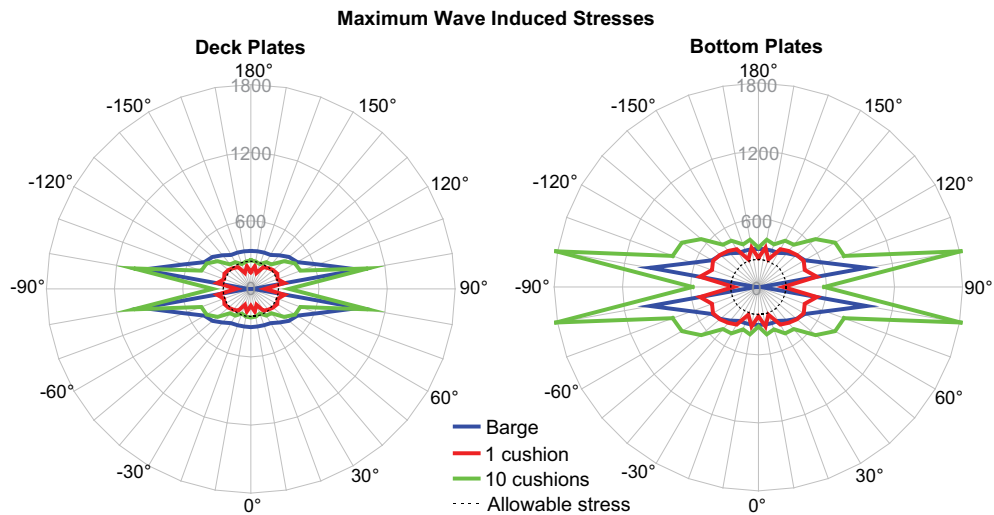


Figure 4.17: Maximum wave induced stresses (in MPa) due to vertical bending in the deck plating (left) and bottom plating (right) based on a 100 year return period

Practically it is not possible to change the dimensions and shape of the conventional structure in a way that the stresses reduce to allowable values. In this case the depth of the structure would reach unrealistic values. A more sensible option is to protect the structure by breakwaters which will reduce the wave loads on the structure. Another interesting option may be to add aircushions around the structure. Both options are interesting studies for future research in which the new program will be a suitable tool in the early design process.

4.5 Conclusions

It is unlikely that a conventional steel mega-float structure will be built in open seas without breakwaters. This chapter showed that the stresses in the bottom and deck of a conventional structure will exceed the allowable stresses. A practical way to reduce these stresses is to protect the structure by breakwaters, which will reduce the wave loads on the structure. Another option may be to apply aircushions around the structure, since these will reduce the wave induced bending moments as well.

The reduction of the wave induced bending moments is largest in case the structure is supported by one aircushion. In the present application of a floating runway the wave induced bending moments will be reduced by 64% for a single aircushion supported structure compared to a conventional floater. The stresses in the deck of the aircushion supported structure are in most cases in the allowable range. Although the stresses in the bottom exceed the allowable values, there are different options to reduce these stresses. One of the options is to support the structure by ten aircushions. A drawback of this configuration is the fact that the stresses in the deck will increase.

Although both aircushion configurations in this chapter do not comply with the criteria, it is likely that the wave induced stresses of an aircushion supported structure can be reduced to allowable values in the design process. This can be done by using different materials, increasing the material thickness, changing the dimensions, modifying the shape or using a different arrangement of the aircushions. These options are outside the scope of the present research, but may be of interest in future mega-float projects.

Chapter 5

Conclusions and recommendations

In the previous chapters a new numerical method to compute the dynamic behavior of aircushion supported structures has been described. Much of the research effort was put into the validation and verification of the method. This chapter summarizes the main conclusions and provides thoughts for future investigations.

5.1 Main conclusions

The numerical method presented in this thesis makes it possible to accurately compute the dynamic behavior of large floating structures with and without aircushions. It is the first method that is able to accurately predict the three-dimensional dynamic behavior and stresses of flexible aircushion supported structures of arbitrary shape in waves. The method is based on a linear diffraction theory with modal expansions; as such the fluid-structure interactions of flexible floating bodies are also taken into account.

The results have indicated that the behavior of aircushion supported structures can be well predicted by means of a three-dimensional linear potential method. In case of rigid bodies, the numerical results were validated with model tests. Experiments of a flexible barge without aircushions served to validate the numerical results. However, no experimental data is available for flexible aircushion supported structures, therefore the computed results were verified with analytical computations and FEM analysis.

Both model tests and computations have shown that aircushions can significantly influence the behavior of floating structures. The effect is particularly pronounced if the structure is supported by a large single aircushion. In this case the roll and pitch motions are small and the mean

second order drift forces will be reduced. A drawback is that the torsion of a single aircushion supported structure in oblique waves may be relatively large compared to a conventional barge. However it is possible to alter the dynamic behavior of an aircushion supported structure by changing the air pressure within the cushions. Especially the heave motions and natural roll frequencies in beam seas are sensitive to a change of the aircushion pressure.

The effect of the aircushions on the structural loads is significant and is particularly pronounced in the wave induced bending moments. It was shown that aircushions considerably reduce the wave induced bending moments. Normally, the maximum wave induced bending moment of a conventional floating structure occurs amidships. The magnitude and location of the maximum value may significantly change if the structure is supported by aircushions.

The number of principal modes required to accurately compute the hydroelastic behavior of flexible floating bodies highly depends on the required analysis, characteristics of the floating body and the wave conditions. In general, it was shown that a limited number of principal modes are required to compute the motions and deflections of the structure. On the other hand, more principal modes are necessary to accurately compute the wave induced bending moments. In addition, many principal modes are required if the wave induced shear forces are to be computed. It has been shown (chapter 4) that the allowable stresses of a conventional non-air supported mega-float structure will be exceeded in open seas if the structure is not protected by breakwaters. Breakwaters will add to the total costs of a future mega-float project, but they can be avoided by supporting the structure by aircushions as these will significantly reduce the wave induced bending moments and consequently the stresses.

In general, the results in this thesis have shown that an aircushion supported structure has significant advantages compared to a conventional large floating structure. In addition, the computational method as developed and proposed proved to be a suitable tool to optimize cushion configurations for a particular application.

5.2 Recommendations

The research presented in this thesis provides a foundation for future work with respect to mega-floaters. The next step will be to design a mega-floater for a particular application in which different floating structures like a conventional barge, semi-submersible, Tension Leg Platform (TLP) or aircushion supported structure should be considered. Besides, combinations such as a conventional barge with aircushions should be assessed in the design process as well.

Studies performed in the past showed that, in water depths of 20 m and more, floating structures are economically more attractive than traditional land reclamation projects [80]. However, these studies were performed more than a decade ago and in the meantime research with respect to mega-floaters has been ongoing and dredging processes improved as well. These technical

developments changed the economic limit of land reclamation projects. For that reason it would be interesting to make a new assessment of the total costs of an optimized mega-floater compared to land reclamation with present knowledge and technology.

There has been a strong focus on renewable energy in recent years. Wave energy is one of the sources of renewable energy and can be extracted by an Oscillating Water Column (OWC). OWCs are basically aircushion supported structures which are connected to generators. The air pressure variations in the cushion result in air flows through a generator from which energy is extracted.

The numerical method, which was presented in this thesis makes use of a linearized adiabatic law to describe the air pressure and assumes that no air will be extracted from the cushion. It would be interesting to modify the software to take into account the energy absorption of the generators and the exchange of air (and heat) with the ambient air. In that case it would be possible to compute the behavior and efficiency of an OWC.

Once it is possible to take into account the leakage of air from the aircushions, it will be interesting to include forward speed as well. With these modifications of the code it may be possible to compute the dynamic behavior of Aircushion Supported Vehicles (ACVs) like hovercrafts and Surface Effect Ships (SEs).

In addition the code can be extended to the time domain calculations. With use of the modal expansion method, which is already incorporated in the software, it will be possible to compute the springing and whipping effects of vessels with forward speed.

Obviously the suggested modifications of the code are outside the scope of the present research and some of the recommendations have no direct relation with Mega-Float structures either. Nevertheless, these thoughts are worth investigating in the future and will contribute to the knowledge of modern society.

Bibliography

- [1] ABS. *Preliminary MOB classification guide*. American Bureau of Shipping, no. AA99018, 1999.
- [2] H.B. Ali. An overview of marine science and technology in the Asia-Pacific region. *US Japan Natural Resources Symposium (UJNR)*, 2000.
- [3] A.I. Andrianov. *Hydroelastic analysis of very large floating structures*. PhD thesis, Delft University of Technology, 2005.
- [4] J.C. Berthin, W.L. Hudson, C.G. Doris, D.O. Myrabo. Installation of Maureen gravity platform over a template. *Offshore Technology Conference*, pg. 321-328, 1985.
- [5] R.E.D. Bishop, W.G. Price. *Hydroelasticity of ships*. Cambridge University Press, 1979.
- [6] R.D. Blevins. *Formulas for natural frequency and mode shape*. Krieger Publishing Company, 1995.
- [7] H. Blood. Model tests of a pneumatically stabilized platform. *Proceedings of International Workshop on Very Large Floating Structures*, pg. 77-84, 1996.
- [8] G.E. Burns, G.C. Holtze. Dynamic submergence analysis of the Khazzan Dubai Subsea Oil Tanks. *Offshore Technology Conference*, vol. 2, pg. 467-479, 1972.
- [9] S.K. Chakrabarti. Scale effects on a unique launch sequence of a gravity-based structure. *Applied Ocean Research*, vol. 17, no. 1, pg. 33-41, 1995.

-
- [10] R. S. Chamberlin. Khazzan Dubai 1 - Design, construction and installation. *Offshore Technology Conference*, pg. 439-454, 1970.
- [11] B. Chenu, M. T. Morris-Thomas, K. P. Thiagarajan. Some hydrodynamic characteristics of an air-cushion supported concrete gravity structure. *15th Australasian Fluid Mechanics Conference*, 2004.
- [12] L.B. Curtis, J.C. Shepler. Dubai Khazzan - Pioneer of large undersea storage systems. *Offshore Technology Conference*, vol. 1, pg. 455-469, 1970.
- [13] DNV. *Environmental conditions and environmental loads*. Det Norske Veritas, 2007.
- [14] DNV. *Hull structural design - ships with length 100 metres and above*. Det Norske Veritas, vol. 3, no. 1, 2009.
- [15] Department of Economic & Social Affairs. *World population in 2300*. United Nations, 2004.
- [16] O.M. Faltinsen, J.B. Helmers, K.J. Minsaas, R. Zhao. Speed loss and operability of catamarans and SES in a seaway. *Proceedings of FAST'91*, pg. 709-724, 1991.
- [17] O.M. Faltinsen. *Hydrodynamics of high-speed marine vehicles*. Cambridge University Press, 2005.
- [18] T. Fuse. Legal Framework for the Use of Ocean Space -Considerations from International Law of the Sea-. *Proceedings of International Symposium on Ocean Space Utilization Technology*, pg. 3/7/2009, 2003.
- [19] N. Goebert. Baggeraars terug naar Singapore; Doorbraak in 'zandconflict' met Maleisië. *Volkskrant (In Dutch)*, pg. 9, 15 January 2005.
- [20] R. Guéret, A.J. Hermans. Air cushion under floating offshore structure. *16th International Workshop on Water Waves and Floating Bodies*, pg. 45-49, 2001.
- [21] R. Guéret. *Interaction of free surface waves with elastic and air-cushion platforms*. PhD thesis, Delft University Press, 2002.

-
- [22] A.J. Hermans. Interaction of free-surface waves with floating flexible strips. *Journal of Engineering Mathematics*, no. 49, pg. 133–147, 2004.
- [23] T. Ikoma, K. Masuda, H. Maeda, C.-K. Rheem. Hydroelastic behavior of air-supported flexible floating structures. *Proceedings of the 21st International Conference on Offshore Mechanics and Arctic Engineering*, 2002.
- [24] T. Ikoma, H. Maeda, K. Masuda, C.-K. Rheem, M. Arita. Effects of submerged vertical plates and air chamber units in hydroelastic response reductions. *Proceedings of the 12th International Offshore and Polar Engineering Conference*, pg. 547-552, 2002.
- [25] T. Ikoma, H. Maeda, K. Masuda, C.-K. Rheem. Effects of the air-chambers on the hydroelastic response reduction. *Proceedings of International Symposium on Ocean Space Utilization Technology*, pg. 180-188, 2003.
- [26] T. Ikoma, K. Masuda, H. Maeda, C.-K. Rheem. Effects of aircushion division to hydroelastic responses of an aircushion type very large floating structure. *Proceedings of the 22nd International Conference on Offshore Mechanics and Arctic Engineering*, 2003.
- [27] T. Ikoma, K. Masuda, C.-K. Rheem, H. Maeda, R. Iwasa. Hydroelastic behavior of air-supported flexible floating structures. *Proceedings of the 23rd International Conference on Offshore Mechanics and Arctic Engineering*, 2004.
- [28] T. Ikoma, K. Masuda, C.-K. Rheem, H. Maeda. Three-dimensional analysis of hydroelastic behaviors of an aircushion type large floating structure. *Proceedings of the 24th International Conference on Offshore Mechanics and Arctic Engineering*, 2005.
- [29] T. Ikoma, K. Masuda, C.-K. Rheem, H. Maeda. Response reduction of motion and steady wave drifting forces of floating bodies supported by aircushions in regular waves. *Proceedings of the 25th International Conference on Offshore Mechanics and Arctic Engineering*, 2006.

- [30] T. Ikoma, K. Masuda, C.-K. Rheem, H. Maeda. Response reduction of motion and steady wave drifting forces of floating bodies supported by aircushions in regular waves - The 2nd report, response characteristics in oblique waves. *Proceedings of the 26th International Conference on Offshore Mechanics and Arctic Engineering*, 2007.
- [31] T. Ikoma, M. Kobayashi, K. Masuda, C.-K. Rheem, H. Maeda. A prediction method of hydroelastic motion of aircushion type floating structures considering with draft effect into hydrodynamic forces. *Proceedings of the 27th International Conference on Offshore Mechanics and Arctic Engineering*, 2008.
- [32] D. Innis, C. McMillan, H. Blood, J. Leary. *Beyond the horizon*. Float Incorporated, 2002.
- [33] J.M.J. Journee, W.W. Massie. *Offshore hydromechanics*. Delft University of Technology, 2001.
- [34] P. Kaplan. Dynamics and hydrodynamics of Surface Effect Ships (SES). *Transactions of the Society of Naval Architecture and Marine Engineering*, 1981.
- [35] P. Kaplan. Scaling problems of dynamic motions in waves from model tests of surface effect ships and air cushion vehicles. *22nd American Towing Tank Conference*, pg. 77-84, 1989.
- [36] M. Kashiwagi. A time-domain mode-expansion method for calculating transient elastic responses of a pontoon-type VLFS. *Journal of Marine Science and Technology*, vol. 5, no. 2, pg. 89-100, 2001.
- [37] G. Kure, O.J. Lindaas. Record-breaking air lifting operation on the Gullfaks C project. *Offshore Technology Conference (OTC)*, pg. 283-290, 1988.
- [38] A. Ledoux, C. Mary, N. Couty. Modelling of springing and whipping of FPSO's in a time domain sea-keeping tool. *Proceedings of the 14th International Offshore and Polar Engineering Conference*, pg. 666-671, 2004.

- [39] C.-H. Lee, J.N. Newman. Wave effects on large floating structures with air cushions. *15th International Workshop on Very Large Floating Structures*, vol. 1, pg. 139-148, 1999.
- [40] MCA Engineers. *An independent review*. Office of Naval Research, 1999.
- [41] MOB Project Team. *Mobile Offshore Base (MOB) - Science and technology program - Final report*. Naval Facilities Engineering Service Center, no. TR-2125-OCN, 2000.
- [42] S. Malenica, M. Zalar. An alternative method for linear hydrodynamics of air cushion supported floating bodies. *15th International Workshop on Water Waves and Floating Bodies*, 2000.
- [43] S. Malenica, B. Molin, F. Remy, I. Senjanović. Hydroelastic response of a barge to impulsive and non-impulsive wave loads. *3rd International Conference on Hydroelasticity in Marine Technology*, pg. 107-116, 2003.
- [44] S. Malenica, I. Senjanović, S. Tomasevi, E. Stumpf. Some aspects of hydroelastic issues in the design of ultra large container ships. *22nd International Workshop on Water Waves and Floating Bodies*, pg. 133-136, 2007.
- [45] J.C. Moulíjn. *Scaling of air cushion dynamics*. Delft University of Technology, Laboratory of Ship Hydrodynamics, Report 1151, 1998.
- [46] J.C. Moulíjn. *Added resistance due to waves of surface effect ships*. PhD thesis, Delft University of Technology, 2000.
- [47] D.E. Nakos, A. Nestegard, T. Ulstein, P.D. Sclavounos. Seakeeping Analysis of Surface Effect Ships. *Proceedings of FAST'91*, pg. 413-428, 1991.
- [48] S.B. Nelson. Airports across the ocean. *Invention and Technology*, vol. 17, no. 1, pg. 32-37, 2001.
- [49] J.N. Newman. Wave effects on deformable bodies. *Applied Ocean Research*, vol. 16, no. 1, pg. 47-59, 1994.

-
- [50] J.N. Newman. Diffraction of water waves by an air chamber. *15th International Workshop on Water Waves and Floating Bodies*, 2000.
- [51] M. Ohkusu, Y. Namba. Analysis of hydroelastic behavior of a very large floating platform of thin plate configuration in waves. *Proceedings of International Workshop on Very Large Floating Structures*, pg. 143-148, 1996.
- [52] M.F. Perutz. A description of the iceberg aircraft carrier and the bearing of the mechanical properties of frozen wood pulp upon some problems of glacier flow. *Journal of Glaciology*, vol. 1, no. 3, pg. 95-104, 1948.
- [53] J.A. Pinkster. The effect of air cushions under floating offshore structures. *Behavior of Offshore Structures, BOSS'97*, vol. 8, pg. 143-158, 1997.
- [54] J.A. Pinkster, A. Fauzi. Motions and drift forces of air-supported structures in waves. *Fifth WEGEMT Workshop on Non linear Wave Action on Structures and Ships*, 1998.
- [55] J.A. Pinkster, A. Fauzi, Y. Inoue, S. Tabeta. The behavior of large air cushion supported structures in waves. *Hydroelasticity in Marine Technology*, pg. 497-506, 1998.
- [56] J.A. Pinkster, E.J.A. Meevers Scholte. The behavior of a large air-supported MOB at sea. *Proceedings of International Workshop on Very Large Floating Structures*, vol. 2, pg. 567-576, 1999.
- [57] J.A. Pinkster, E.J.A. Meevers Scholte. The behavior of a large air-supported MOB at sea. *Marine Structures*, no. 14, pg. 163-179, 2001.
- [58] F. Remy, B. Molin, A. Ledoux. Experimental and numerical study of the wave response of a flexible barge. *Hydroelasticity in Marine Technology*, pg. 255-264, 2006.
- [59] I. Senjanović, S. Malenica, S. Tomašević. Investigation of ship hydroelasticity. *Ocean Engineering*, no. 35, pg. 523–535, 2008.

- [60] Vernon A. Squire. Synergies between VLFS hydroelasticity and sea-ice research. *International Journal of Offshore and Polar Engineering*, vol. 18, no. 3, pg. 1–13, 2008.
- [61] S. Steen. *Cobblestone effect on SES*. PhD thesis, The Norwegian Institute of Technology, 1993.
- [62] H. Suzuki. Overview of mega-float: concept, design criteria and analysis and design. *Workshop on Very Large Floating Structures (VLFS'04)*, 2004.
- [63] H. Suzuki, B. Bhattacharya, M. Fujikubo, D.A. Hudson and H.R. Riggs, H. Seto, H. Shin, T.A. Shugar, Y. Yasuzawa and Z. Zong. Very large floating structures. *16th International Ship and Offshore Structures Congress*, vol. 2, no. 2, pg. 391-442, 2006.
- [64] S. Tabeta. Model experiments on barge type floating structures supported by air cushions. *Delft University of Technology, Ship Hydromechanics Laboratory Report 1125*, 1998.
- [65] R.J. Taylor. MOB Project Summary and Technology Spin-offs. *Proceedings of International Symposium on Ocean Space Utilization Technology*, pg. 29-36, 2003.
- [66] K.P. Thiagarajan. An effective scaling device for model testing of air cushion vehicles in a Laboratory. *25th Symposium on Naval Hydrodynamics*, 2004.
- [67] K.P. Thiagarajan., M.T. Morris-Thomas, A. Spargo. Heave and pitch response of an offshore platform with air cushion support in shallow water. *Proceedings of the 23rd International Conference on Offshore Mechanics and Arctic Engineering (OMAE2004)*, 2004.
- [68] K.P. Thiagarajan, M.T. Morris-Thomas. Wave-induced motions of an air cushion structure in shallow water. *Ocean Engineering*, vol. 33, pg. 1143-1160, 2006.
- [69] S. Tomašević. *Hydroelastic model of dynamic response of container ships in waves*. PhD thesis, FSB Zagreb (In Croatian), 2007.

- [70] T. Tsubogo, H. Okada. Hydroelastic behavior of an aircushion-type floating structure. *Proceedings of the 12th International Offshore and Polar Engineering Conference*, 2002.
- [71] T. Ulstein, O.M. Faltinsen. Nonlinear effects of a flexible stern seal bag on cobblestone oscillations of a SES. *Proceedings of FAST'95*, 1995.
- [72] H. van den Berg, M. Serne. Maasvlakte: gebed zonder end; 'Het mag duidelijk zijn dat dit een geduchte tegenvaller is'. *NRC Handelsblad (in Dutch)*, pg. 15, 27 January 2005.
- [73] J.L.F. van Kessel, J.A. Pinkster. Wave-induced structural loads on different types of aircushion supported structures. *Proceedings of the 17th International Offshore and Polar Engineering Conference*, 2007.
- [74] J.L.F. van Kessel, J.A. Pinkster. The effect of aircushion division on the structural loads of large floating offshore structures. *Proceedings of the 26th International Conference on Offshore Mechanics and Arctic Engineering*, 2007.
- [75] J.L.F. van Kessel, F. Fathi. A comparison between CFD, potential theory and model tests for oscillating aircushion supported structures. *Proceedings of the 28th International Conference on Offshore Mechanics and Arctic Engineering*, 2009.
- [76] C.M. Wang, N.J. Shankar, W.Y. Mao, A.M. Hee. Sea space utilization in Singapore. *Proceedings of International Symposium on Ocean Space Utilization Technology*, pg. 37-46, 2003.
- [77] C.M. Wang, E. Watanabe, T. Utsunomiya. *Very large floating structures*. Taylor & Francis, 2008.
- [78] E. Watanabe, C. M. Wang, T. Utsunomiya, T. Moan. *Very large floating structures: applications, analysis and design*. Centre for Offshore Research and Engineering, CORE Report No: 2004-02, 2004.
- [79] Q. Xin-Yuan. Experimental study on behavior of an open bottom floating platform in wave, wind and current. *Proceedings of the 4th International Offshore and Polar Engineering Conference*, pg. 334-337, 1994.

- [80] K. Yoshida. Developments and Researches on VLFS in Japan. *Proceedings of International Workshop on Very Large Floating Structures*, pg. 5/12/2009, 1996.
- [81] L. Yun, A. Bliault. *Theory and design of air cushion craft*. Elsevier, 2000.
- [82] R. Zueck, R. Taylor, P. Palo. Development options for mobile offshore base technology. *Proceedings of the 11th International Offshore and Polar Engineering Conference*, pg. 13-18, 2001.

Websites

- [83] Kansai International Airport. *Website: http://www.onelang.com/encyclopedia/index.php/Kansai_International_Airport*, 2 May 2005.
- [84] Maasvlakte2. *Website: <http://www.maasvlakte2.com>*, 3 April 2009.
- [85] World Population Prospects: The 2006 Revision. *<http://data.un.org/Data.aspx?q=WORLD+POPULATION&d=PopDiv&f=variableID%3A14%3BcrID%3A900>*.

Appendix A

Compressibility of aircushions

Based on equation (2.6), the polytropic process of the aircushion may be expressed as.

$$\left(\frac{P(t)}{P_0} \right)^{1/\kappa} \cdot h_c(t) = \text{constant} \quad (\text{A.1})$$

If the structure moves ΔT downward and the compressibility of the air is written as a small dimensionless parameter ε , then the aircushion will be compressed by $\varepsilon \Delta T$. In this case equation (A.1) may be written as follows:

$$\left(1 + \frac{\rho g}{P_a} T_c(t) \right)^{1/\kappa} h_c(t) = \left(1 + \frac{\rho g}{P_a} [T_c(t) + (1 - \varepsilon) \Delta T] \right)^{1/\kappa} (h_c(t) - \varepsilon \Delta T) \quad (\text{A.2})$$

If:

$$f(\Delta T) = \left\{ 1 + \frac{\rho g}{P_a} (T_c + (1 - \varepsilon) \Delta T) \right\}^{1/\kappa} (h_c - \varepsilon \Delta T) \quad (\text{A.3})$$

it follows that:

$$\begin{aligned} f'(\Delta T) = & \frac{1}{\kappa} \left\{ 1 + \frac{\rho g}{P_a} (T_c + (1 - \varepsilon) \Delta T) \right\}^{\frac{1}{\kappa}-1} \frac{\rho g}{P_a} (1 - \varepsilon) (h_c - \varepsilon \Delta T) \\ & - \left\{ 1 + \frac{\rho g}{P_a} (T_c + (1 - \varepsilon) \Delta T) \right\}^{\frac{1}{\kappa}} \varepsilon \end{aligned} \quad (\text{A.4})$$

A Taylor expansion of $f(\Delta T)$ around $\Delta T = 0$ provides:

$$f_l(\Delta T) = \left(1 + \frac{\rho g}{P_a} T\right)^{\frac{1}{\kappa}} h_c + \left\{ \frac{1}{\kappa} \left(1 + \frac{\rho g}{P_a} T\right)^{\frac{1}{\kappa}-1} \frac{\rho g}{P_a} (1 - \varepsilon) h_c - \left(1 + \frac{\rho g}{P_a} T\right)^{\frac{1}{\kappa}} \varepsilon \right\} \Delta T \quad (\text{A.5})$$

This expansion can be rewritten in a simplified form by making use of expression (A.1):

$$\begin{aligned} f_l(\Delta T) &= \left(\frac{P}{P_a}\right)^{\frac{1}{\kappa}} h_c + \left\{ \frac{1}{\kappa} \left(\frac{P}{P_a}\right)^{\frac{1}{\kappa}-1} \frac{\rho g}{P_a} (1 - \varepsilon) h_c - \left(\frac{P}{P_a}\right)^{\frac{1}{\kappa}} \varepsilon \right\} \Delta T \\ &= \left(\frac{P}{P_a}\right)^{\frac{1}{\kappa}} h_c + \Delta T \frac{\left(\frac{P}{P_a}\right)^{\frac{1}{\kappa}} \rho g h_c}{\kappa \frac{P}{P_a}} (1 - \varepsilon) - \left(\frac{P}{P_a}\right)^{\frac{1}{\kappa}} \varepsilon \Delta T \end{aligned} \quad (\text{A.6})$$

Substitution of the Taylor expansion in equation (A.2) yields:

$$\begin{aligned} \left(\frac{P}{P_a}\right)^{\frac{1}{\kappa}} h_c &= f_l(\Delta T) \\ h_c &= h_c + \frac{\rho g h_c \Delta T}{\kappa P} - \frac{\rho g h_c \varepsilon \Delta T}{\kappa P} - \varepsilon \Delta T \end{aligned} \quad (\text{A.7})$$

Resulting in the compressibility factor of the aircushion:

$$\varepsilon = \frac{\rho g h_c}{\kappa P + \rho g h_c} \quad (\text{A.8})$$

with P being equal to $P(t)$ as described in expression (2.7).

If the structure moves a distance ΔT downwards, the aircushion will be compressed by $\varepsilon \Delta T$ and the displaced volume will increase with $(A_w - \varepsilon A_c) \Delta T$. Due to the compressibility of air, the vertical restoring coefficient of an aircushion supported structure is smaller than that of a corresponding conventional barge. The heave restoring coefficient of the aircushion supported structure is equal to:

$$C_{33} = (A_w - \varepsilon A_c) \rho g \quad (\text{A.9})$$

Substitution of expression (A.8) into the previous equation results in:

$$\begin{aligned}
C_{33} &= \rho g A_w - \frac{\rho^2 g^2 h_c A_c}{\kappa P + \rho g h_c} \\
&= \frac{\kappa P \rho g A_w + \rho^2 g^2 h_c A_w - \rho^2 g^2 h_c A_c}{\kappa P + \rho g h_c} \\
&= \frac{\kappa P \rho g A_w \frac{A_w}{h_c} + \rho^2 g^2 A_w^2 - \rho^2 g^2 A_c A_w}{\kappa P \frac{A_w}{h_c} + \rho g A_w} \\
&= \frac{\rho g A_w \left(\kappa P \frac{A_w}{h_c} \right) + \rho^2 g^2 A_w^2 - \rho^2 g^2 A_c A_w}{\kappa P \frac{A_w}{h_c} + \rho g A_w} + \frac{\left(\kappa P \frac{A_w}{h_c} \right)^2 - \left(\kappa P \frac{A_w}{h_c} \right)^2}{\kappa P \frac{A_w}{h_c} + \rho g A_w} \\
&= \kappa P \frac{A_w}{h_c} + \frac{\rho^2 g^2 A_w (A_w - A_c) - \left(\kappa P \frac{A_w}{h_c} \right)^2}{\kappa P \frac{A_w}{h_c} + \rho g A_w}
\end{aligned} \tag{A.10}$$

With use of equation (2.5), the heave stiffness of the total structure may be rewritten as:

$$C_{33} = C_{33,w} - \frac{C_{33,w}^2 - \rho^2 g^2 A_w \left(A_w - \sum_{i=1}^{N_{AC}} A_c \right)}{C_{33,w} + \rho g A_w} \tag{A.11}$$

in which:

$$C_{33,w} = \kappa P \frac{A_w}{h_c} \tag{A.12}$$

A more comprehensive expression of the heave stiffness may be obtained by rewriting equation (A.9) as:

$$C_{33} = \rho g (A_w - A_c) + \rho g A_c (1 - \varepsilon) \tag{A.13}$$

In this case the first term of the expression represents the buoyant part of the structure. The latter term corresponds to the aircushion contribution.

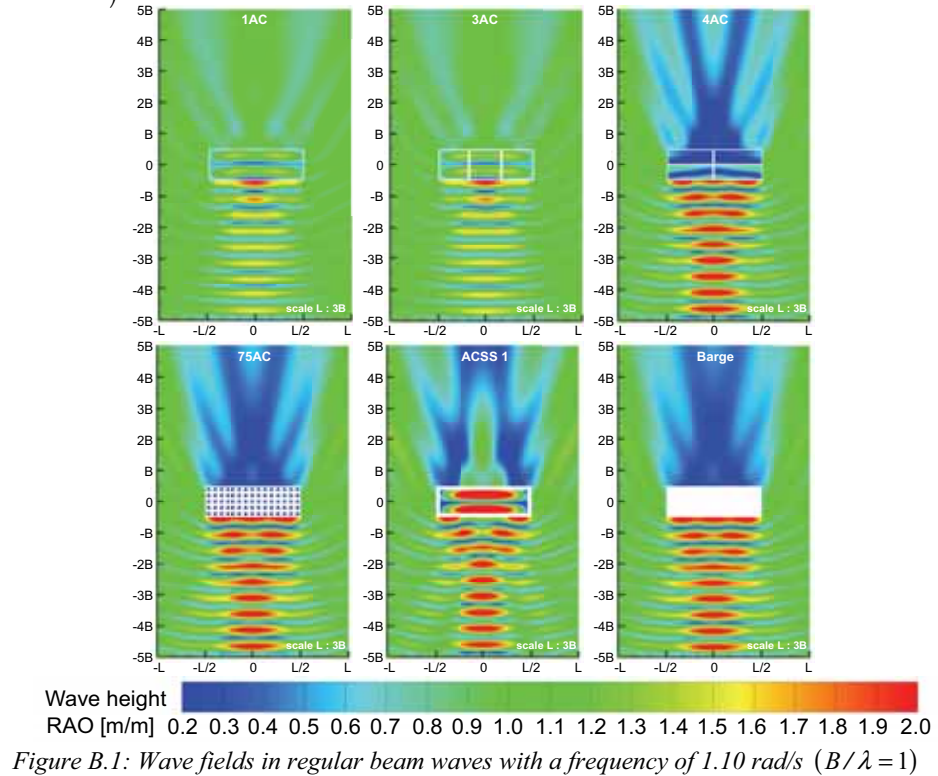
After substitution of equation (A.8) into (A.13), the aircushion contribution may be rewritten in the same way as expression (A.10). However in this case A_w should be replaced by A_c in equation (A.10). Eventually, this results in the final expression of the heave stiffness:

$$C_{33} = \rho g (A_w - A_c) + C_{33,c} - \frac{C_{33,c}^2}{C_{33,c} + \rho g A_c} \quad (\text{A.14})$$

Appendix B

Behavior of a large rigid aircushion supported structure

This appendix shows the wave field around different types of structures as described in section 2.7.2. Figure B.1 shows the results in regular beam waves of 1.10 rad/s ($B/\lambda = 1$). Figure B.2 shows the wave field in case of oblique waves of 135 degrees and a frequency of 0.95 rad/s ($B\sqrt{2}/\lambda = 1$).



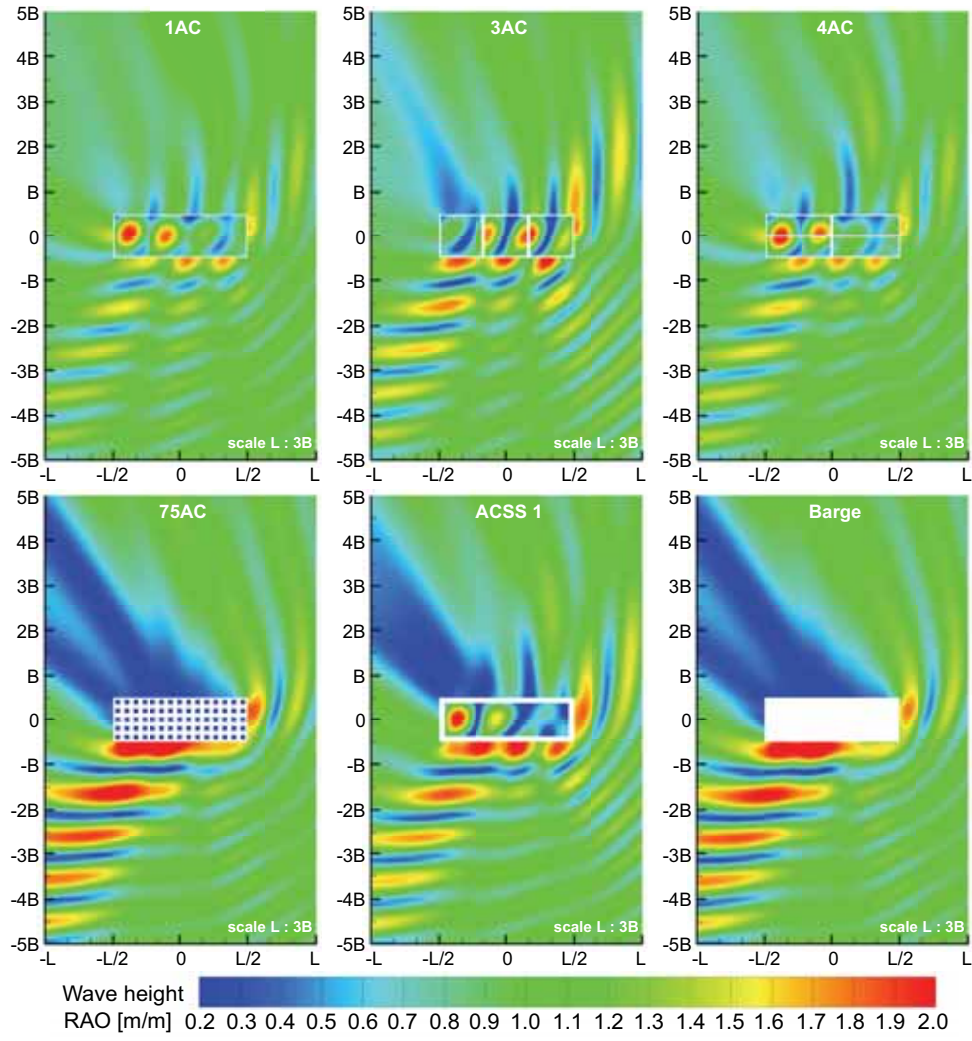


Figure B.2: Wave fields in regular waves with a heading of 135 degrees and a frequency of 0.95 rad/s ($B\sqrt{2}/\lambda = 1$)

Appendix C

Orthogonality condition

Since the matrices \mathbf{M} and \mathbf{K} are real and symmetric the eigenvectors of two different eigenvalues are orthogonal with respect to \mathbf{M} and \mathbf{K} . Given any two eigenvalues ω_s^2 and ω_r^2 and making use of equation (3.3), this results in:

$$\begin{aligned}\omega_s^2 \mathbf{M} \mathbf{D}_s &= \mathbf{K} \mathbf{D}_s \\ \omega_r^2 \mathbf{M} \mathbf{D}_r &= \mathbf{K} \mathbf{D}_r\end{aligned}\tag{C.1}$$

Pre-multiplying the first equation by \mathbf{D}_r^T and post-multiplying the transpose of the second by \mathbf{D}_s provides:

$$\begin{aligned}\omega_s^2 \mathbf{D}_r^T \mathbf{M} \mathbf{D}_s &= \mathbf{D}_r^T \mathbf{K} \mathbf{D}_s \\ \omega_r^2 \mathbf{D}_r^T \mathbf{M} \mathbf{D}_s &= \mathbf{D}_r^T \mathbf{K} \mathbf{D}_s\end{aligned}\tag{C.2}$$

subtracting one from the other gives:

$$(\omega_s^2 - \omega_r^2) \mathbf{D}_r^T \mathbf{M} \mathbf{D}_s = 0\tag{C.3}$$

It follows that:

$$\mathbf{D}_r^T \mathbf{M} \mathbf{D}_s = \delta_{rs} a_{rs}\tag{C.4}$$

where δ_{rs} is the Kronecker delta function, defined by:

$$\delta_{rs} = \begin{cases} 0 & \text{for } r \neq s \\ 1 & \text{for } r = s \end{cases}\tag{C.5}$$

Substituting this result back into equation (C.2) yields:

$$\left. \begin{aligned}\mathbf{D}_r^T \mathbf{K} \mathbf{D}_s &= \delta_{rs} \omega_s^2 a_{rs} \\ \mathbf{D}_r^T \mathbf{K} \mathbf{D}_s &= \delta_{rs} \omega_r^2 a_{rs}\end{aligned} \right\} = \delta_{rs} c_{rs}\tag{C.6}$$

The relation between \mathbf{D}_r and \mathbf{D}_s shown in equations (C.4) and (C.6) are those of orthogonality with respect to \mathbf{M} and \mathbf{K} respectively. The quantities a_{ss} and c_{ss} represent the generalized mass and generalized stiffness associated with the s^{th} mode. Their values depend upon the scaling of the s^{th} principal mode. In general the following relationships are true for rigid-body modes:

$$\begin{aligned} a_{ss} &= \rho \nabla & \text{for } s = 1, 2, 3 \\ a_{ss} &= I_{ss} & \text{for } s = 4, 5, 6 \end{aligned} \tag{C.7}$$

Appendix D

Flexible aircushion supported structures

The heave and pitch responses in regular head waves at six different locations of a flexible barge with and without aircushions are shown in figures D.1 and D.2. The dots and the black line represent experimental and numerical results of the conventional flexible barge that was discussed in paragraph 3.4.2. The other results are associated with different aircushion configurations as described in paragraph 3.4.3 and illustrated in figures 3.38 to 3.40. The locations at which the responses are computed are shown in figure 3.16.

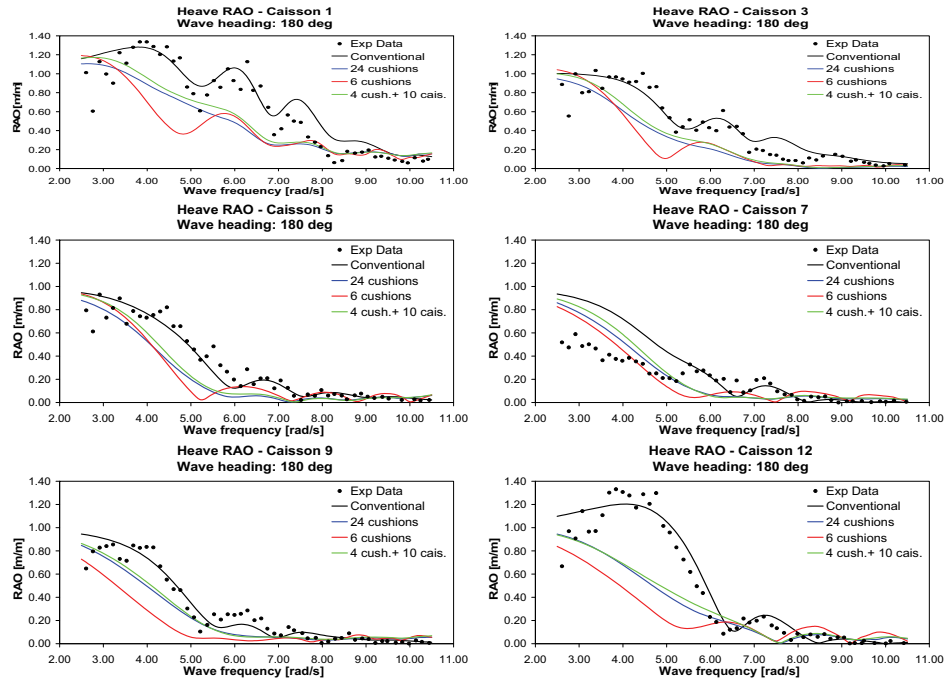


Figure D.1: Heave RAOs at six locations at a flexible barge with and without aircushions in regular head waves

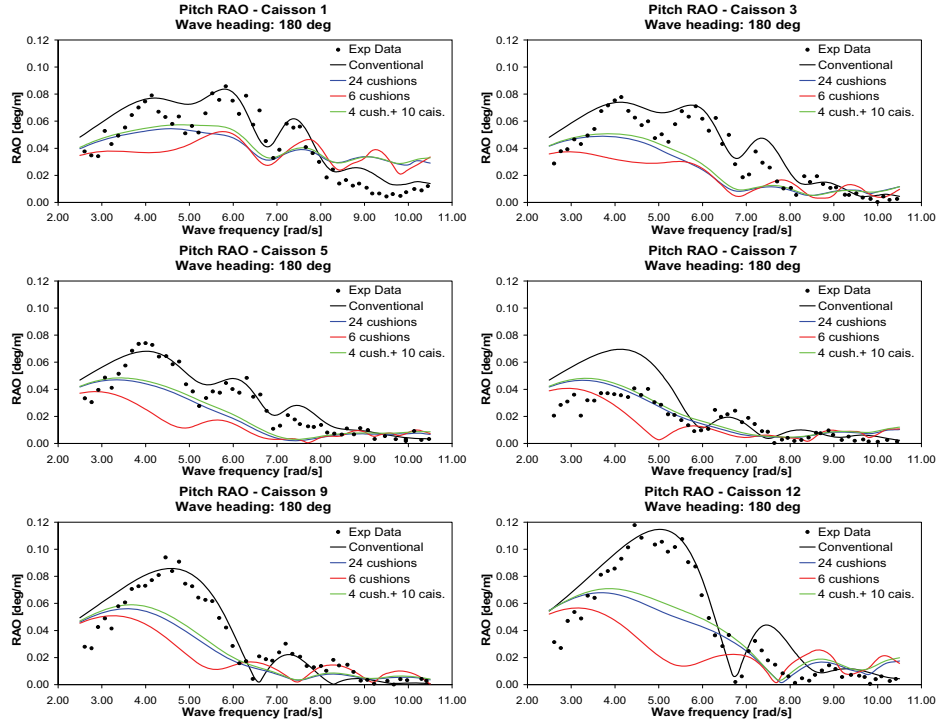


Figure D.2: Pitch RAOs at six locations at a flexible barge with and without aircushions in regular head waves

The maximum wave induced bending moment in the beam on top of the conventional barge occurs in waves of 5.50 rad/s. Figure D.3 shows the maximum deflection of the beam on top of the barge in waves of 100 mm wave height. The red line corresponds to the computed displacement with the new program. The green dotted line shows the 6-parameter fit of equation (3.51). The correlation coefficient R between both lines is 1.0, which is based on least square fitting.

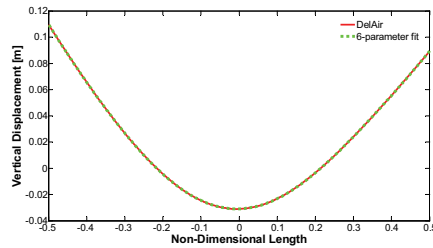


Figure D.3: Vertical deflection along the beam on top of the conventional flexible structure in head waves of 100 mm at 5.50 rad/s

The roll RAOs of the conventional flexible barge and the aircushion configurations at six locations in quartering waves of 120 deg are shown in figure D.4.

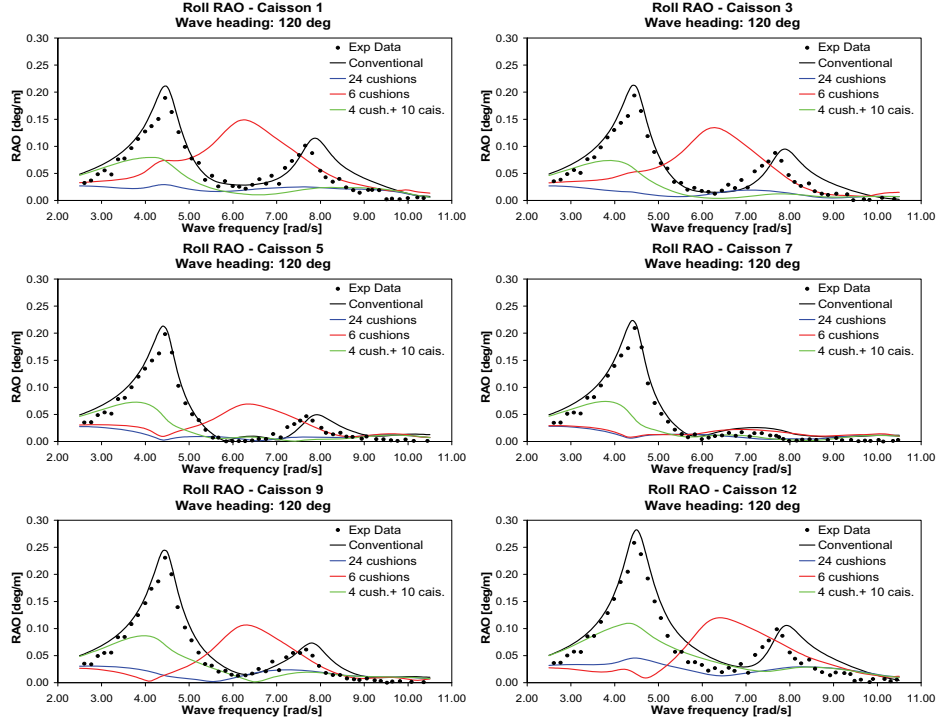


Figure D.4: Roll RAOs at six locations at a flexible barge with and without aircushions in quartering waves of 120 deg

The wave induced bending moments of the different structures are presented in figures D.5 to D.8. These bending moments are computed in the beam on top of the floaters. Each figure shows the results along the length of the beam in regular waves of 100 mm and frequencies ranging from 2.50 to 10.50 rad/s. The colors are associated with the phase differences. The wave induced bending moments of the conventional flexible barge are presented in figure D.5.

Figures D.6 and D.7 show the wave induced bending moments of the structures with 24 and 6 aircushions respectively. The results of the structure supported by four aircushions and ten conventional caissons are presented in figure D.8.

Conventional barge**Wave Bending Moments around y-axis**

Wave heading : 180 deg

Wave height : 0.1 m

Maximum value : 43 N.m

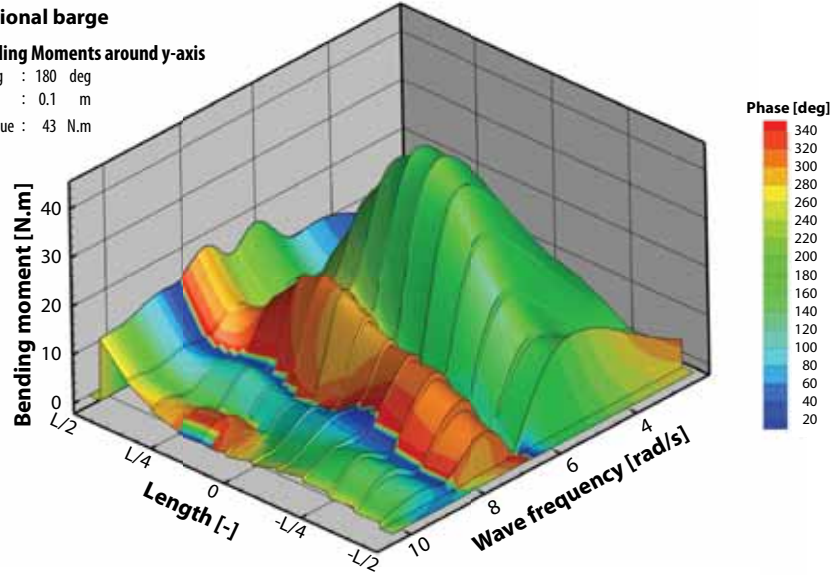


Figure D.5: Wave induced bending moments of the conventional flexible barge in regular head waves of 0.10 m at different wave frequencies

24 cushions**Wave Bending Moments around y-axis**

Wave heading : 180 deg

Wave height : 0.1 m

Maximum value : 27 N.m

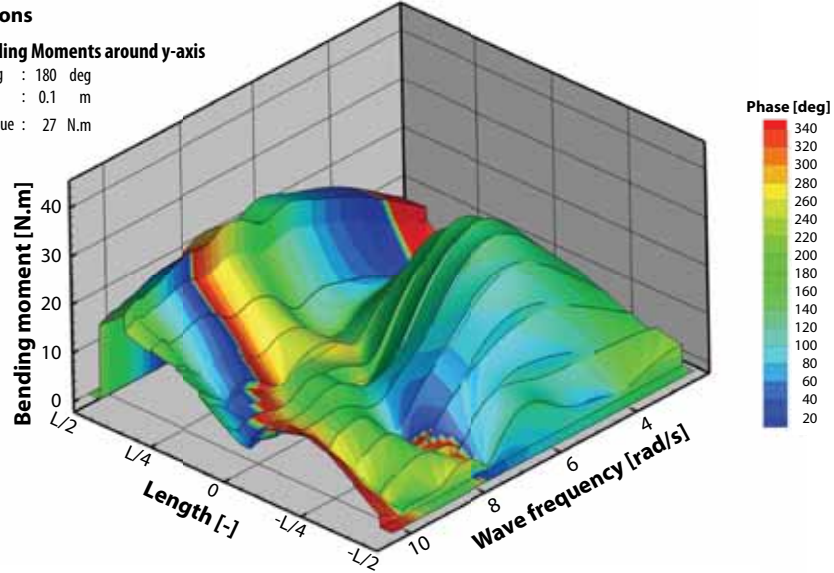


Figure D.6: Wave induced bending moments of the structure supported by 24 cushions in regular head waves of 0.10 m at different wave frequencies

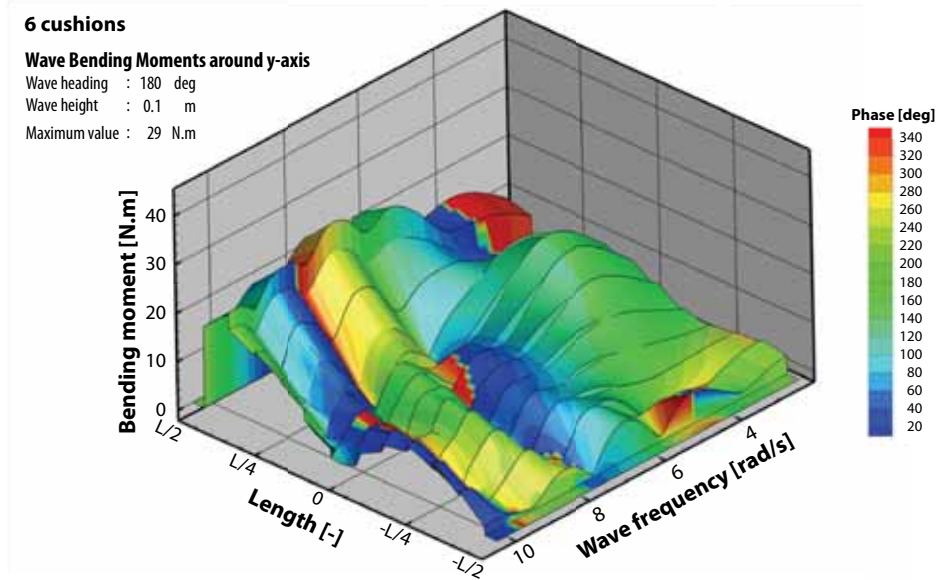


Figure D.7: Wave induced bending moments of the structure supported by 6 cushions in regular head waves of 0.10 m at different wave frequencies

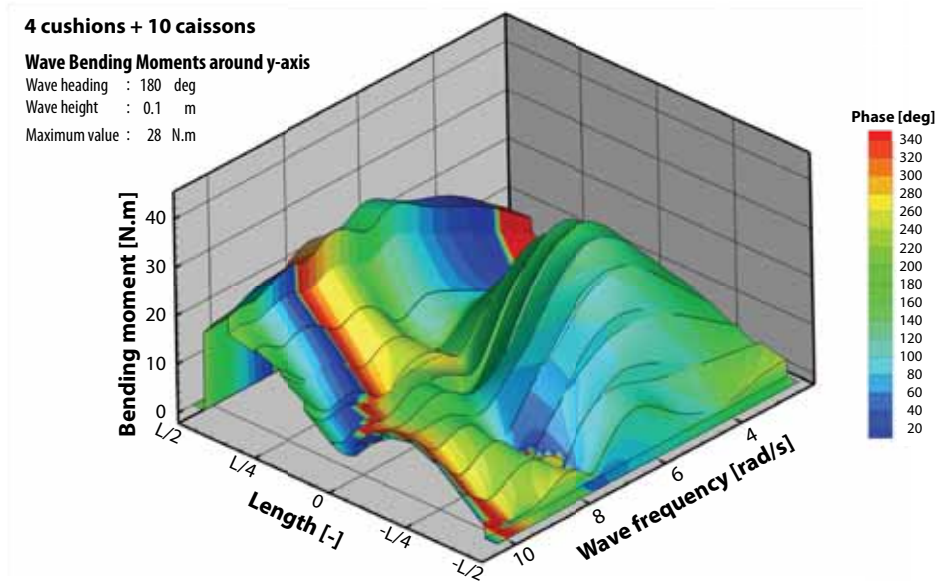


Figure D.8: Wave induced bending moments of the structure consisting of 4 aircushions and 10 caissons in regular head waves of 0.10 m at different wave frequencies

Appendix E

Responses in irregular seas

The response spectrum of a floating body may be obtained by multiplying the wave spectrum by the square of the transfer function:

$$S_z(\omega) = \left| \frac{z_a}{\zeta_a}(\omega) \right|^2 S_\zeta(\omega) \quad (\text{E.1})$$

In this case the area underneath the spectral response curve is equal to:

$$m_{0z} = \int_0^\infty S_z(\omega) d\omega \quad (\text{E.2})$$

and the significant response¹ of the floating body is equal to:

$$z_{a1/3} = 2 \sqrt{m_{0z}} \quad (\text{E.3})$$

The wave elevations are Gaussian distributed, the wave amplitudes ζ may be written by a Rayleigh distribution:

$$f(\zeta | \sigma) = \frac{\zeta}{\sigma^2} \exp\left(-\frac{\zeta^2}{2\sigma^2}\right) \quad (\text{E.4})$$

In which σ is the standard deviation of the wave heights. The probability that the wave amplitude exceeds the maximum value ζ_{max} may be expressed as:

¹ The significant response is defined as the mean response of the highest one-third part of the responses.

$$\begin{aligned}
P(\zeta > \zeta_{max}) &= \int_{\zeta_{max}}^{\infty} f(\zeta) d\zeta \\
&= \frac{1}{\sigma^2} \int_{\zeta_{max}}^{\infty} \zeta \cdot \exp\left\{-\left(\frac{\zeta}{\sigma\sqrt{2}}\right)^2\right\} d\zeta \\
&= \exp\left\{-\frac{\zeta_{max}^2}{2\sigma^2}\right\}
\end{aligned} \tag{E.5}$$

Therefore the probability that the maximum wave height H_{max} is exceeded once in n events is:

$$\exp\left\{-2\left(\frac{H_{max}}{H_s}\right)^2\right\} = \frac{1}{n} \tag{E.6}$$

in which H_s is the significant wave height a storm.

It is common practice in engineering applications to statistically determine the maximum responses of a floating structure. Normally it is assumed that a chosen wave height will only be exceeded once in a three hours storm in which 1000 waves pass [33]. As a result equation (E.6) may be rewritten as:

$$\exp\left\{-2\left(\frac{H_{max}}{H_s}\right)^2\right\} = \frac{1}{1000} \tag{E.7}$$

resulting in:

$$H_{max} = 1.86 H_s \tag{E.8}$$

Samenvatting

De snel toenemende wereldbevolking zorgt ervoor dat we efficiënt met de beschikbare ruimte om moeten gaan. Vooral de ruimte rondom snel groeiende wereldsteden is meestal beperkt omdat ze vaak aan het water gelegen zijn. *Mega-Floaters* bieden in dit geval een oplossing voor het gebrek aan land. Drijvende eilanden zijn vaak minder milieu belastend dan traditionele landwinningprojecten. Bovendien zijn ze ongevoelig voor aardbevingen en kunnen in een relatief korte tijd, onafhankelijk van waterdiepte en bodemgesteldheid, gebouwd worden. Daarnaast kunnen bestaande operationele faciliteiten eenvoudig uitgebreid worden. De enorme inwendige ruimte van een drijvende constructie biedt bovendien veel extra mogelijkheden.

Dit proefschrift beschrijft een methode om het gedrag van grote drijvende luchtkussenconstructies te berekenen. De methode is gebaseerd op een driedimensionale potentiaal theorie met trilvormen. De druk in de luchtkussens wordt beschreven door een lineaire adiabatische theorie. Het ondergedompelde gedeelte van het drijvende lichaam wordt beschreven door een panelenmodel dat belegd is met pulserende bronnen. Het vrije vloeistof oppervlak onder de constructies dient bovendien verdeeld te zijn met panelen. De panelen op het vrije vloeistofoppervlak hebben geen massa, maar wel toegevoegde massa, demping, hydrostatische stijfheid en aerostatische stijfheid.

De resultaten in dit proefschrift laten zien dat het gedrag van drijvende luchtkussenconstructies goed voorspeld kan worden met een driedimensionale potentiaal methode. Resultaten van diverse experimenten zijn gebruikt om de methode te valideren voor onvervormbare luchtkussenconstructies. Experimenten van een elastische constructie zijn gebruikt om de methode te valideren voor conventionele flexibele lichamen zonder luchtkussens. Vooralsnog zijn er geen resultaten beschikbaar van model proeven met flexibele luchtkussenconstructies, de numerieke resultaten zijn geverifieerd met een Eindige Elementen Methode (EEM) en analytische berekeningen.

Zowel model proeven en berekeningen hebben aangetoond dat luchtkussens het gedrag van drijvende constructies aanzienlijk kunnen beïnvloeden. Het effect op de inwendige belastingen

is groot en met name de golf buigende momenten kunnen aanzienlijk gereduceerd worden door het gebruik van luchtkussens.

Golfbrekers zijn noodzakelijk in open water om een conventionele mega-floater tegen de golven te beschermen. Een andere optie is om de constructie te ondersteunen door luchtkussens die de inwendige spanningen dusdanig kunnen reduceren zodat golfbrekers overbodig zijn.

De resultaten in dit proefschrift hebben aangetoond dat luchtkussenconstructies een goed alternatief zijn voor grote drijvende constructies. Daarnaast kan de nieuwe software gebruikt worden in het ontwerp proces om de optimale luchtkussenconfiguratie te bepalen voor een drijvende constructie.

Curriculum Vitae

Jan van Kessel was born in Bergeijk, the Netherlands, on 24 December 1979. He finished his secondary education at Were Di College in Valkenswaard in 1999. From 1999 to 2004 he studied Naval Architecture at Delft University of Technology. During these years he participated in various extracurricular activities. He went on study tours to South-Korea, Japan, Sweden, Spain and the USA. He studied Economics at Erasmus University in Rotterdam from 2001 to 2003. Finally, Jan completed his M.Sc. in naval architecture cum laude with an annotation in Offshore Engineering in August 2004. His Master's degree was obtained with a study on the '*Development of a pipelay/heavy-lift vessel*', which was performed at SBM Gusto in Schiedam, the Netherlands.

During the last year of his M.Sc. study he wrote a research proposal for funding of a Ph.D. research on '*Aircushion Supported Mega-Floaters*'. After having obtained his Master's degree and having received funding for the Ph.D. research, he started as a Ph.D. student at the departments of Offshore Engineering and Ship Hydromechanics of Delft University of Technology in December 2004. In 2007 he moved back to the SBM Gusto office where he carried out the second part of his Ph.D. research. In addition to this research he worked one day a week for SBM Gusto from 2007 to 2009. At present, Jan is working as an engineer at the Product Development Department of SBM Gusto.